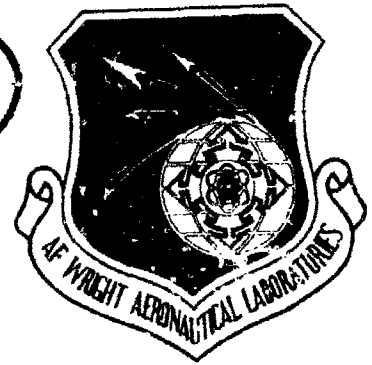


AD-A134503

AFWAL-TR-83-2004

12



# FUEL EFFECTS ON GAS TURBINE COMBUSTION

A. H. Lefebvre

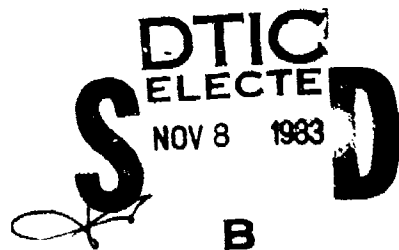
Combustion Laboratory  
Thermal Science and Propulsion Center  
School of Mechanical Engineering  
Purdue University  
West Lafayette, Indiana 47907

January 1983

Final Report for Period 21 September 1981— 23 December 1982

Approved for public release; distribution unlimited.

DTIC FILE COPY



AERO PROPULSION LABORATORY  
AIR FORCE WRIGHT AERONAUTICAL LABORATORIES  
AIR FORCE SYSTEMS COMMAND  
WRIGHT-PATTERSON AFB, OH 45433

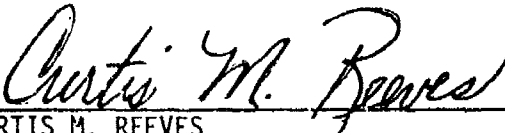
83 11 07 014

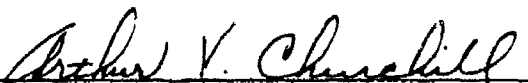
NOTICE

When Government drawings, specifications, or other data are used for any purpose other than in connection with a definitely related Government procurement operation, the United States Government thereby incurs no responsibility nor any obligation whatsoever; and the fact that the government may have formulated, furnished, or in any way supplied the said drawings, specifications, or other data, is not to be regarded by implication or otherwise as in any manner licensing the holder or any other person or corporation, or conveying any rights or permission to manufacture use, or sell any patented invention that may in any way be related thereto.


This report has been reviewed by the Office of Public Affairs (ASD/PA) and is releasable to the National Technical Information Service (NTIS). At NTIS, it will be available to the general public, including foreign nations.

This technical report has been reviewed and is approved for publication.

  
CURTIS M. REEVES  
Project Engineer  
Fuels Branch  
Fuels and Lubrication Division

  
ARTHUR V. CHURCHILL  
Chief, Fuels Branch  
Fuels and Lubrication Division

FOR THE COMMANDER

  
ROBERT D. SHERRILL, Chief  
Fuels and Lubrication Division  
Aero Propulsion Laboratory

"If your address has changed, if you wish to be removed from our mailing list, or if the addressee is no longer employed by your organization please notify AFWAL/POSF, W-PAFB, OH 45433 to help us maintain a current mailing list".

Copies of this report should not be returned unless return is required by security considerations, contractual obligations, or notice on a specific document.

UNCLASSIFIED

SECURITY CLASSIFICATION OF THIS PAGE (When Data Entered)

REPORT DOCUMENTATION PAGE		READ INSTRUCTIONS BEFORE COMPLETING FORM															
1. REPORT NUMBER AFWAL-TR-83-2004	2. GOVT ACCESSION NO. <b>A134503</b>	3. RECIPIENT'S CATALOG NUMBER															
4. TITLE (and Subtitle) FUEL EFFECTS ON GAS TURBINE COMBUSTION		5. TYPE OF REPORT & PERIOD COVERED Final Report for Period 21 Sep 81 - 23 Dec 82															
		6. PERFORMING ORG. REPORT NUMBER															
7. AUTHOR(s) A. H. LEFEBVRE		8. CONTRACT OR GRANT NUMBER(s) F33615-81-C-2067															
9. PERFORMING ORGANIZATION NAME AND ADDRESS School of Mechanical Engineering Purdue University West Lafayette IN 47907		10. PROGRAM ELEMENT, PROJECT, TASK AREA & WORK UNIT NUMBERS  30480513															
11. CONTROLLING OFFICE NAME AND ADDRESS Aero Propulsion Laboratory (AFWAL/POS) Air Force Wright Aeronautical Laboratories, AFSC Wright-Patterson Air Force Base, Ohio 45433		12. REPORT DATE January 1983															
		13. NUMBER OF PAGES 170															
14. MONITORING AGENCY NAME & ADDRESS (if different from Controlling Office)		15. SECURITY CLASS. (of this report) UNCLASSIFIED															
		15a. DECLASSIFICATION/DOWNGRADING SCHEDULE															
16. DISTRIBUTION STATEMENT (of this Report) APPROVED FOR PUBLIC RELEASE; DISTRIBUTION UNLIMITED																	
17. DISTRIBUTION STATEMENT (of the abstract entered in Block 20, if different from Report)																	
18. SUPPLEMENTARY NOTES																	
19. KEY WORDS (Continue on reverse side if necessary and identify by block number) <table border="0"> <tr> <td>Fuels</td> <td>Fuel Atomization</td> <td>Pattern Factor</td> </tr> <tr> <td>Alternate Fuels</td> <td>Combustion Efficiency</td> <td></td> </tr> <tr> <td>Gas Turbine Combustion</td> <td>Lean Blow Out</td> <td></td> </tr> <tr> <td>Exhaust Emissions</td> <td>Ignition</td> <td></td> </tr> <tr> <td></td> <td>Liner Wall Temperature</td> <td></td> </tr> </table>			Fuels	Fuel Atomization	Pattern Factor	Alternate Fuels	Combustion Efficiency		Gas Turbine Combustion	Lean Blow Out		Exhaust Emissions	Ignition			Liner Wall Temperature	
Fuels	Fuel Atomization	Pattern Factor															
Alternate Fuels	Combustion Efficiency																
Gas Turbine Combustion	Lean Blow Out																
Exhaust Emissions	Ignition																
	Liner Wall Temperature																
20. ABSTRACT (Continue on reverse side if necessary and identify by block number) This program is an analytical study correlating fuel properties and engine design and operating parameters with engine combustion performance and hot section (combustor and turbine) durability. Standard fuel specification data and fuel composition data are considered, along with special fuel properties and characteristics not routinely measured. Engine combustor design parameters considered are fuel injection and atomization, fuel/air mixing, residence times, temperatures and pressures, and flow velocities and other important design parameters. Engine performance parameters include low temperature starting and																	

DD FORM 1473

JAN 73

EDITION OF 1 NOV 65 IS OBSOLETE

UNCLASSIFIED

SECURITY CLASSIFICATION OF THIS PAGE (When Data Entered)

UNCLASSIFIED

SECURITY CLASSIFICATION OF THIS PAGE(When Data Entered)

20. high altitude relight, flame stability (i.e., lean blow-off limits), combustion efficiency, exhaust emissions including smoke, and thermal loading of the combustor liner and turbine nozzles.

Data for this program were obtained from recent and current Aero Propulsion Laboratory sponsored programs, NASA programs, and similar work performed by other Government agencies and industry.

UNCLASSIFIED

SECURITY CLASSIFICATION OF THIS PAGE(When Data Entered)

# FOREWORD

This final report is submitted by the Combustion Laboratory of the Thermal Science and Propulsion Center, School of Mechanical Engineering, Purdue University. The report documents work conducted under Contract No. F33615-81-C-2067 during the period 21 September 1981 to 23 December 1982. Program sponsorship and guidance were provided by the Fuels Branch of the Air Force Aero Propulsion Laboratory (AFAPL), Air Force Wright Aeronautical Laboratories, Wright-Patterson Air Force Base, Ohio. The Air Force Technical Monitors employed on this program were Mr. Thomas A. Jackson for the first 10 months and Mr. Curtis M. Reeves for the remainder of the program.

Accession For	
NTIS	<input checked="" type="checkbox"/>
DTIC TAB	<input type="checkbox"/>
Unannounced	<input type="checkbox"/>
Justification	<input type="checkbox"/>
By	
Distribution/	
Availability Codes	
Dist	Avail and/or Special
A-1	



## TABLE OF CONTENTS

SECTION	PAGE
I INTRODUCTION	1
II BASIC DATA	5
III FUEL ATOMIZATION	9
IV ANALYSIS	11
V COMBUSTION EFFICIENCY	13
1. Reaction Rate-Controlled Systems	13
2. Mixing Rate-Controlled Systems	14
3. Evaporation Rate-Controlled Systems	15
4. General Case	23
5. Reaction Rate- and Evaporation Rate-Controlled Systems	23
VI LEAN BLOWOUT	35
VII IGNITION	57
1. The Ignition Process	57
2. Theory	59
3. Data Analysis	62
VIII LINER WALL TEMPERATURE	77
1. Internal Radiation, $R_1$	77
2. External Radiation, $R_2$	85
3. Internal Convection, $C_1$	86
4. External Convection, $C_2$	87
IX EMISSIONS	93
1. Carbon Monoxide	93
2. Unburned Hydrocarbons	95
3. Oxides of Nitrogen	95
4. $NO_2$ Emissions	98

Preceding Page Blank

5. Smoke	98
6. Prediction of Emissions Characteristics	103
7. NO <sub>x</sub> and CO	105
8. Smoke	120
X. PATTERN FACTOR	135
1. Correlation of Data	137
2. Data Analysis	141
XI. DISCUSSION AND SUMMARY	151
1. Combustion Efficiency	151
2. Lean Blowout	152
3. Lean Lightup	153
4. Liner Wall Temperature	153
5. NO <sub>x</sub> Emissions	154
6. CO Emissions	155
7. Smoke	155
8. Pattern Factor	156
XII CONCLUSIONS	159
XIII RECOMMENDATIONS	161
REFERENCES	163

# LIST OF ILLUSTRATIONS

FIGURE		PAGE
1	Distillation Characteristics of Test Fuels (Ref. 2).	8
2	Variation of Effective Evaporation Constant with Normal Boiling Point at a Pressure of 100 kPa.	17
3	Variation of Effective Evaporation Constant with Normal Boiling Point at a Pressure of 1000 kPa.	18
4	Variation of Effective Evaporation Constant with Normal Boiling Point at a Pressure of 2000 kPa.	19
5	Illustration of Use of Eq. (19) to Predict the Combustion Efficiencies of Various Alternative Fuels from Data Obtained with Baseline Fuel. Experimental Data from Moses (Ref. 12).	22
6	Comparison of Measured and Predicted Values of Combustion Efficiency for J79-17A Combustor.	27
7	Comparison of Measured and Predicted Values of Combustion Efficiency for J79-17C Combustor.	28
8	Comparison of Measured and Predicted Values of Combustion Efficiency for F101 Combustor.	29
9	Comparison of Measured and Predicted Values of Combustion Efficiency for TF41 Combustor.	30
10	Comparison of Measured and Predicted Values of Combustion Efficiency for TF39 Combustor.	31
11	Comparison of Measured and Predicted Values of Combustion Efficiency for J85 Combustor.	32
12	Comparison of Measured and Predicted Values of Combustion Efficiency for TF33 Combustor.	33
13	Comparison of Measured and Predicted Values of Combustion Efficiency for F100 Combustor.	34
14	Comparison of Measured and Predicted Values of $q_{LBO}$ for J79-17A Combustor. (Fuels 1 to 6).	41
15	Comparison of Measured and Predicted Values of $q_{LBO}$ for J79-17A Combustor. (Fuels 7 to 13).	42
16	Comparison of Measured and Predicted values of $q_{LBO}$ for J79-17C Combustor. (Fuels 2A to 7A).	43

17	Comparison of Measured and Predicted Values of $q_{LBO}$ for J79-17C Combustor. (Fuels 1A, 8A to 12A).	44
18	Comparison of Measured and Predicted Values of $q_{LBO}$ for F101 Combustor.	45
19	Comparison of Measured and Predicted Values of $q_{LBO}$ for TF 41 Combustor. (Fuels 1 to 6).	46
20	Comparison of Measured and Predicted Values of $q_{LBO}$ for TF 41 Combustor. (Fuels 7 to 12).	47
21	Comparison of Measured and Predicted Values of $q_{LBO}$ for TF 39 Combustor.	48
22	Comparison of Measured and Predicted Values of $q_{LBO}$ for J85 Combustor.	49
23	Comparison of Measured and Predicted Values of $q_{LBO}$ for TF 33 Combustor.	50
24	Comparison of Measured and Predicted Values of $q_{LBO}$ for F100 Combustor.	51
25	Relationship Between Fuel Viscosity and Lean Blowout Limits.	53
26	Comparison of Predicted Influence of Fuel Temperature on $q_{LBO}$ with Experimental Data.	54
27	Comparison of Measured and Predicted Values of $q_{LLO}$ for J79-17A Combustor. (Fuels 1 to 6).	64
28	Comparison of Measured and Predicted Values of $q_{LLO}$ for J79-17A Combustor. (Fuels 7 to 12).	65
29	Correlation of Experimental Data on $q_{LLO}$ for J79-17C Combustor. (Fuels 1A to 6A).	66
30	Correlation of Experimental Data on $q_{LLO}$ for J79-17C Combustor. (Fuels 7A to 12A).	67
31	Comparison of Measured and Predicted Values of $q_{LLO}$ for J79-17C Combustor. (Fuels 1A to 6A).	68
32	Comparison of Measured and Predicted Values of $q_{LLO}$ for J79-17C Combustor. (Fuels 7A to 12A).	69
33	Comparison of Measured and Predicted Values of $q_{LLO}$ for F101 Combustor.	70
34	Comparison of Measured and Predicted Values of $q_{LLO}$ for TF 41 Combustor.	71
35	Comparison of Measured and Predicted Values of $q_{LLO}$ for TF 39 Combustor.	72

36	Comparison of Measured and Predicted Values of $q_{LLO}$ for J85 Combustor.	73
37	Comparison of Measured and Predicted Values of $q_{LLO}$ for TF 33 Combustor.	74
38	Comparison of Measured and Predicted Values of $q_{LLO}$ for F100 Combustor.	75
39	Effect of Fuel Hydrogen Content on Liner Temperature Parameter at Cruise Operating Conditions (Refs. 22 and 23).	80
40	Effect of Fuel Hydrogen Content on Liner Temperature Parameter for J79-17A Combustor.	81
41	Effect of Fuel Hydrogen Content on Liner Temperature Parameter for J79-17C Combustor.	82
42	Effect of Fuel Hydrogen Content on Liner Temperature Parameter for F101 Combustor.	83
43	Effect of Fuel Hydrogen Content on Liner Temperature Parameter for TF 41 Combustor.	84
44	Comparison of Measured and Predicted Values on the Effect of $H_2$ Content on Liner Temperature for J79-17A Combustor.	88
45	Comparison of Measured and Predicted Values on the Effect of $H_2$ Content on Liner Temperature for J79-17C Combustor.	89
46	Comparison of Measured and Predicted Values on the Effect of $H_2$ Content on Liner Temperature for F101 Combustor.	90
47	Comparison of Measured and Predicted Values on the Effect of $H_2$ Content on Liner Temperature for TF 41 Combustor.	91
48	Comparison of Measured and Predicted Values of $NO_x$ Emissions for J79-17A Combustor. (Fuels 1 to 6).	109
49	Comparison of Measured and Predicted Values of $NO_x$ Emissions for J79-17A Combustor. (Fuels 7 to 13).	110
50	Comparison of Measured and Predicted Values of $NO_x$ Emissions for J79-17C Combustor. (Fuels 1A to 6A).	111
51	Comparison of Measured and Predicted Values of $NO_x$ Emissions for J79-17C Combustor. (Fuels 7A to 13A).	112
52	Comparison of Measured and Predicted Values of $NO_x$ Emissions for F101 Combustor. (Fuels 1 to 6).	113
53	Comparison of Measured and Predicted Values of $NO_x$ Emissions for F101 Combustor. (Fuels 7 to 13).	114

54	Comparison of Measured and Predicted Values of NO <sub>x</sub> Emissions for TF 41 Combustor. (Fuels 1 to 6).	115
55	Comparison of Measured and Predicted Values of NO <sub>x</sub> Emissions for TF 41 Combustor. (Fuels 7 to 12).	116
56	Comparison of Measured and Predicted Values of NO <sub>x</sub> Emissions for TF 39 Combustor.	117
57	Comparison of Measured and Predicted Values of NO <sub>x</sub> Emissions for TF 33 Combustor.	118
58	Comparison of Measured and Predicted Values of NO <sub>x</sub> Emissions for F100 Combustor.	119
59	Comparison of Measured and Predicted Values of CO Emissions for J79-17A Combustor.	121
60	Comparison of Measured and Predicted Values of CO Emissions for J79-17C Combustor.	122
61	Comparison of Measured and Predicted Values of CO Emissions for F101 Combustor.	123
62	Comparison of Measured and Predicted Values of CO Emissions for TF 41 Combustor.	124
63	Comparison of Measured and Predicted Values of CO Emissions for F100 Combustor.	125
64	Graphs Illustrating Influence of Aromatics Content and Engine Operating Conditions on Soot Emissions for J79-17A Combustor.	128
65	Graphs Illustrating Influence of Aromatics Content and Engine Operating Conditions on Soot Emissions for J79-17C Combustor.	129
66	Graphs Illustrating Influence of Aromatics Content and Engine Operating Conditions of Soot Emissions for F101 Combustor.	130
67	Graphs Illustrating Influence of Aromatics Content and Engine Operating Conditions on Soot Emissions for TF 41 Combustor.	131
68	Pattern Factor Correlation for Turbo-Annular Combustors.	139
69	Pattern Factor Correlation for Annular Combustors.	140
70	Comparison of Measured and Predicted Values of Pattern Factor for J79-17A Combustor.	144

71	Comparison of Measured and Predicted Values of Pattern Factor for J79-17C Combustor.	145
72	Comparison of Measured and Predicted Values of Pattern Factor for TF 41 Combustor.	146
73	Comparison of Measured and Predicted Values of Pattern Factor for F101 Combustor.	147
74	Graphs Illustrating the Effects of Fuel Density and Combustor Operating Conditions on Pattern Factor.	149

## LIST OF TABLES

TABLE		PAGE
1	Test Fuel Chemical and Physical Properties	6
2	Test Fuel Chemical and Physical Properties (Reference 6)	7
3	Fuel Properties used to Construct Figure 5.	24
4	Re-assigned Fuel Numbers for Lean Blowout Data in Tables C-8 to C-11. [1]	56
5	Values of A' and B' employed in Eqs. (33) and (37).	56
6	Values of A, B and C employed in Eq. (60).	132

# LIST OF SYMBOLS

A	area, $m^2$
B	mass transfer number
A', B'	constants in Eqs. (33) and (37)
C <sub>1</sub>	heat flux from combustion gases to liner wall by convection, $W/m^2$
C <sub>2</sub>	heat flux from liner wall to annulus air by convection, $W/m^2$
C <sub>3</sub> , C <sub>4</sub> , C <sub>5</sub>	constants in Eq. (20)
C <sub>7</sub> , C <sub>8</sub>	constants in Eq. (38)
c <sub>p</sub>	specific heat at constant pressure, J/kg K
C/H	carbon/hydrogen ratio of fuel, by mass
D <sub>h</sub>	hydraulic mean diameter of atomizer air duct at exit plane, m
D <sub>L</sub>	liner diameter or height, m
D <sub>0</sub>	initial mean drop size of fuel spray, m
D <sub>p</sub>	atomizer prefilmer diameter, m
D <sub>r</sub>	mean drop size relative to that for JP4
E <sub>min</sub>	minimum ignition energy, J
f <sub>c</sub>	fraction of total combustor air employed in combustion
f <sub>pz</sub>	fraction of total combustor air employed in primary-zone combustion
f <sub>f</sub>	fraction of fuel vaporized within combustion zone
k	thermal conductivity, J/ms K
L	length, or luminosity factor
L <sub>c</sub>	length of combustion zone, m
L <sub>e</sub>	liner length employed in fuel evaporation, m
L <sub>L</sub>	total liner length, m

LCV	lower calorific value of fuel, J/kg
LCV <sub>r</sub>	lower calorific value relative to JP4
$\ell_b$	mean beam length of radiation path, m
$\dot{m}$	mass flow rate, kg/s
n	reaction order
P	pressure, kPa
$\Delta P$	pressure differential, Pa
q	fuel/air ratio
q <sub>c</sub>	fuel/air ratio in combustion zone
q <sub>ov</sub>	combustor overall fuel/air ratio
q <sub>ref</sub>	reference dynamic head, Pa
q <sub>LBO</sub>	fuel/air ratio at lean blowout, g fuel/kg air
q <sub>LL0</sub>	fuel/air ratio at lean lightup, g fuel/kg air
R	gas constant (286.9 m <sup>2</sup> /s <sup>2</sup> K)
R <sub>1</sub>	radiation heat flux from combustion gases to liner wall, W/m <sup>2</sup>
R <sub>2</sub>	radiation heat flux from liner to casing, W/m <sup>2</sup>
Re <sub>D<sub>0</sub></sub>	Reynolds number based on initial mean drop size, (U <sub>PA</sub> D <sub>0</sub> /μ <sub>A</sub> )
SMD	Sauter mean diameter of fuel spray, m
SN	smoke number
T	temperature, K
T <sub>bn</sub>	boiling temperature at normal atmospheric pressure, K
T <sub>LO</sub>	maximum liner wall temperature for JP4, K
T <sub>Lmax</sub>	maximum liner wall temperature for given fuel, K
ΔT	temperature rise, K
U	velocity, m/s

$U_j$	jet velocity, m/s
$V$	combustion volume (general), $m^3$
$V_c$	total combustion zone volume (=predilution zone volume), $m^3$
$V_e$	evaporation volume, $m^3$
$V_{pz}$	primary zone volume, $m^3$
$X$	concentration, mg pollutant/kg gas
$\epsilon$	emissivity
$\sigma$	Stefan-Boltzmann constant ( $5.67 \times 10^{-8} \text{ W/m}^2 \text{ K}$ ), or surface tension, $\text{kg/s}^2$
$\mu$	dynamic viscosity, $\text{kg/ms}$
$\nu$	kinematic viscosity, $\text{m}^2/\text{s}$
$\phi$	equivalence ratio
$\lambda_{\text{eff}}$	effective value of evaporation constant, $\text{m}^2/\text{s}$
$\lambda_r$	value of $\lambda_{\text{eff}}$ relative to that for JP4
$\eta_c$	combustion efficiency
$\eta_{c\theta}$	combustion efficiency based on chemical kinetics
$\eta_{ce}$	combustion efficiency based on fuel evaporation
$\eta_{cm}$	combustion efficiency based on mixing rates
$\rho$	density, $\text{kg/m}^3$
$f$	function of

#### Subscripts

A	air
F	fuel, or formation
o	oxidation
g	gas
ad	adiabatic value

st	stoichiometric value
c	combustion zone, or air casing, value
an	annulus value
pz	primary zone value
sz	secondary zone value
w	wall value
3	combustor inlet value
4	combustor outlet value
8	engine discharge value
L	liner value

## SECTION 1

### INTRODUCTION

In the early days of gas turbine development, the view was widely held that within a few years engines would be capable of operating efficiently on a wide variety of cheap fuels. Although Whittle had chosen kerosine on the grounds of cost, availability and ease of handling, it was generally believed that normal development procedures would yield engines capable of burning a wide range of gaseous, liquid and even pulverized solid fuels. However, this early optimism was short-lived, at least for aircraft engines, as experience soon revealed the important and restrictive effects of aircraft and engine requirements on the physical and chemical properties of the fuel.

In due course, the extensive research initiated by the major fuel and engine companies and the various governmental research establishments yielded increasing knowledge of fuel properties and the manner in which they affect aircraft performance, safety and reliability. This improved understanding helped to eliminate or ease many formidable problems, but from time to time various new problems emerged, mainly as a result of the continuing demand for increases in aircraft speed, range and operating altitude. In the late 1960s the growth of public concern over air pollution caused by combustion processes eventually culminated in legislation for closer control of exhaust emissions, notably in terms of reductions in carbon monoxide, unburned hydrocarbons, smoke and nitric oxides. The restraining effects of these requirements, coupled with the fact that the aircraft user has traditionally been able to draw his fuel supplies from the highest quality feedstock, fostered conservatism to the extent that current airline fuels do not differ markedly from the kerosine used by Whittle.

In general, for any given aircraft application, the optimum fuel is one that represents the best compromise solution to the various problems confronting the fuel companies, the engine and aircraft manufacturers and the operator. For civil aircraft the main requirements are safety, reliability, low cost and ease of handling. For military aircraft fuel cost is of secondary importance compared with availability, supply logistics and the need for trouble-free operation over a wide range of conditions.

The most dominant fuel issues of today are those of cost and availability. The steps now being taken to ensure future supplies of fuels for gas turbines, in addition to various measures of fuel conservation, include the exploitation of alternative fuel sources and the acceptance of a broader specification for aviation fuels. It is clearly of paramount importance that prediction techniques be established for estimating accurately, for any given combustor, the impact of any change in fuel specification on hardware durability and the key aspects of combustion performance.

A complicating factor in the attainment of this goal is that the effect of a change in fuel properties is not constant for all combustors but varies between one combustor and another, due to differences in operating conditions and differences in design. For example, the effect of an increase in carbon/hydrogen ratio on liner wall temperature is much greater for combustors featuring fuel-rich primary zones than for combustors in which the primary zone is fuel-weak. This is because with rich primary zones most of the heat transferred to the liner wall is by radiation, which is proportional to  $\epsilon T_g^4$ . Thus liner wall temperature is dependent on the flame emissivity,  $\epsilon$ , which, in turn, is dependent on the C/H ratio of the fuel. With fuel-weak primary zones, however, most of the heat

transferred to the liner wall is by forced convection. Here the dominant term is the gas temperature,  $T_g$ , which is fairly insensitive to changes in C/H ratio. In consequence, quite large changes in C/H ratio produce only a slight effect on liner wall temperature.

Another complicating factor is that the various properties and characteristics of petroleum fuels are so closely interrelated that it is virtually impossible to change any one property without affecting many others. Thus the classical approach to experimental research, which is based on examination of the effects of varying one independent parameter, while maintaining the others constant, is precluded from the outset.

Fortunately, there are several mitigating factors that help to ease the situation. For example, atomization quality is influenced only by the physical properties of the fuel, namely, viscosity, surface tension, and density, all of which are easily measured by standard laboratory techniques. Moreover, it can also be shown that evaporation rates are closely linked to the physical properties of the fuel, for example,  $\rho_F$  provides a useful indication of fuel volatility.

As far as the actual combustion process is concerned, it is found that chemical reaction rates vary only slightly between the various hydrocarbon fuels of interest to the aircraft gas turbine. This is partly because these fuels exhibit only slight differences in adiabatic flame temperature, but also because before entering the true reaction zone all the fuels are largely pyrolyzed to methane, other 1-2 carbon atom hydrocarbons, and hydrogen. Hence the gas composition in the reaction zone is substantially independent of the parent fuel. Thus, provided the discussion is restricted to the anticipated range of aircraft fuels, as reflected in Table 1, any

differences that occur in ignition performance, lean-blowout limits and combustion efficiency, will be caused mainly by differences in the physical properties of the fuel insofar as they control the quality of atomization and the ensuing rate of evaporation.

These same physical properties, along with the critical liner design features, and the combustor operating conditions, also play a role in determining the rates of formation of carbon monoxide (CO), unburned hydrocarbons (UHC) and, to a lesser extent  $\text{NO}_x$ . Smoke, and the soot formation in the combustion zone that gives rise to smoke, are strongly dependent on fuel chemistry. Thus fuels of different chemical composition (especially in regard to hydrogen and aromatics content) are found to exhibit wide variations, both in radiant heat flux to the liner walls and in the level of smoke concentration in the engine exhaust gases. It follows that the success of any proposed relationships for luminous flame radiation, liner wall temperature, and soot and particulate emissions will depend upon accurate identification of the initial fuel components that govern the nature and rate of soot formation in the flame.

In subsequent sections the main combustor performance parameters are discussed in turn. In each case an outline is given of the general approach employed in identifying the basic relationships between the relevant fuel properties and each individual aspect of combustor performance. Meaningful relationships are sought, not on the basis of statistical techniques, but from an understanding of the fundamental physical and chemical processes involved. The general approach has been either to enhance existing correlations or to replace them with new correlations that are based on a firmer scientific footing. It is hoped that the relationships developed in this program will make a useful contribution to future combustor designs.

## SECTION II

### BASIC DATA

In recent years the USAF, Army, Navy, and NASA, along with engine manufacturers, have initiated programs to determine the effects of anticipated future fuels on existing engines. As a result of these studies data have become available that yield new and useful insights into fuel property effects on combustion performance. These data, that are contained in references 1 to 6, provide the basic material for this investigation.

In addition to a considerable body of evidence on the effects of fuel property variations on the performance, exhaust emissions, and durability characteristics of the combustors investigated, references 1 to 6 also contain detailed information on all the relevant chemical and physical properties of the fuels employed. These fuels were supplied by the USAF for combustion system evaluation. They included a current JP4, a current JP8, five blends of the JP4, five blends of the JP8 and, in some cases, a No. 2 diesel fuel. The blends were intended to achieve three different levels of hydrogen content; i.e. 12, 13 and 14 percent by mass.

The rationale for the diesel fuel was to approximate the Experimental Referee Broad Specification (ERBS) aviation fuel that emanated from the NASA-Lewis Workshop on Jet Aircraft Hydrocarbon Fuel Technology [7]. The JP4, JP8 fuels and their blends were chosen to span systematically the possible fuel variations in key properties that might be dictated in the future on grounds of availability and cost, and the use of non-petroleum sources for jet fuel production,

The key chemical and physical properties of the fuels selected are listed in Tables 1 and 2. Additional information on the distillation characteristics of the test fuels is contained in Fig. 1.

TABLE 1. Test Fuel Chemical and Physical Properties.

Reference					Fuel Components		Hydrogen Content H Weight %	Heating Value (net) MJ/kg	Density $\rho_{300\text{ K}}$ kg/m <sup>3</sup>	Viscosity $\nu_{300\text{ K}}$ mm <sup>2</sup> /s	Surface Tension $\sigma_{300\text{ K}}$ mN/m	Vapor Pressure $P_{300\text{ K}}$ kPa
1	2	3	4	5	Base Fuel	Blending Agents						
1	1	1	1	1B, 1C	JP-4	-	14.5	43.603	752.7	0.924	23.27	12.04
2	2	7	2	2B1	JP-8	-	14.0	43.210	799.5	1.849	25.85	2.15
3	3	12	3	-	JP-8	Gulf Mineral Seal Oil	13.9	43.189	801.2	2.071	25.92	1.97
4	4	8	4	-	JP-8	2040 Solvent	12.0	41.947	852.3	1.809	27.62	1.16
5	5	11	5	-	JP-8	Xylene Bottoms	13.0	42.724	813.4	1.428	26.38	1.48
6	6	10	6	-	JP-8	Xylene Bottoms	12.0	42.129	827.6	1.160	26.66	1.33
7	7	9	7	-	JP-8	2040	13.0	42.556	825.2	1.804	26.42	1.38
8	8	2	8	8B, 8C	JP-4	2040	12.0	42.203	829.7	1.141	25.22	7.38
9	9	3	9	9B, 9C	JP-4	2040	13.0	42.629	796.3	1.028	23.75	8.61
10	10	4	10	-	JP-4	Xylene	12.0	42.196	808.0	0.830	25.21	6.17
11	11	5	11	-	JP-4	Xylene	13.0	42.682	786.5	0.835	24.20	9.06
12	12	6	12	-	JP-4	Xylene & GMSO	14.0	43.366	769.6	1.057	23.45	10.25
13	13	13	13	13B1, 13C	2-D	-	13.1	42.691	837.2	3.245	27.35	1.59

TABLE 2. Test Fuel Chemical and Physical Properties. (Reference 6)

Fuel Types	Hydrogen Content H Weight %	Heating Value (net) MJ/kg	Density $\rho_{311K}$ kg/m <sup>3</sup>	Viscosity $\nu_{311K}$ mm <sup>2</sup> /s	Surface Tension $\sigma_{311K}$ mN/m	Vapor Pressure $P_{311K}$ kPa
JP-4	14.54	43.401	0.7411	0.7956	21.28	18.13
JP-4 Shale	14.39	43.469	0.7637	1.027	22.99	19.73
Blend No. 1	14.24	43.287	0.7715	1.331	23.07	11.40
Blend No. 2	13.44	43.001	0.7785	0.9415	23.30	8.80
Blend No. 3	14.04	43.232	0.7843	1.323	24.38	2.47
Blend No. 4	12.27	42.560	0.7778	0.6216	22.04	23.26
Blend No. 5	13.44	42.818	0.8008	1.419	24.93	2.47
Blend No. 6	12.94	42.537	0.7968	1.159	23.03	23.33
Blend No. 7	11.56	41.212	0.8624	1.933	23.66	3.27
Blend No. 8	11.50	41.451	0.8695	2.027	27.53	3.80

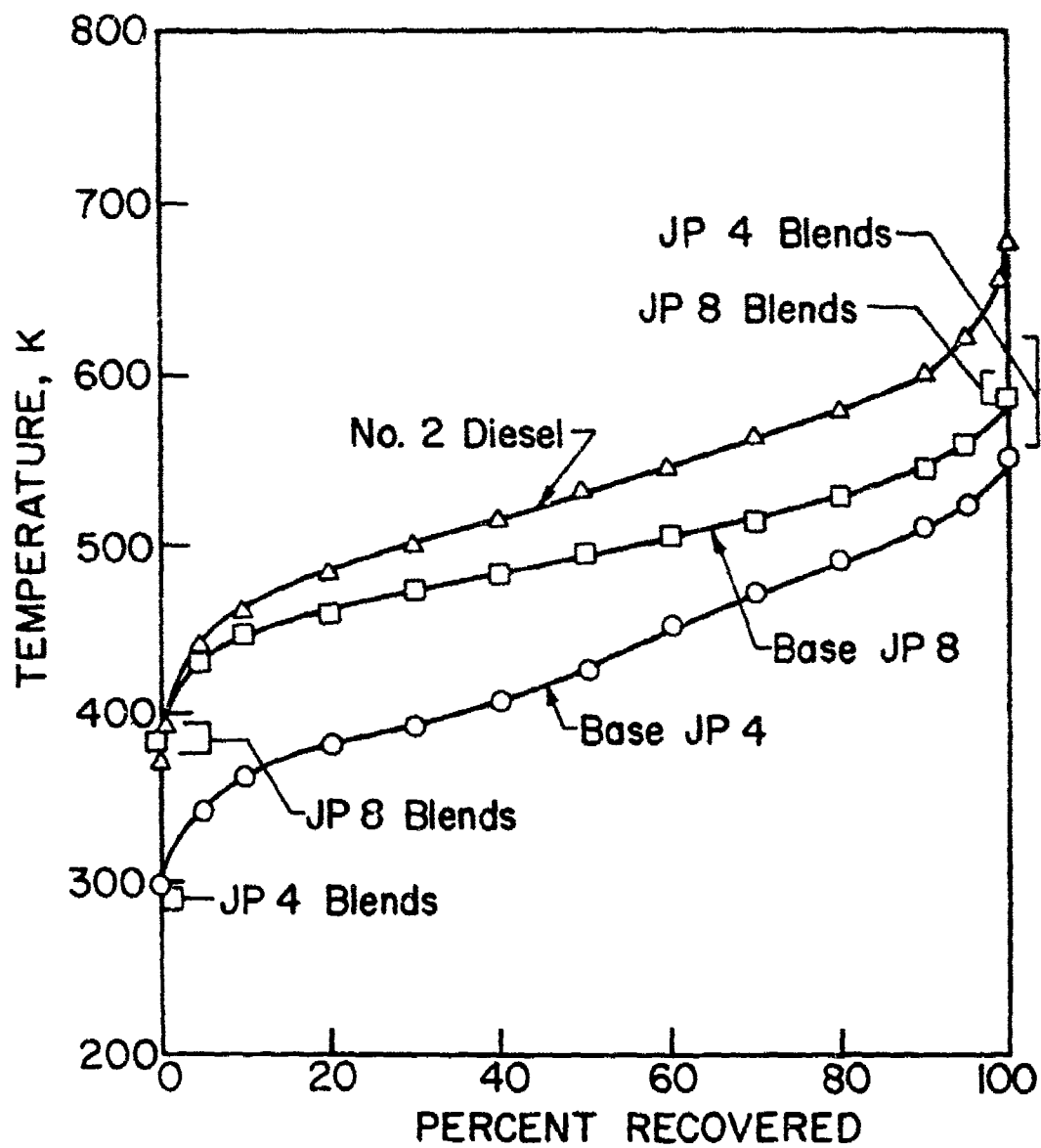


Figure 1. Distillation Characteristics of Test Fuels (Ref. 2).

### SECTION III

#### FUEL ATOMIZATION

The quality of the experimental data contained in references 1 to 6 is generally high. Although detailed information on the main liner dimensions and airflow distribution is somewhat sparse, it was usually possible to deduce these parameters to an acceptable level of accuracy. Only in one area, namely that of fuel atomization, did lack of accurate information prove a real impediment to the investigation. It is strongly advised that in future experimental studies on fuel effects every effort should be made to determine mean drop size and drop size distribution for all fuels over wide ranges of combustor operating conditions. Sufficient measurements should be undertaken to allow the spray characteristics at intermediate test conditions to be obtained by interpolation.

In the absence of actual measured values, the mean drop size (SMD) was calculated using one of the following two expressions:

For airblast atomizers [8]

$$\frac{SMD}{D_h} = \left[ 1 + \frac{\dot{m}_F}{\dot{m}_A} \right] \left[ 0.33 \left( \frac{\sigma_F}{\rho_A U_A^2 D_p} \right)^{0.6} \left( \frac{\rho_F}{\rho_A} \right)^{0.1} + 0.068 \left( \frac{u_F^2}{\rho_F \sigma_F D_p} \right)^{0.5} \right] \quad (1)$$

For pressure swirl atomizers [9]

$$SMD = 0.071 \sigma_F^{0.25} v_F^{0.25} \dot{m}_F^{0.25} \Delta P_F^{-0.5} \rho_g^{-0.25} \quad (2)$$

Equation (1) takes full account of variations in fuel properties ( $\sigma_F$ ,  $\rho_F$  and  $u_F$ ), air properties ( $\rho_A$  and  $U_A$ ) and atomizer geometry ( $D_p$  and  $D_h$ ). The values of the constants and exponents in this equation were established in a number of experimental studies that covered much wider ranges of fuel and air properties than are needed for the present investigation. Thus the main source of error in the use of Eq. (1) stems from uncertainties surrounding the values to be assigned to the atomizer dimensions. With Eq. (2) problems arise in the calculation of  $\rho_g$ , since the primary-zone temperature cannot be estimated accurately. Another potentially serious source of error that applies to both equations, is that all the experimental work involved in their formulation was carried out under cold, i.e. non-burning, and fairly quiescent conditions. Clearly drop sizes could be appreciably different in the true combustor environment due to the combined effects of high temperature, high turbulence, and strong airflow currents.

## SECTION IV

### ANALYSIS

The objective of the analysis was to develop appropriate relationships and correlations between combustion performance and the relevant fuel properties, combustor design features, and combustor operating conditions. The method followed was to study each aspect of combustion performance from as fundamental a viewpoint as possible, making full use of existing knowledge on the basic chemical and physical processes involved. Only under circumstances where strict adherence to this dictum would clearly yield an impractical solution was a less rigorous approach adopted.

It was found convenient to divide the analytical work into the following separate tasks:

1. Combustion efficiency
2. Lean blowout limits
3. Ignition performance
4. Liner wall temperature
5. Emissions: carbon monoxide, unburned hydrocarbons, oxides of nitrogen, and smoke
6. Pattern factor

As stated in the previous section, the paucity of available data on the fuel spray characteristics of the combustors described in references 1 to 6 proved to be a serious obstacle to the successful accomplishment of these tasks. This will become apparent in subsequent sections of the report, where it can be seen that the quality of the correlations achieved is distinctly higher for those aspects of performance where the dependence on mean drop size is either small or non-existent. For some performance

parameters, such as lean blowout and lean lightoff limits, it is possible to express the mean drop size for any given fuel in terms of its value relative to that obtained with JP4 for the same fuel nozzle at the same flow rate, so that any errors incurred through lack of detailed information on mean drop size are thereby greatly diminished. However, for certain other performance aspects, such as pattern factor and carbon monoxide emissions, it is important to know for each fuel at all the key operating conditions the absolute value of mean drop size in order to calculate the volume expended within the combustion zone in fuel evaporation. In the absence of accurate values of SMD and, bearing in mind that one of the recommendations for the second phase of this program is that measurements of SMD should be carried out on all the fuel nozzles of relevance to the investigation [see references 1 to 6], it was decided that for Task I the analysis of those performance aspects which demanded a precise knowledge of SMD would be confined to a relatively small number of combustors, just sufficient to demonstrate the validity of the analytical procedures employed. The combustors selected for more detailed study were the J79-17A, F101, TF41, and J79-17C. These combustors were chosen, partly because their atomization characteristics were fairly well known, but also because the relevant reports [references 1 to 4] were available at the outset of Task I. More detailed analysis of the TF39, J85, TF33 and F100 combustors will be performed as part of Task II of the WPAFB "Fuel Effects on Gas Turbine Performance" program, which also includes plans for acquiring a comprehensive body of drop size data for these combustors.

The analyses that were conducted to obtain correlations for combustion efficiency, lean blowout limits, lean lightup limits, liner wall temperature, pollutant emissions, and pattern factor, are described in the following sections.

## SECTION V

### COMBUSTION EFFICIENCY

The main factors affecting the level of combustion efficiency are evaporation rates, mixing rates, chemical reaction rates and the air loading on the combustor. Thus combustion efficiency may be expressed as [10]

$$\eta_c = (\text{air flow rate})^{-1} \left( \frac{1}{\text{evaporation rate}} + \frac{1}{\text{mixing rate}} + \frac{1}{\text{reaction rate}} \right)^{-1} \quad (3)$$

In practical combustion systems, the maximum rate of heat release at any given operating condition may be governed either by evaporation, mixing or chemical reaction, but rarely by all three at the same time. However, over the range of operating conditions where the combustion process is in transition from one regime to another, it is inevitable that two of the three key steps will participate in determining the overall combustion efficiency. Before exploring this situation, it is of interest to examine the separate effects on combustion efficiency of chemical reaction, mixing and evaporation.

#### 1. Reaction Rate-Controlled Systems

If evaporation and mixing rates are both infinitely fast, then Eq. (3) leads directly to the well-known  $\theta$  parameter

$$\eta_c = f(\theta)$$

or, 
$$\eta_{c_\theta} = f \left[ \frac{p_3^{1.75} A_L D_L^{0.75} \exp T_3/300}{\dot{m}_A} \right] \quad (4)$$

This equation is ideally suited, and has been widely used, in the correlation of experimental data on combustion efficiency obtained with well atomized, light distillate fuels, such as JP4 and Jet A.

As the length of the combustion zone is usually proportional to its diameter or height,  $H$ , the above equation may be expressed in terms of combustor volume,  $V_c$ , with little loss of accuracy, i.e.

$$\eta_{c_\theta} = f \left[ \frac{P_3^{1.75} V_c \exp (T_3/300)}{\dot{m}_A} \right] \quad (5)$$

## 2. Mixing Rate-Controlled Systems

If evaporation and chemical reaction rates are both infinitely fast, Eq. (3) becomes

$$\eta_c = f(\text{mixing rate/air flow rate})$$

Now the rate of mixing between a turbulent air jet and the surrounding gas is given by the product of the eddy diffusivity, the mixing area and the density gradient. If it is assumed that the eddy diffusivity is proportional to the product of a mixing length,  $\ell$ , and the turbulent velocity in the air jet, then

$$\text{mixing rate} \propto (\text{eddy diffusivity}) \times (\text{mixing area}) \times (\text{density gradient})$$

$$\text{mixing rate} \propto (\ell U_j) (\ell^2) (\rho/\ell)$$

$$\text{mixing rate} \propto \rho U_j \ell^2 \quad (6)$$

Substituting in Eq. (6) for

$$U_j \propto \left( \frac{\Delta P_L}{\rho} \right)^{0.5}$$

yields

$$\text{Mixing rate} \propto \frac{P_3 L^2}{T_3^{0.5}} \left( \frac{\Delta P_L}{P_3} \right)^{0.5} \quad (7)$$

Under conditions where mixing is limiting to performance, combustion efficiency will depend on the ratio of the mixing rate to the air flow rate. Thus, by assuming that turbulence scale is proportional to combustor size, Eq. (7) becomes

$$\eta_{cm} = f \left[ \frac{P_3 A_L}{\dot{m}_A T_3^{0.5}} \right] \left[ \frac{\Delta P_L}{P_3} \right]^{0.5} \quad (8)$$

### 3. Evaporation Rate-Controlled Systems

The third case to consider is when mixing and reaction rates are fast enough for fuel evaporation to be the rate-controlling step. Now, for a volume of air,  $V$ , containing fuel drops whose initial drop size is  $D_0$ , the average rate of fuel evaporation is given by [9]

$$\dot{m}_F = 8(\rho_g/\rho_F)(k/c_p)_g(V_c/D_0^2)q_c \ln(1+B)(1+0.22 \text{Re}_{D_0}^{0.5}) \quad (9)$$

It is assumed that as the fuel evaporates, it instantly mixes and burns with the surrounding air. Thus, combustion efficiency is obtained as the ratio of the mass of fuel evaporated within the combustion zone to the mass of fuel supplied, i.e.

$$\eta_{ce} = \frac{\dot{m}_F}{q_{ov} \dot{m}_A} \quad (10)$$

$$= \frac{\dot{m}_F}{f_c q_c \dot{m}_A} \quad (11)$$

where  $f_c$  is the fraction of the total air flow,  $\dot{m}_A$ , that participates in combustion.

Substitution of  $\dot{m}_F$  from Eq. (9) into Eq. (11) gives

$$\eta_{ce} = 8(\rho_g/\rho_F)(k/c_p)_g(V_c/f_c\dot{m}_A D_o^2) \ln(1+B)(1+0.22 Re_D^{0.5}) \quad (12)$$

By making the substitution

$$\lambda_{eff} = \frac{8(k/c_p)_g \ln(1+B)(1+0.22 Re_{D_o}^{0.5})}{\rho_F} \quad (13)$$

where  $\lambda_{eff}$  is an average or "effective" value of the evaporation constant during the drop lifetime [11], Eq. (12) becomes

$$\eta_{ce} = \lambda_{eff} \rho_g V_c \left[ f_c \dot{m}_A D_o^2 \right]^{-1} \quad (14)$$

Equations (12) and (14) relate combustion efficiency to combustor dimensions (via  $V_c$ ), combustor operating conditions (via  $k_g$ ,  $c_{p_g}$  and  $\rho_g$ ), fuel nozzle characteristics (via  $D_o$ ) and fuel type (via  $\rho_F$  and  $B$ , or  $\lambda_{eff}$ ).

Values of  $\lambda_{eff}$  are shown plotted in Figs. 2, 3 and 4. These figures contain plots of  $\lambda_{eff}$  versus  $T_{bn}$  at three levels of pressure, namely 100, 1000 and 2000 kPa, and three levels of ambient temperature, namely 500, 1200 and 2000K. For each value of temperature several lines are drawn to represent different values of  $UD_o$ , where  $U$  is the relative velocity between the fuel drop and the surrounding gas, and  $D_o$  is the initial drop diameter. The parameter  $T_{bn}$ , fuel boiling temperature (K) at normal atmosphere pressure, was chosen to represent the fuels' propensity for evaporation. It is recognized that no single chemical or physical property is completely satisfactory for this purpose. However, the average boiling

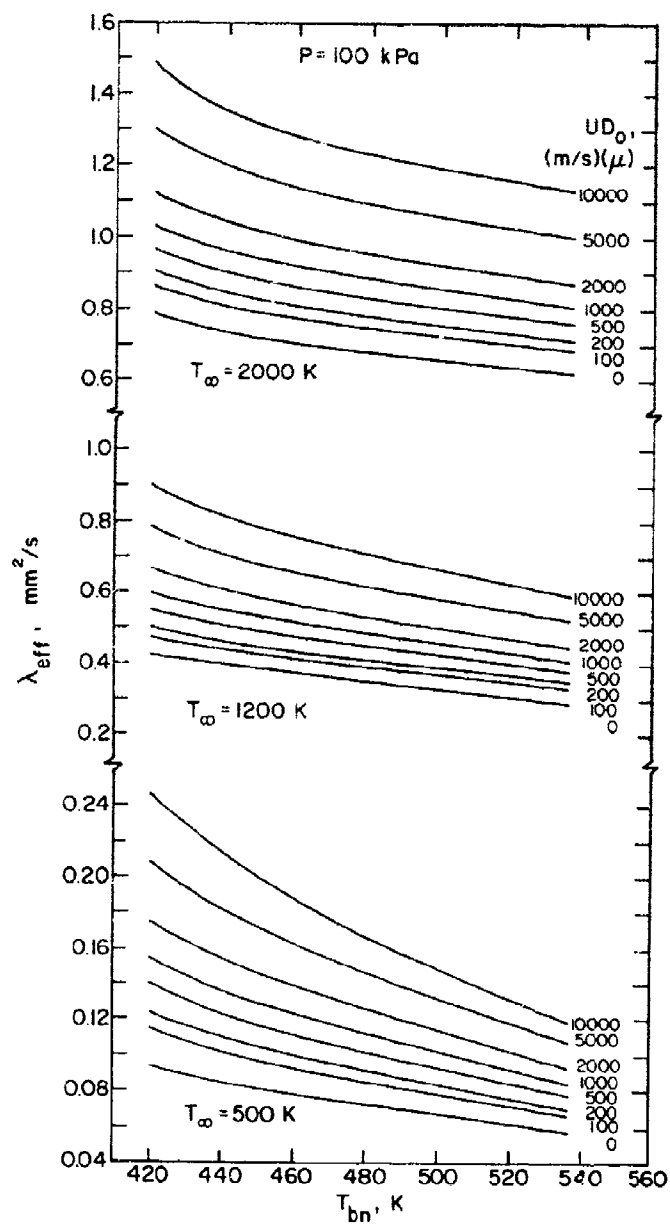


Figure 2. Variation of Effective Evaporation Constant with Normal Boiling Point at a Pressure of 100 kPa.

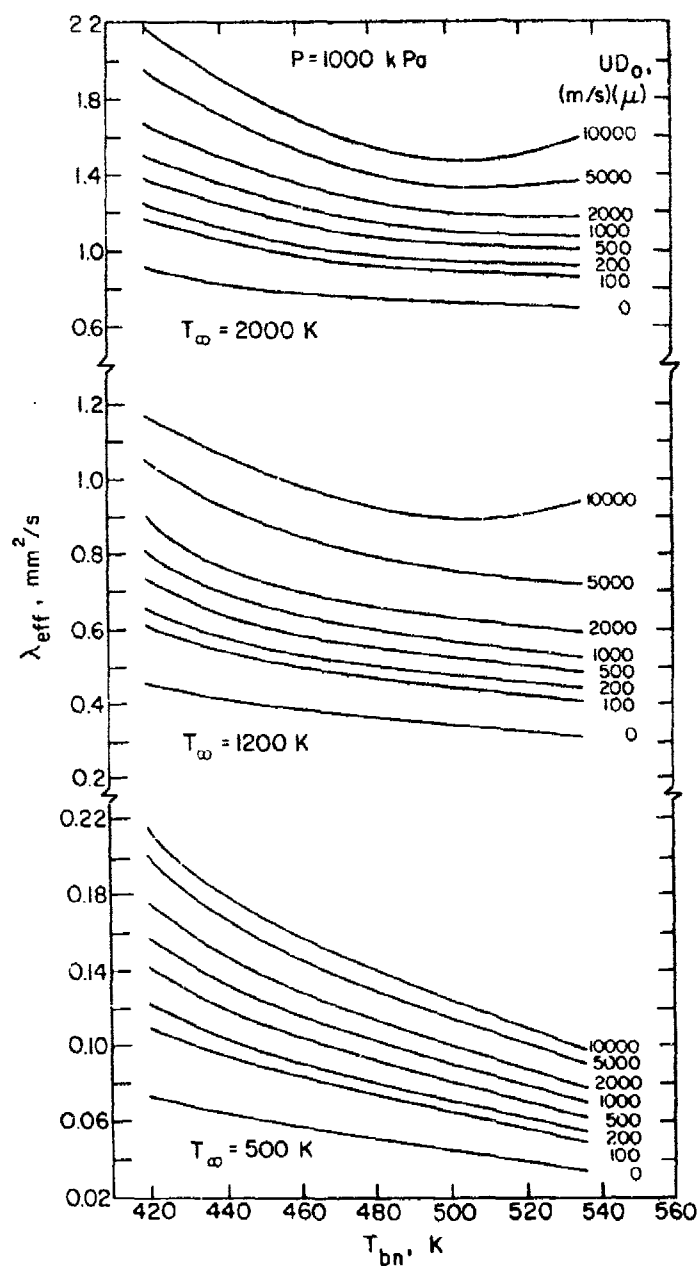


Figure 3. Variation of Effective Evaporation Constant with Normal Boiling Point at a Pressure of 1000 kPa.

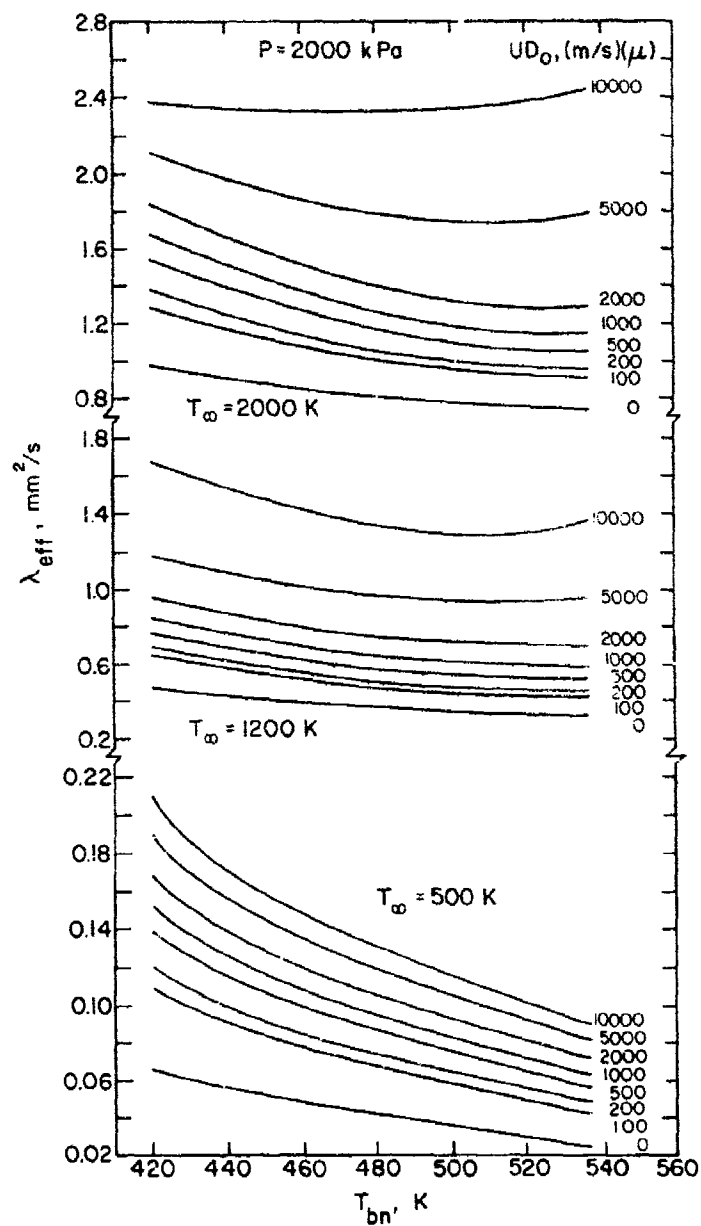


Figure 4. Variation of Effective Evaporation Constant with Normal Boiling Point at a Pressure of 2000 kPa.

point (50 percent recovered) has much to commend it, since it is directly related to fuel volatility and fuel vapor pressure. It also has the virtue of being easy to measure, and is usually quoted in fuel specifications.

From a practical standpoint the concept of  $\lambda_{eff}$  has considerable advantages since it takes into account the reduced rate of evaporation that occurs during the initial droplet heat-up period, as well as the enhancement of fuel evaporation rates due to the effects of forced convection. Thus plots of  $\lambda_{eff}$  of the type shown in Figs. 2 to 4 greatly simplify calculations on rates of spray evaporation and drop lifetimes.

For any given combustor the influence of fuel type on combustion efficiency can be examined by defining a dimensionless efficiency ratio which is the ratio of the combustion efficiency of any alternative fuel 'a' to that of the baseline fuel 'b', when burning at the same operating conditions. From Eq. (12) we have, for low  $Re_{D_0}$ ,

$$\frac{\eta_{c_a}}{\eta_{c_b}} = \frac{\rho_{F_b} D_b^2 \ln(1+B_a)}{\rho_{F_a} D_a^2 \ln(1+B_b)} \quad (15)$$

This equation may be used to predict the change in combustion efficiency due to a change in fuel type provided, of course, that fuel evaporation is known to be the rate-controlling step. If the level of combustion efficiency of interest is high, say > 90 percent, a more accurate prediction of combustion efficiency is obtained by rewriting Eq. (15) as

$$\frac{(1-\eta_{c_b})}{(1-\eta_{c_a})} = \frac{\rho_{F_b} D_b^2 \ln(1+B_a)}{\rho_{F_a} D_a^2 \ln(1+B_b)} \quad (16)$$

Although the derivation of Eq. (16) from Eq. (15) cannot be justified on mathematical grounds, the substitution of reciprocal inefficiency for efficiency has become accepted practice because it leads to a more accurate result in cases where combustion efficiencies are close to 100 percent.

For pressure-swirl atomizers the mean drop size depends on the surface tension and viscosity of the fuel. However, conventional fuels exhibit merely slight differences in surface tension values so that only the influence of viscosity on SMD need be considered. From Eq. (2) we have

$$SMD = \mu_F^{0.25} \quad (17)$$

Substitution of SMD from Eq. (17) into Eqs. (15) and (16) respectively gives

$$\frac{n_{c_a}}{n_{c_b}} = \frac{\rho_{F_b} \mu_{F_b}^{0.5} \ln(1+B_a)}{\rho_{F_a} \mu_{F_a}^{0.5} \ln(1+B_b)} \quad (18)$$

$$\text{and} \quad \frac{(1-n_{c_b})}{(1-n_{c_a})} = \frac{\rho_{F_b} \mu_{F_b}^{0.5} \ln(1+B_a)}{\rho_{F_a} \mu_{F_a}^{0.5} \ln(1+B_b)} \quad (19)$$

The practical utility of Eq. (19) for predicting the influence on combustion efficiency of a change in fuel type is demonstrated in Fig. 5, which contains experimental data obtained by Moses [12] on several fuels, using a T63 combustor. By designating Jet A as the baseline fuel, the combustion efficiencies of the other fuels are readily calculated from

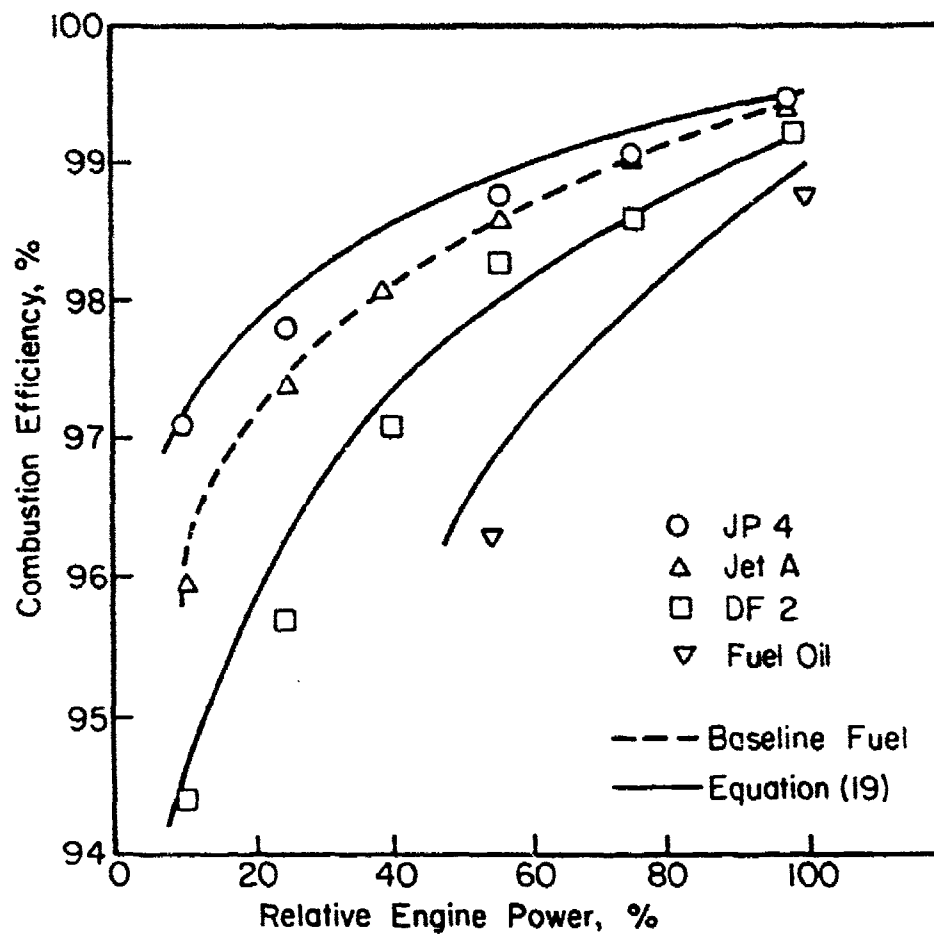


Figure 5. Illustration of Use of Eq. (19) to Predict the Combustion Efficiencies of Various Alternative Fuels from Data Obtained with Baseline Fuel. Experimental Data from Moses (Ref. 12).

Eq. (19) using values for  $B$ ,  $\rho_F$ , and  $\mu_F$  from Table 3. Owing to lack of detailed information on the fuel spray characteristics, the effect of any differences in mean drop size between the various fuels cannot be included. The results of the calculations are shown in Fig. 5. The dashed line drawn in this figure describes the combustion efficiency of the baseline fuel as determined experimentally. The full lines represent the predictions of Eq. (19) for the other fuels. The level of agreement between the predicted and measured values is clearly very satisfactory.

#### 4. General Case

For the general case in which evaporation, mixing and chemical reaction processes could all influence the total rate of combustion, either singly or in combination, an appropriate expression for combustion efficiency may be obtained by substituting Eqs. (5), (8) and (14) into Eq. (3) to obtain

$$\eta_c = \left[ \frac{P_3 V_c}{\dot{m}_A} \right] \left[ \frac{C_3^f D_o^2 T_g}{\lambda_{eff}} + \frac{C_4 L_c T_3^{0.5}}{(\Delta P_L / P_3)^{0.5}} + \frac{C_5}{P_3^{0.75} \exp(T_3/300)} \right]^{-1} \quad (20)$$

The constant  $C_3$  in the above equation is included in order to take into account possible effects of droplet interaction on the rate of fuel evaporation.  $C_4$  represents a turbulent diffusion coefficient, while  $C_5$  is the collision factor for the chemical reaction.

#### 5. Reaction Rate- and Evaporation Rate-Controlled Systems

In practice it is difficult to assess the importance of mixing rates to combustion efficiency. This is due partly to lack of accurate information on the liner pressure drop parameter,  $\Delta P_L / P_3$ , but mainly to the fact that

TABLE 3. Fuel Properties used to Construct Fig. 5

Fuel	Density kg/m <sup>3</sup>	Mass-transfer number $B_{st}$	Viscosity kg/ms
Gasoline (JP 4)	692	6.10	0.00070
Kerosine (Jet A)	775	3.75	0.00129
Diesel oil (DF 2)	850	2.80	0.0020
Light fuel oil	875	2.50	0.0037

mixing rates tend to be limiting only at conditions where the level of combustion efficiency is close to 100 percent, so that deficiencies in performance due to mixing are difficult to discern. For these reasons it is often preferable to express combustion efficiency as the product of the  $\theta$  efficiency,  $\eta_{c_\theta}$ , and the evaporation efficiency,  $\eta_{c_e}$ , i.e.

$$\eta_c = \eta_{c_\theta} \times \eta_{c_e} \quad (21)$$

The second term on the right hand side of Eq. (21) i.e.,  $\eta_{c_e}$  from Eq. (14), represents the fraction of the fuel that is vaporized within the combustion zone. For  $\eta_{c_e} \geq 1$ ,  $\eta_c = \eta_{c_\theta}$ , and Eq. (21) reverts to the

$\theta$  parameter which denotes the fraction of fuel vapor that is converted into combustion products by chemical reaction.

From analysis of the available experimental data on combustion efficiency the following expressions for  $\eta_{c\theta}$  and  $\eta_{ce}$  were derived.

$$\eta_{c\theta} = 1 - \exp \left[ \frac{-0.022 P_3^{1.3} V_c \exp (T_c/400)}{f_c \dot{m}_A} \right] \quad (22)$$

$$\text{and } \eta_{ce} = 1 - \exp \left[ \frac{-36 \times 10^6 P_3 V_c \lambda_{eff}}{T_c D_o^2 f_c \dot{m}_A} \right] \quad (23)$$

It should be noted in Eq. (22) that the pressure dependence is reduced from 1.75 to 1.3. This is because the exponent of 1.75 was determined from tests conducted in the pressure range from 40 to 200 kPa. In the present study the data on combustion efficiency were obtained at higher pressure levels, where the intervention of mixing rates tends to lower the pressure exponent, in this case to a value of 1.3. Another noteworthy point is that temperature dependence is now expressed in terms of  $T_c$  rather than  $T_3$ . Either may be used (with suitable adjustment to the constant) but  $T_c$  was found to give the best correlation.  $T_c$  is the adiabatic flame temperature in the primary zone, assuming complete combustion of the fuel. It is calculated from the expression

$$T_c = T_3 + \Delta T_c$$

where  $\Delta T_c$  is obtained from standard temperature rise charts for the fuel in question, using appropriate values of  $P_3$ ,  $T_3$  and  $q_c (=q_{ov}/f_c)$ .

Values of mean drop size,  $D_0$  may be calculated from Eq. (1) or Eq. (2) using the information on fuel nozzle characteristics supplied in references 1 to 6. The very satisfactory correlation of combustion efficiency data provided by Eq. (21) is demonstrated in Figs. 6 to 13. These figures include all the relevant data on combustion efficiency contained in references 1 to 6. However, it should be noted that for some combustors the measurements of combustion efficiency did not include all fuels. Moreover, where both predicted and measured values of combustion lie close to 100 percent, the results obtained for all fuels are virtually the same and are indicated on the graphs by a single point.

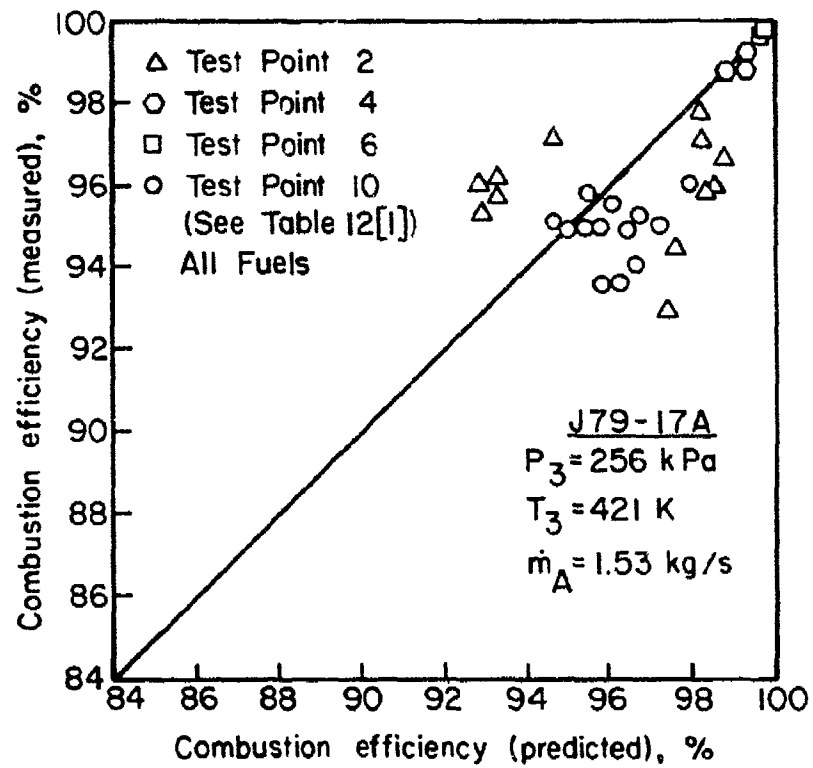


Figure 6. Comparison of Measured and Predicted Values of Combustion Efficiency for J79-17A Combustor.

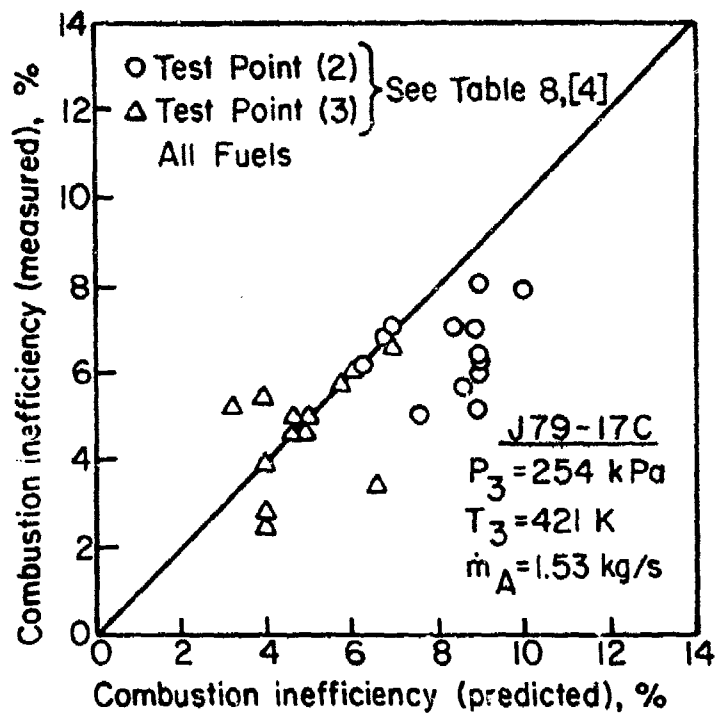


Figure 7. Comparison of Measured and Predicted Values of Combustion Efficiency for J79-17C Combustor.

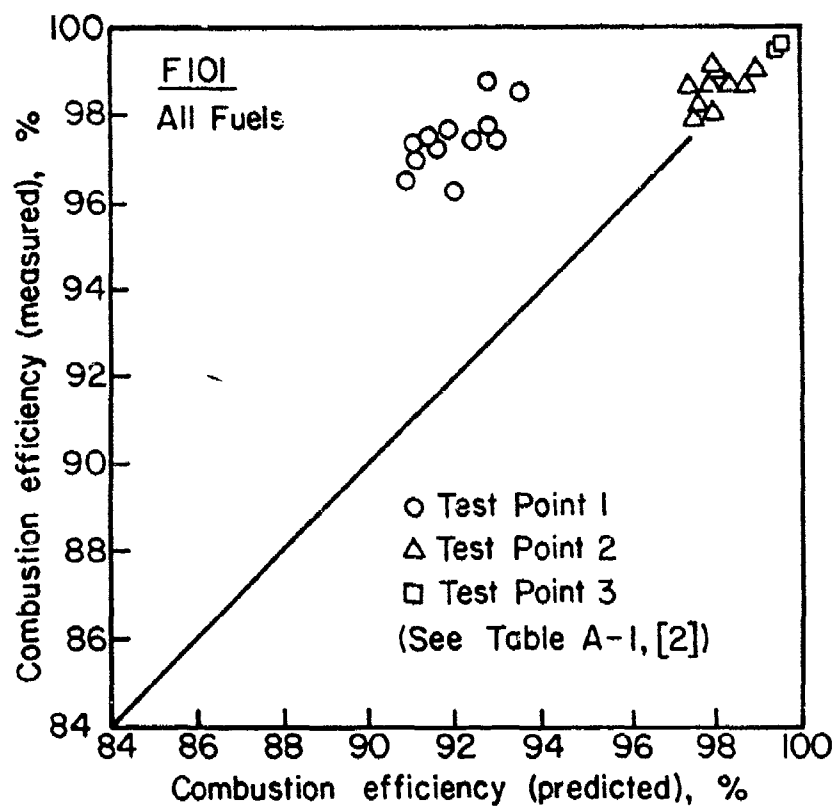


Figure 8. Comparison of Measured and Predicted Values of Combustion Efficiency for F101 Combustor.

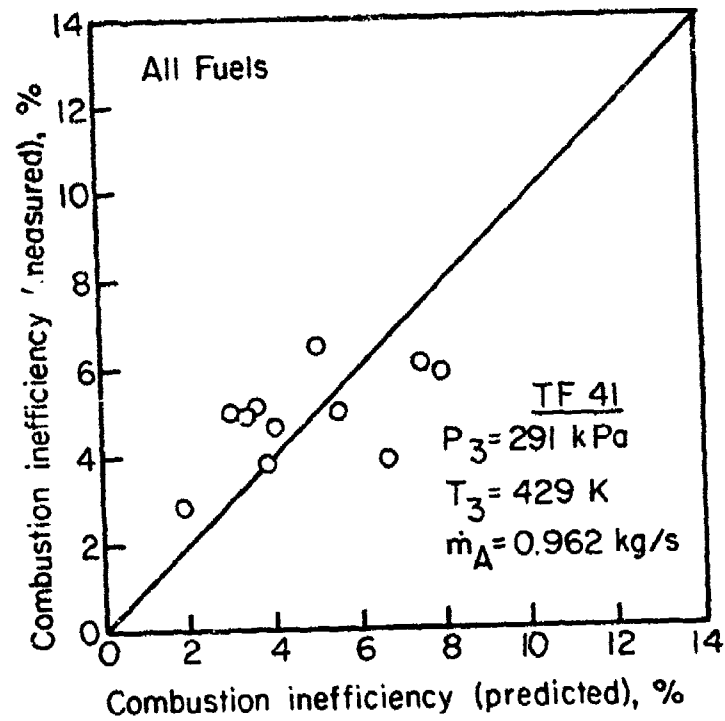


Figure 9. Comparison of Measured and Predicted Values of Combustion Efficiency for TF 41 Combustor.

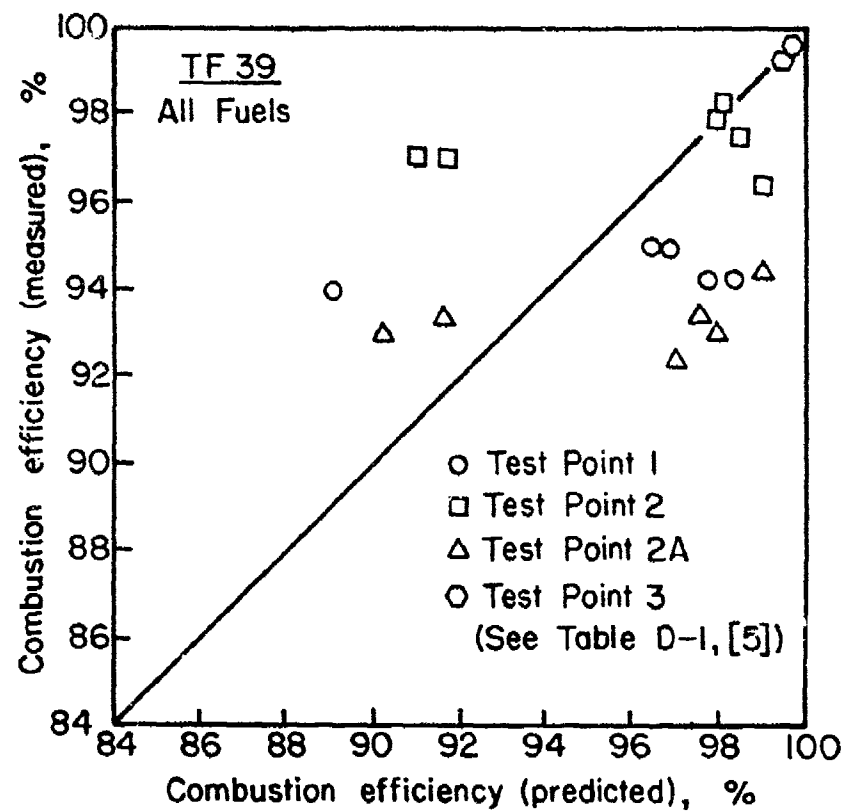


Figure 10. Comparison of Measured and Predicted Values of Combustion Efficiency for TF39 Combustor.

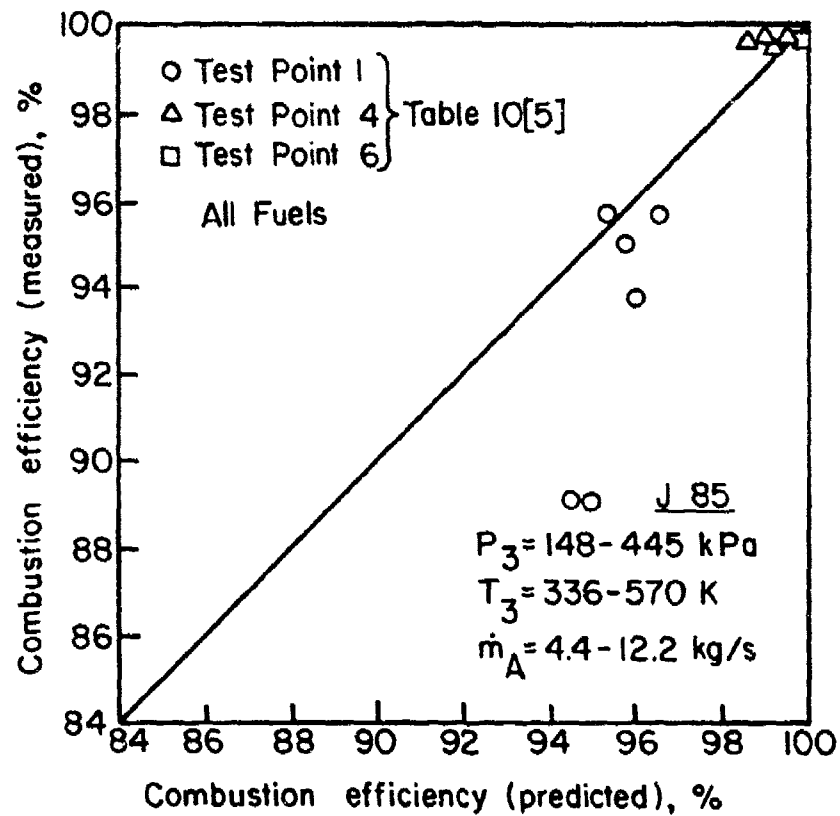


Figure 11. Comparison of Measured and Predicted Values of Combustion Efficiency for J85 Combustor.

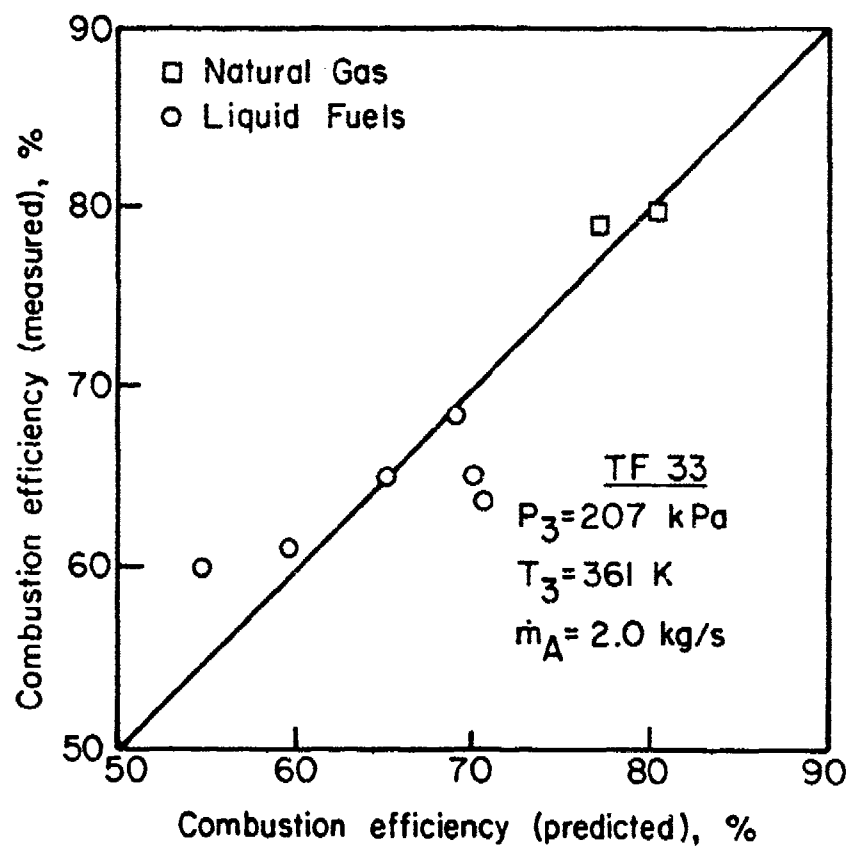


Figure 12. Comparison of Measured and Predicted Values of Combustion Efficiency for TF 33 Combustor.

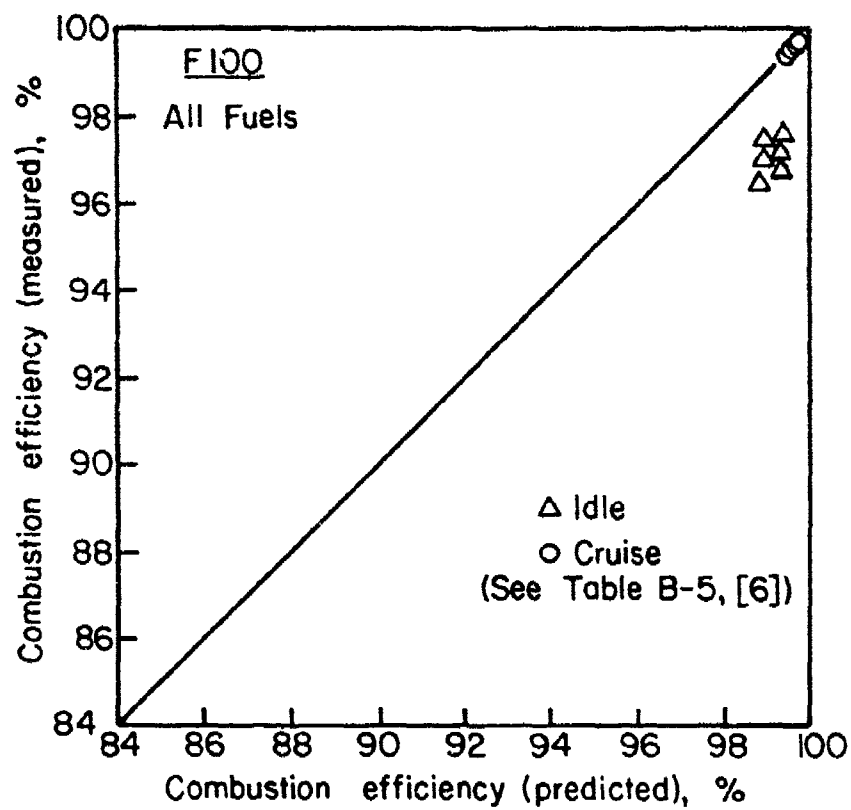


Figure 13. Comparison of Measured and Predicted Values of Combustion Efficiency for F100 Combustor.

## SECTION VI

### LEAN BLOWOUT

Until the early 1970's the problem of lean blowout was always regarded as relatively minor. To a large extent this was due to the almost universal use of pressure-swirl spray atomizers of the duplex or dual-orifice type. The poor mixing characteristics of these pressure-swirl atomizers create many performance problems, not the least being a high rate of soot formation in the primary zone. However, this same poor mixing of fuel and primary air has the useful advantage of allowing combustion to occur, albeit with low combustion efficiency, at mixture strengths well below the normal weak extinction limit. In fact, lean blowout limits in excess of 1000 AFR, based on overall combustor values of air and fuel flow rates, used to be quite commonplace. In recent years the continuing trend toward improved fuel-air mixing prior to combustion (for example, airblast atomizers and prechambers) in order to reduce the generation of pollutant emissions, especially  $\text{NO}_x$  and smoke, has led to a narrowing of stability limits and to increasing concern over the attainment of satisfactory lean blowout performance.

For homogeneous fuel-air mixtures flame blowout occurs when the rate of heat liberation in the primary zone becomes insufficient to heat the incoming fresh mixture up to the required reaction temperature. With heterogeneous mixtures, however, an additional factor is the time required for fuel evaporation. For fuel sprays of low volatility and large mean drop size this time is relatively long and is often the main factor limiting the overall rate of heat release. In the analysis of lean blowout limits it is convenient to consider homogeneous mixtures first and then to examine

how the results obtained should be modified to take account of fuel evaporation.

For homogeneous mixtures it has been shown that the lean blowout fuel/air ratio depends on the inlet air velocity, pressure, and temperature, and on the size of the combustion zone [13]. The relationship is of the form

$$q_{LBO} \propto \left[ \frac{\dot{m}_A}{V P_3^n \exp(T_3/b)} \right]^x \quad (24)$$

This equation was used by Ballal and Lefebvre [13] to correlate measured values of weak extinction equivalence ratio for propane-air flames stabilized on bluff-body flameholders, using experimental data to determine optimum values of  $n$ ,  $b$  and  $x$ .

Equation (24) may also be used to predict the lean blowout limits of combustion chambers supplied with heterogeneous fuel-air mixtures, provided that the rate of fuel evaporation is sufficiently high to ensure that all the fuel is fully vaporized within the primary combustion zone. If the fuel does not fully vaporize, then clearly the "effective" fuel/air ratio will be lower than the nominal value. However, if the fraction of fuel that is vaporized is known, or can be calculated, it can then be combined with Eq. (24) to yield the fuel/air ratio at lean blowout, i.e.,

$$q_{LBO(\text{heterogeneous})} = q_{LBO(\text{homogeneous})} \times f_f^{-1} \quad (25)$$

where  $f_f$  is the fraction of fuel that is vaporized within the primary combustion zone.

From analysis of the factors governing the rate of evaporation of a fuel spray, it was found [14] that

$$f_f = 8 (\rho_g/\rho_F) (k/c_p)_g \ln(1+B) (V_{pz}/\dot{m}_{pz} D_o^2) (1 + 0.22 Re_{D_o}^{0.5}) \quad (26)$$

$$\text{or, substituting for } \lambda_{eff} = \frac{8 (k/c_p)_g \ln(1+B) (1 + 0.22 Re_{D_o}^{0.5})}{\rho_F} \quad (27)$$

$$\begin{aligned} f_f &= \frac{8 \rho_g V_{pz} \lambda_{eff}}{\dot{m}_{pz} D_o^2} \\ &= \frac{8 \rho_g V_{pz} \lambda_{eff}}{f_{pz} \dot{m}_A D_o^2} \end{aligned} \quad (28)$$

It should be noted that Eqs. (26) and (28) allow  $f_f$  to exceed unity. When this occurs it simply means that the time required for fuel evaporation is less than the time available, so that the fuel is fully vaporized within the recirculation zone. In these circumstances  $f_f$  should be assigned a value of 1.0, so that

$$q_{LBO(\text{heterogeneous})} = q_{LBO(\text{homogeneous})} \quad (29)$$

Substitution of  $q_{LBO(\text{hom})}$  from Eq. (24) and  $f_f$  from Eq. (28) into Eq. (25) gives

$$q_{LBO} \propto \frac{f_{pz} \dot{m}_A (1+x) D_o^2}{V_{pz}^{(1+x)} P_3^{(1+nx)} \exp(xT_3/b) \lambda_{eff}} \quad (30)$$

An additional term to be incorporated into Eq. (30) is the heating value of the fuel. This stems from the assumption that for any given

operating condition the lean blowout temperature is the same for all hydrocarbon fuel-air mixtures. This means that fuels with a high gravimetric heat content should be capable of burning down to weaker mixture strengths than fuels having a lower heat content. With this modification Eq. (30) becomes

$$q_{LBO} \propto \left[ \frac{f_{pz}}{V_{pz}^{(1+x)}} \right] \left[ \frac{\dot{m}_A^{(1+x)}}{P_3^{(1+nx)} \exp(x T_3/b)} \right] \left[ \frac{D_o^2}{\lambda_{eff} LCV} \right] \quad (31)$$

The first term on the right-hand side of the above expression is a function of combustor design. The second term represents the combustor operating conditions. The third term embodies the relevant fuel-dependent properties.

Unfortunately the available experimental data do not allow the values of  $n$  and  $x$  to be determined with any degree of accuracy. This is due mainly to the fact that for any given engine the air mass flow rate is always roughly proportional to air pressure which makes it very difficult to isolate their separate effects on  $q_{LBO}$ . All that can reasonably be deduced from Eq. (31) is that the exponents of  $\dot{m}_A$  and  $V_{pz}$  should be the same and that the pressure exponent should be somewhat higher by an amount depending on the effective reaction order. Analysis of the experimental data on  $q_{LBO}$  suggests, in fact, that the pressure exponent is about 30 percent larger than that of the air mass flow rate. Also, the temperature dependence corresponds to the relationship

$$q_{LBO} \propto \exp(-(T_3/300))$$

Thus the simplest form in which Eq. (31) can be expressed that is consistent with the experimental data is

$$q_{LBO} = \left( \frac{A'' f_{pz}}{V_{pz}} \right) \left( \frac{\dot{m}_A}{P_3^{1.3} \exp(T_3/300)} \right) \left( \frac{D_o^2}{\lambda_{eff} LCV} \right) \quad (32)$$

where  $A''$  is a constant whose value depends on the geometry and mixing characteristics of the combustion zone and must be arrived at experimentally. Having determined the value of  $A''$  at any convenient test condition, Eq. (32) may then be used to predict the lean blowout fuel/air ratio at any other operating condition.

One problem with Eq. (32) is that of assigning appropriate values of  $V_{pz}$  to all the combustors under consideration. Although values of  $f_{pz}$ , the fraction of the total combustor airflow entering the primary zone, were either quoted directly in references 1 to 6, or could easily be estimated, only in one or two cases could the corresponding primary-zone volume be assessed to the desired level of accuracy. To surmount this problem it was decided to substitute the predilution volume,  $V_c$ , into Eq. (32), instead of  $V_{pz}$ . This could be justified on the grounds that more accurate values of  $V_c$  were available and, in fact, had already been used in Section V for the correlation of combustion efficiency data. Moreover, as the ratio of primary-zone volume to pre-dilution volume tends to be fairly constant for most conventional combustion chambers, using  $V_c$  instead of  $V_{pz}$  has the virtue of consistency without undue sacrifice in accuracy.

A more serious drawback to Eq. (32) is that its solution demands an accurate knowledge of mean drop size over the entire range of operating conditions. As no measurements of drop size were taken for this investigation,

nor can they be estimated with sufficient accuracy, this obstacle would appear to rule out the application of this equation to the present task. However, since the main objective is to study fuel effects, the problem can be circumvented by rewriting Eq. (32) in a different form, such that the fuel-dependent properties are expressed relative to those of the baseline fuel, JP4. With these modifications Eq. (32) becomes

$$q_{LBO} = \frac{A' f_{pz} \dot{m}_A}{V_c P_3^{1.3} \exp(T_3/300)} \times \frac{D_r^2}{\lambda_r LCV_r} \times \left( \frac{D \text{ at } T_F}{D \text{ at } 277.5 \text{ K}} \right)^2 \quad (33)$$

where  $D_r$  = mean drop size relative to that for JP4  
 $LCV_r$  = lower calorific value relative to that for JP4  
 $\lambda_r$  = effective evaporation constant relative to that for JP4  
 at  $T_{pz}$  and  $P_3$

The term  $(D \text{ at } T_F)^2 / (D \text{ at } 277.5)^2$  is introduced to take into account the variation in drop size arising from a change in fuel temperature from the initial baseline value, which is normally taken as 277.5K.

The correlations of lean blowout limits provided by Eq. (33), using appropriate values of  $A'$ , are illustrated in Figs. 14 to 24. The close agreement exhibited between the predicted and the measured values of lean blowout fuel/air ratio is clearly very satisfactory. However, because the measured values of  $q_{LBO}$  for the F101 seemed much too high, only the correlation obtained with one fuel is shown in Fig. 18 to demonstrate the ability of Eq. (33) to predict the effect of changes in  $T_3$  and  $T_F$  on the lean blowout limits of this combustor. Also, it should be noted that a few test points for the F100 are omitted from Fig. 24. These points were considered spurious since the measured values of  $q_{LBO}$  were lower than the

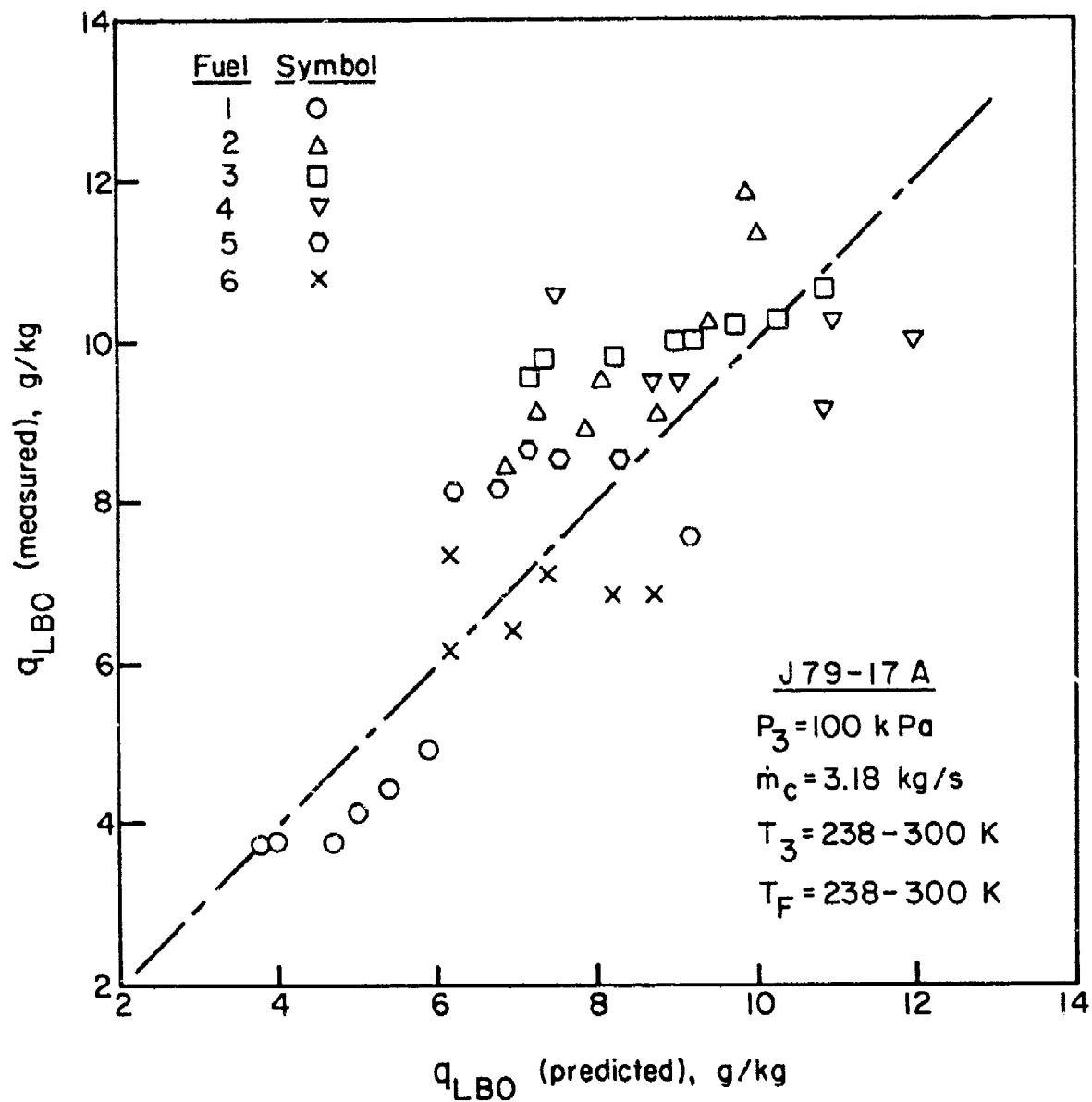


Figure 14. Comparison of Measured and Predicted Values of  $q_{LBO}$  for J79-17A Combustor. (Fuels 1 to 6).

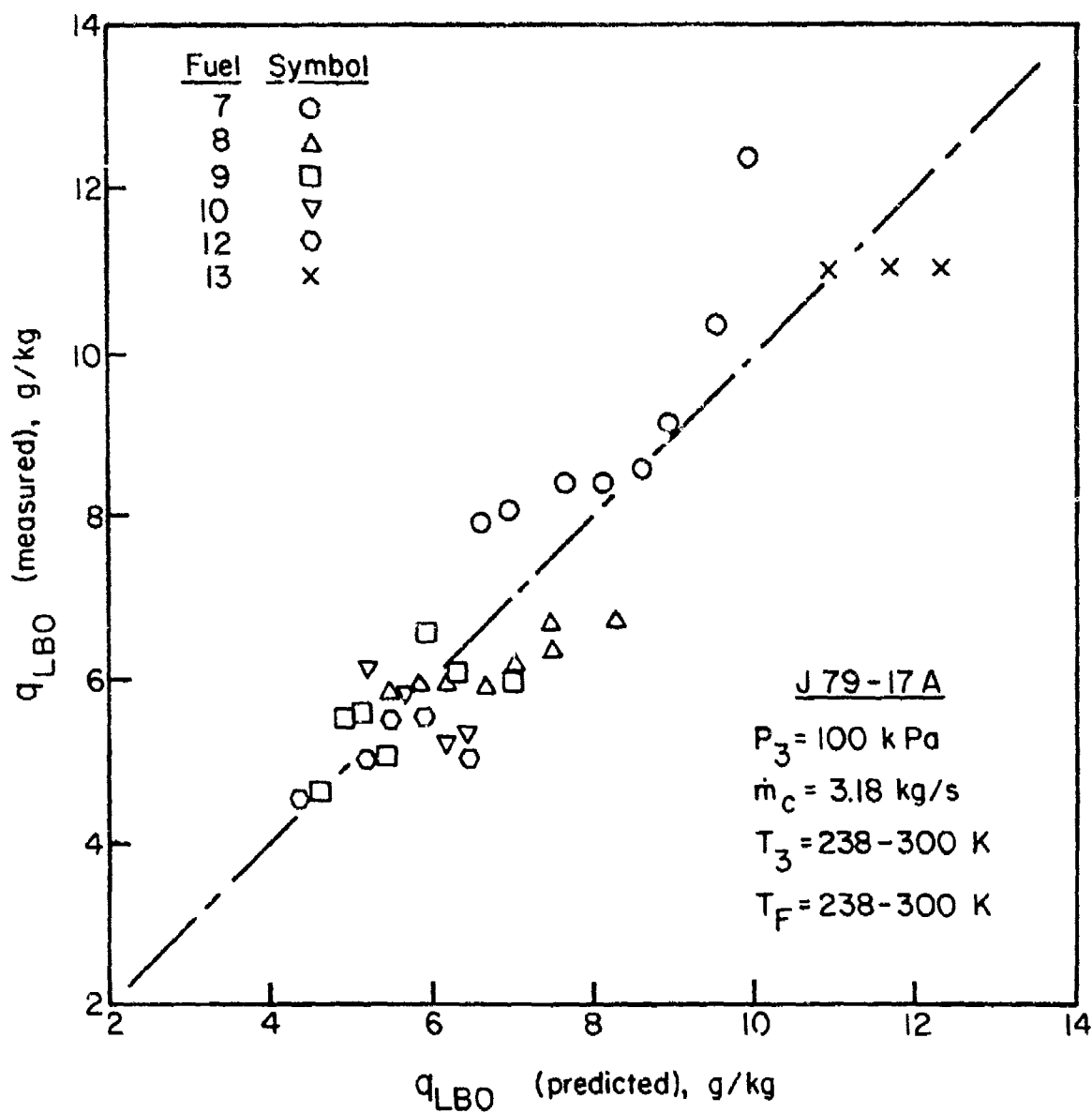


Figure 15. Comparison of Measured and Predicted Values of  $q_{LBO}$  for J79-17A Combustor. (Fuels 7 to 13).

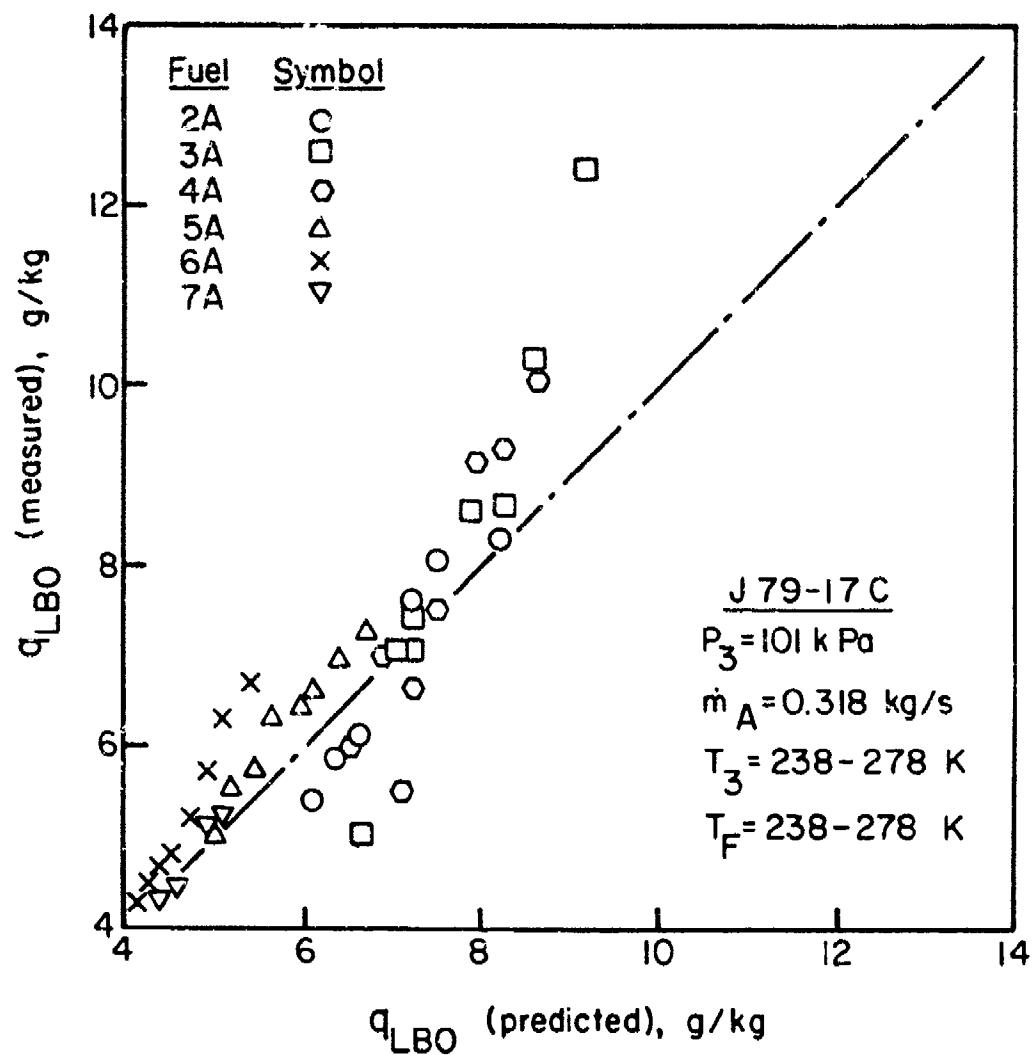


Figure 16. Comparison of Measured and Predicted Values of  $q_{LBO}$  for J79-17C Combustor. (Fuels 2A to 7A).

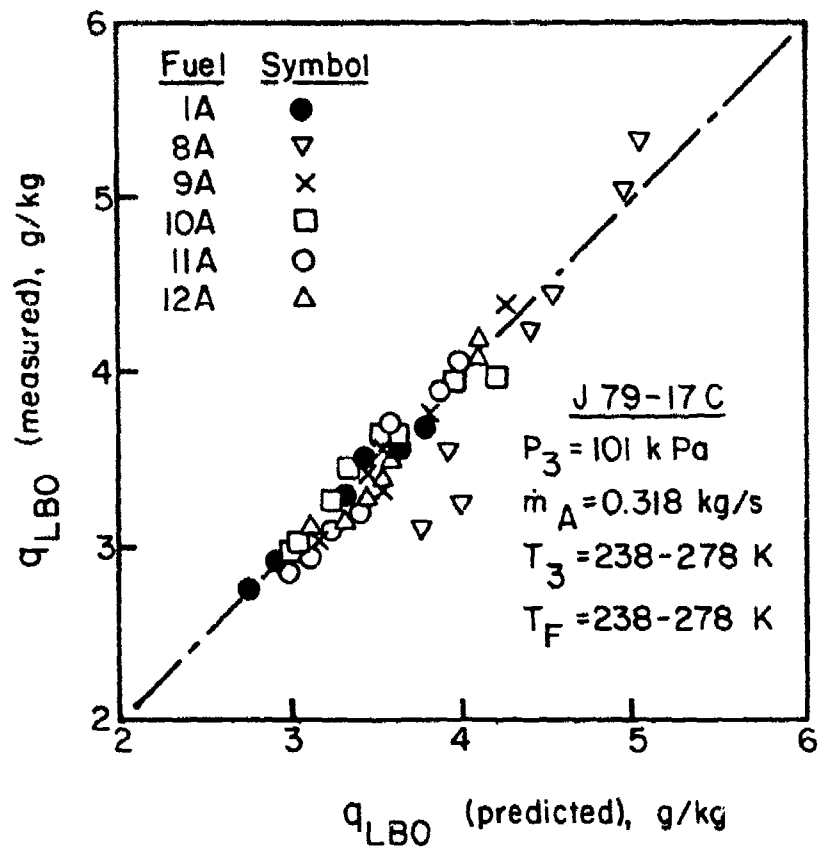


Figure 17. Comparison of Measured and Predicted Values of  $q_{LBO}$  for J79-17C Combustor. (Fuels 1A, 8A to 12A).

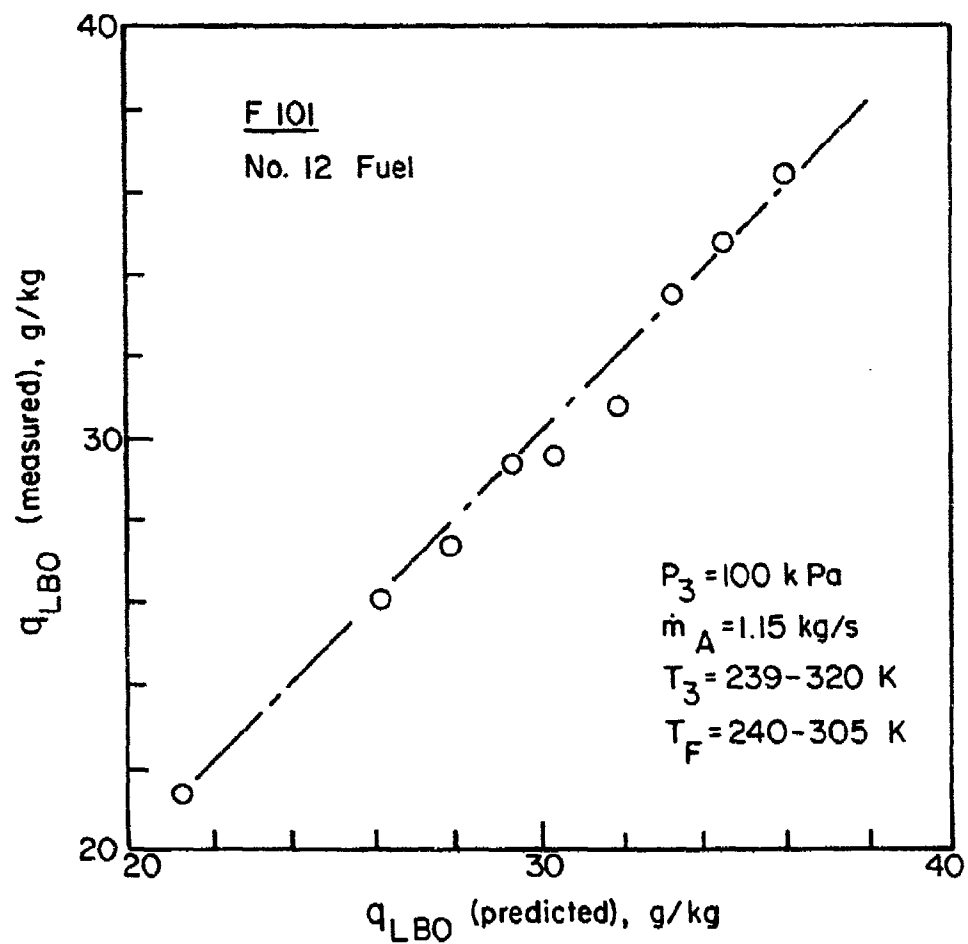


Figure 18. Comparison of Measured and Predicted Values of  $q_{LBO}$  for F101 Combustor.

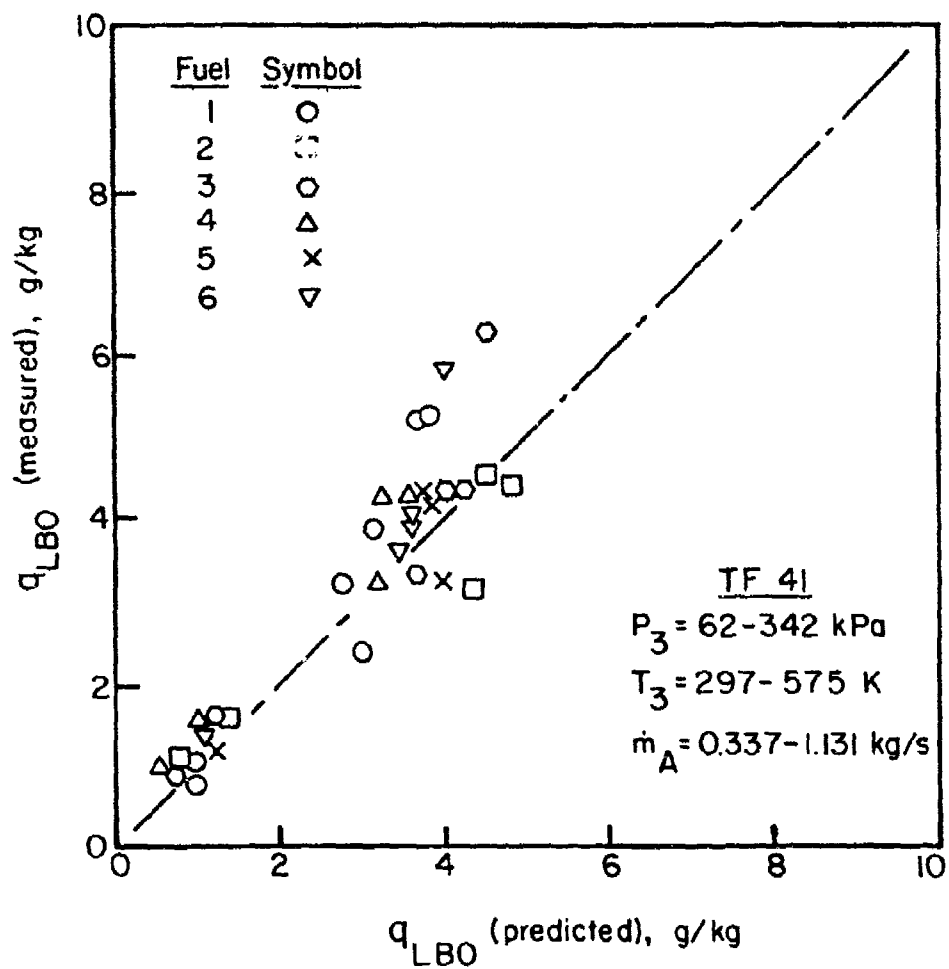


Figure 19. Comparison of Measured and Predicted Values of  $q_{LBO}$  for TF 41 Combustor. (Fuels 1 to 6).

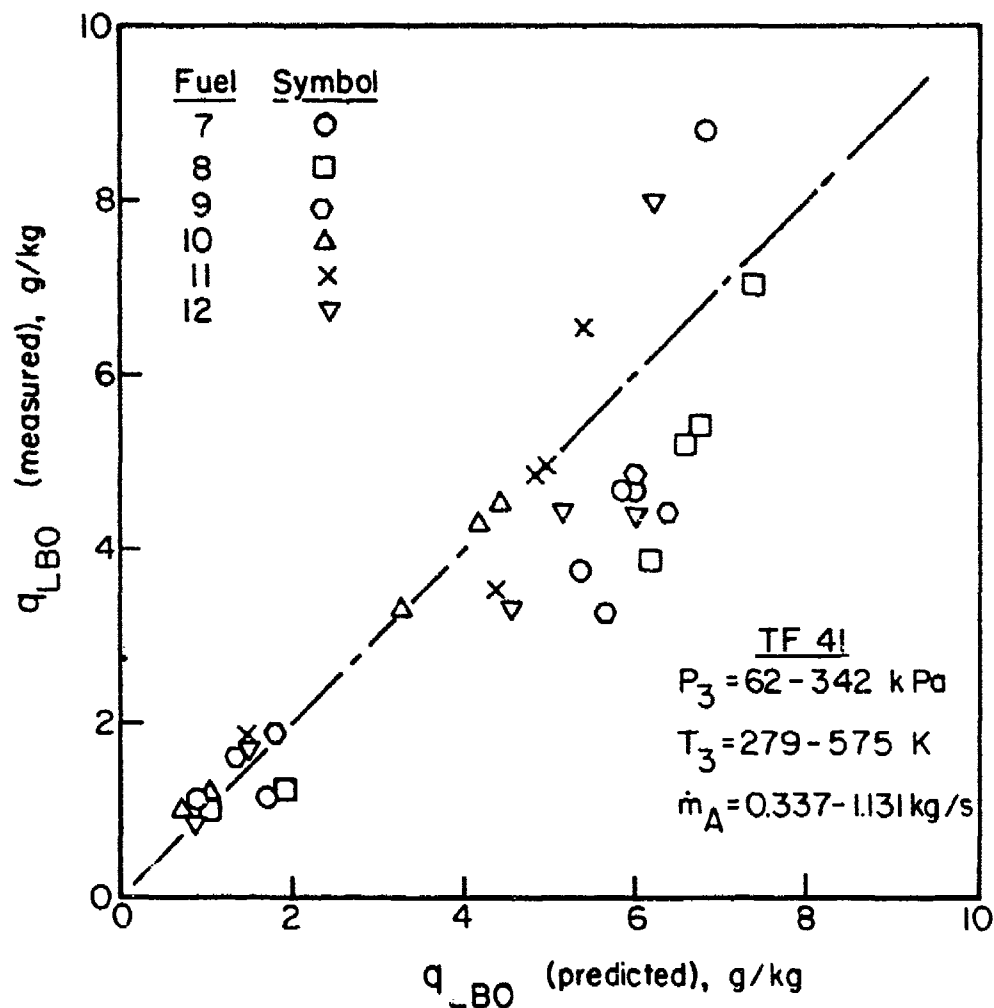


Figure 20. Comparison of Measured and Predicted Values of  $q_{LBO}$  for TF 41 Combustor. (Fuels 7 to 12).

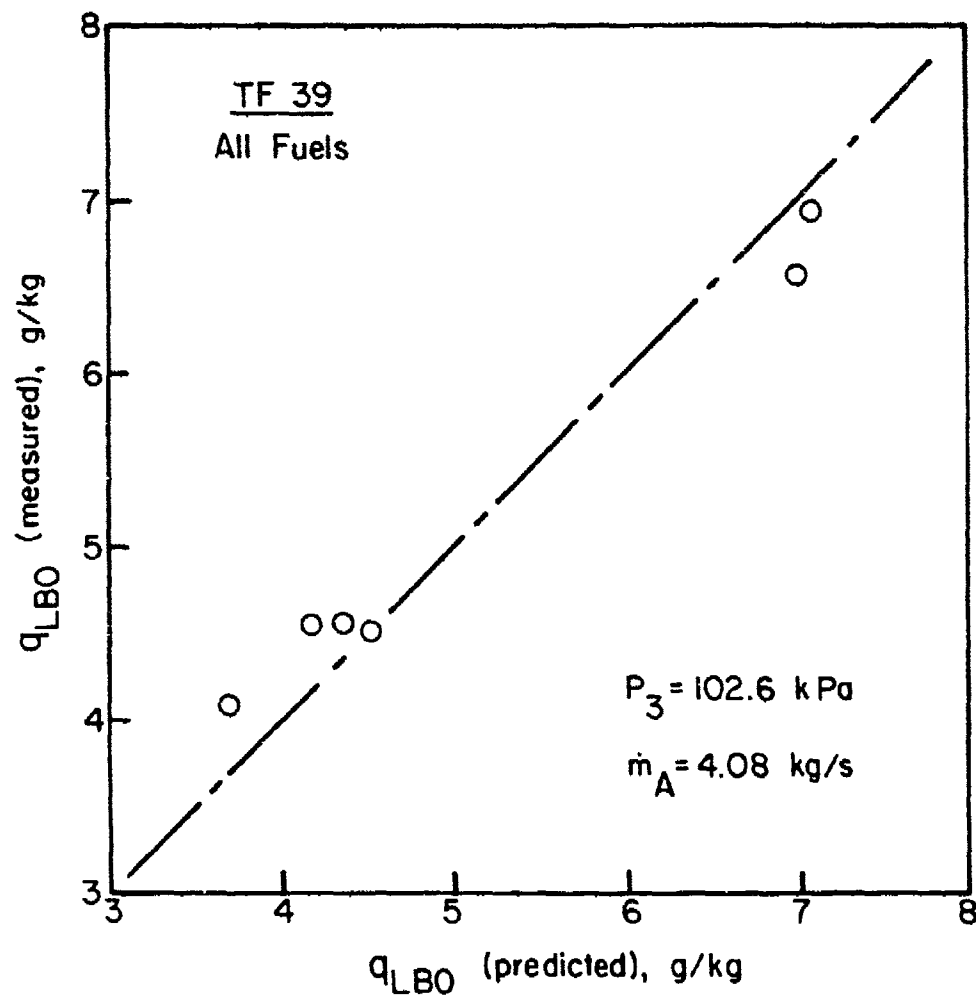


Figure 21. Comparison of Measured and Predicted Values of  $q_{LBO}$  for TF 39 Combustor. Plotted Points Represent Average of Five Values for Fuel and Air Temperatures between 255 and 277K.

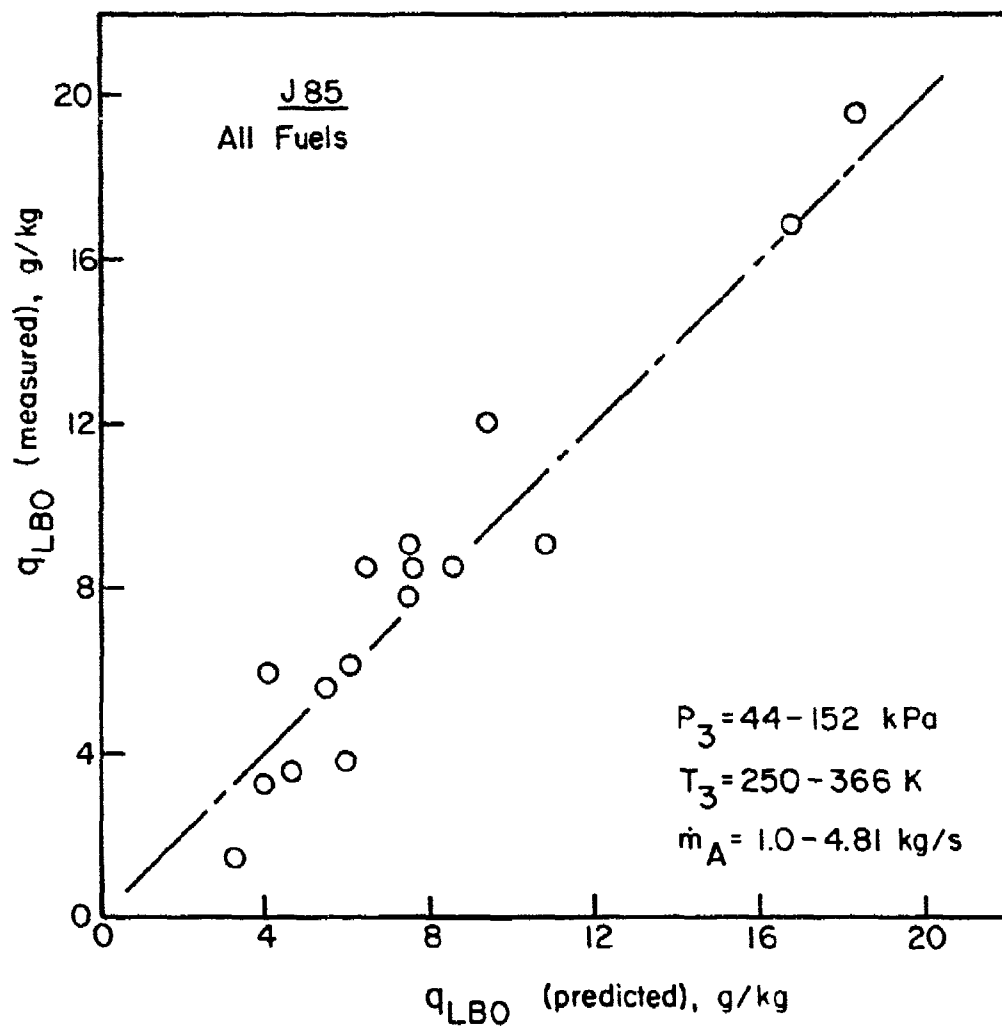


Figure 22. Comparison of Measured and Predicted Values of  $q_{LBO}$  for J85 Combustor.

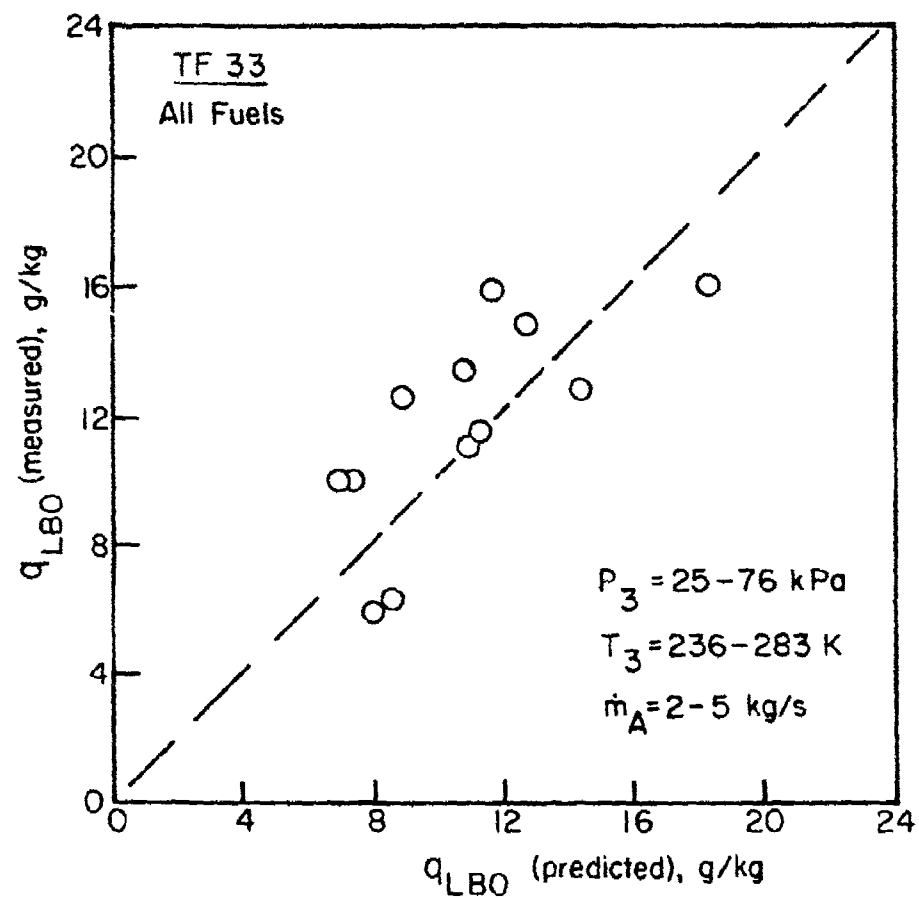


Figure 23. Comparison of Measured and Predicted Values of  $q_{LBO}$  for TF 33 Combustor.

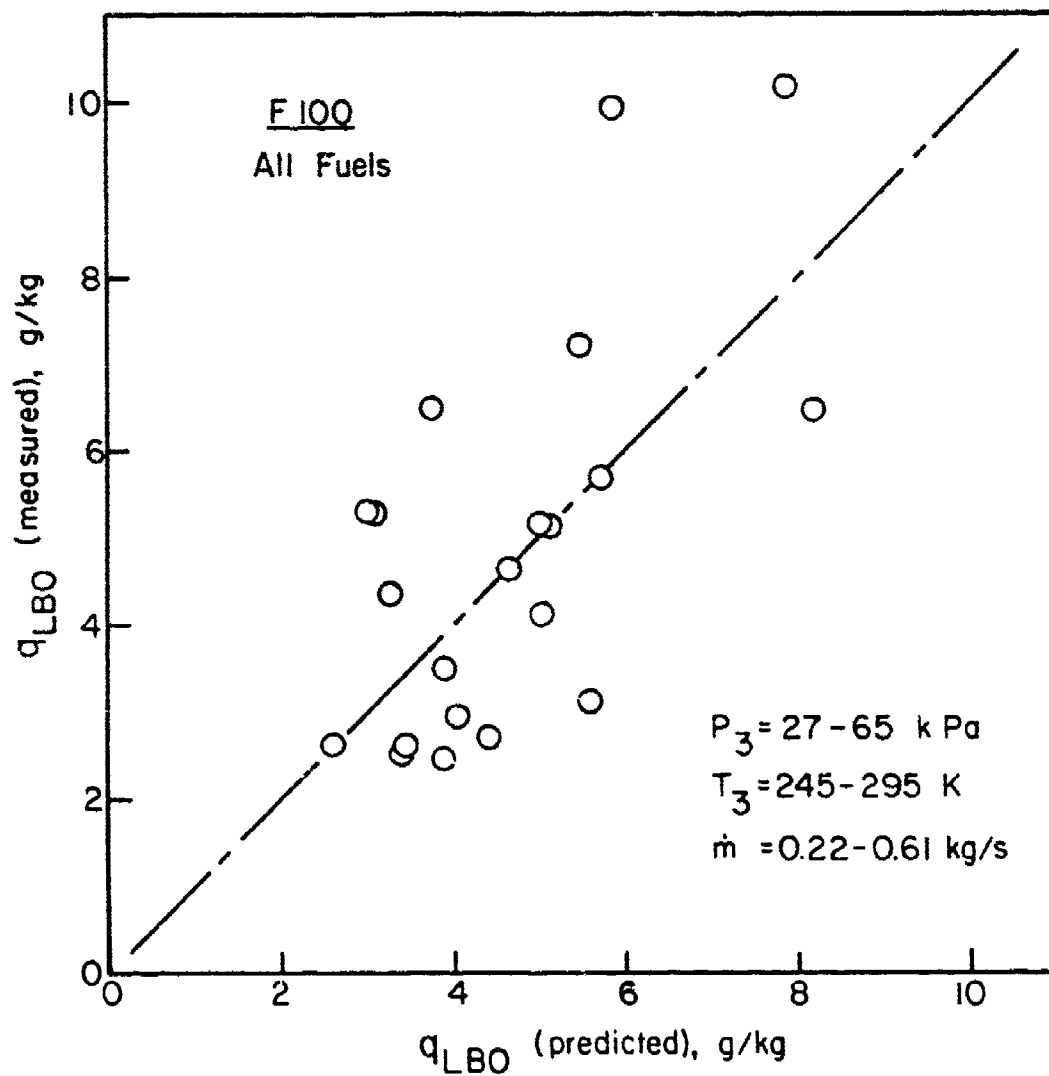


Figure 24. Comparison of Measured and Predicted Values of  $q_{LBO}$  for F100 Combustor.

corresponding predicted values (and other measured values at similar test conditions) by an order of magnitude.

It should also be mentioned that the original correlation obtained for the J79-17A combustor was extremely poor. After further examination of the data it was concluded that the designation of fuels in Tables C-8, C-9, C-10 and C-11 of reference 1 was incorrect and that some mix-up of fuels had occurred during this portion of the test program. From inspection of Eq. (33) it is apparent that  $q_{LBO}$  is strongly influenced by the mean drop size of the spray which, in turn, is very dependent on fuel viscosity,  $\nu_F$ . Thus, to a first approximation, lean blowout limits should correlate with fuel viscosity, and this is confirmed by the upper half of Fig. 25 which demonstrates an excellent correlation between these two parameters for the J79-17C combustor. The lower part of this figure shows similar plots for the J79-17A combustor but, in this instance, there is clearly no correlation between  $\nu_F$  and  $q_{LBO}$ , which tends to suggest that the reported fuel designations are incorrect. To remedy this situation the fuels were renumbered, as indicated in Table 4, in a manner designed to provide a better correlation between  $\nu_F$  and  $q_{LBO}$ . This procedure led to a very satisfactory correlation between the experimental data on  $q_{LBO}$  and the corresponding predictions of Eq. (33), as illustrated in Figs. 14 and 15.

It should be noted that the observations made above apply only to the lean blowout data, and there is no reason to suspect the published fuel numbers for lean lightoff limits in Tables C-8 to C-11 of reference 1.

The full lines drawn in Fig. 26 represent the results of calculations, using Eq. (33), on the effect of variation in initial fuel temperature on  $q_{LBO}$ . Although the experimental data show some scatter, inspection of

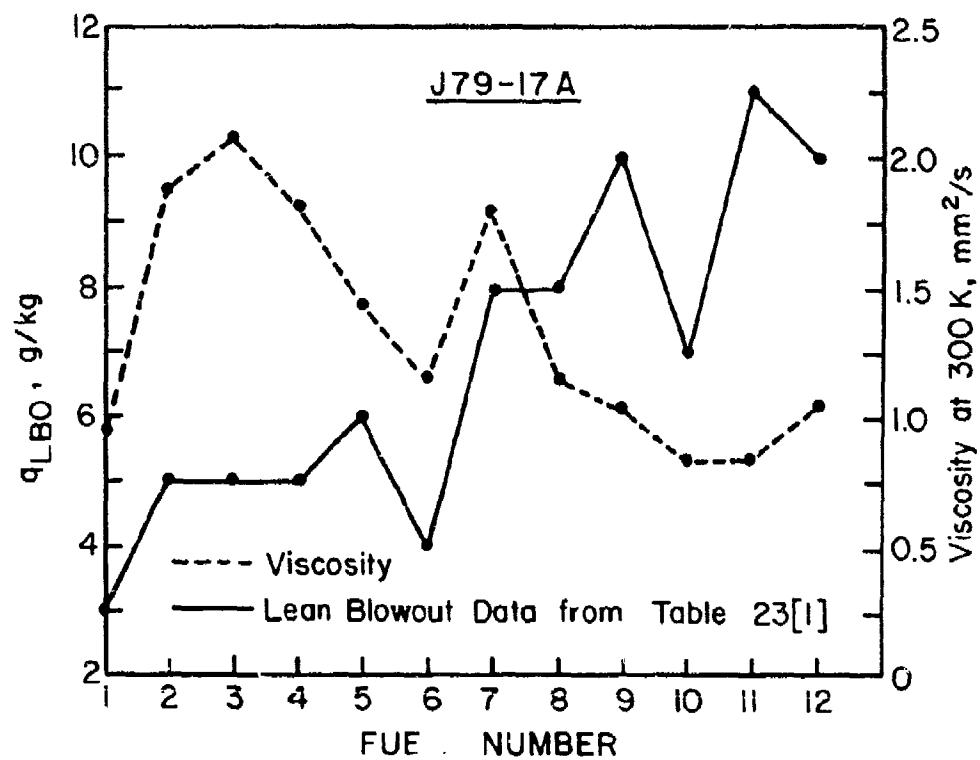
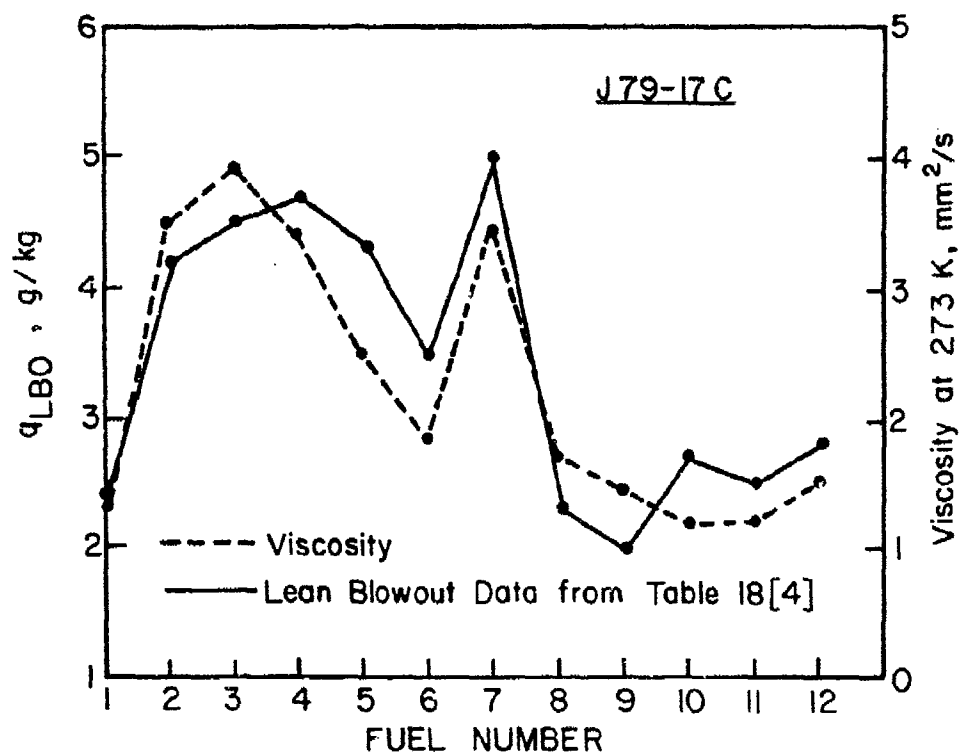


Figure 25. Relationship Between Fuel Viscosity and Lean Blowout Limits.

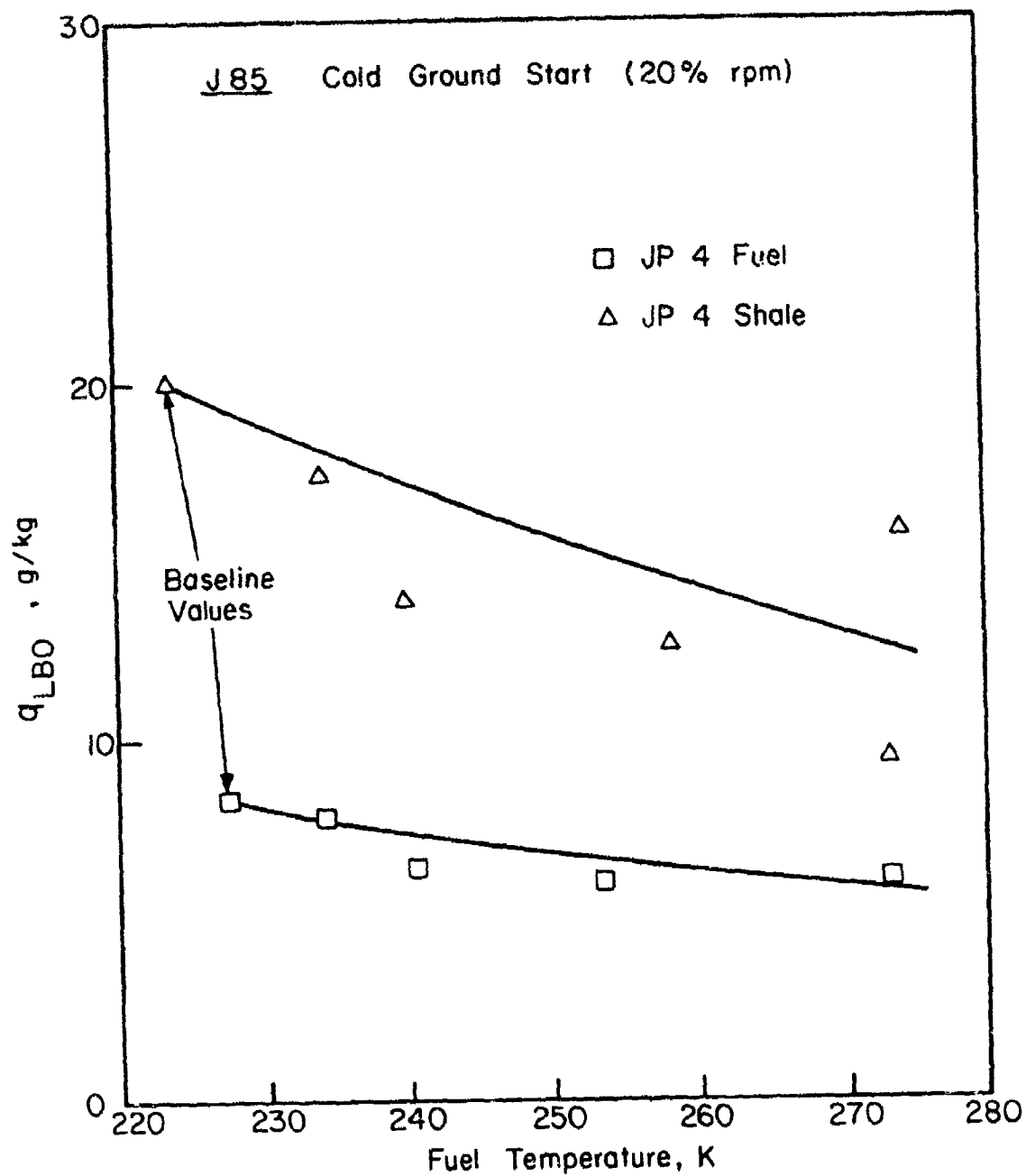


Figure 26. Comparison of Predicted Influence of Fuel Temperature on  $q_{LBO}$  with Experimental Data.

the figure indicates reasonably good agreement between theory and measurement.

For each combustor a value of  $A'$  was chosen for insertion into Eq. (33) that would provide the best fit to the experimental data. These values of  $A'$  are given in Table 5. It was anticipated that similar types of primary zones would yield similar values of  $A'$ , which would clearly be advantageous from the standpoint of predicting the lean blowout limits of future combustor designs. Although the variation in the values of  $A'$  exhibited in Table 5 virtually prohibits such extrapolation, it should be borne in mind that these values embody all the errors incurred in the estimates of combustion volume, the fraction of air involved in primary combustion, and the mean drop size. If these parameters could be established accurately, then it should be possible to determine an appropriate value of  $A'$  for each characteristic primary zone/nozzle configuration. By combining  $A'$  with  $f_{pz}$  the deviation is reduced somewhat, as illustrated in Table 5. The exceptionally low value of  $A'f_{pz}$  for the TF41 combustor can be attributed to its excellent atomization characteristics at low fuel flows stemming from the use of an exceptionally low primary nozzle flow number. Initially, an unusually high value of  $A'f_{pz}$  was calculated for the F101 combustor. This could be the result of an error in the recording of either fuel flow rate or air flow rate, due probably to the fact that the tests were conducted on a  $54^\circ$  segment of the full annular combustor. If the tabulated results in reference [2] were accepted at face value they would imply that the engine was in danger of flame-out at take off, which is highly unlikely. Dividing the published values of  $q_{LBO}$  by  $(360/54)$  reduces  $A'f_{pz}$  to 32 which is fully consistent with the results obtained for the other combustors.

TABLE 4. Re-assigned Fuel Numbers for Lean Blowout Data in  
Tables C-8 to C-11 [1]

Original Fuel Number	1	2	3	4	5	6	7	8	9	10	11	12	13
New Fuel Number	1	12	10	9	8	11	2	5	3	6	13	4	7

TABLE 5. Values of  $A'$  and  $B'$  employed in Eqs. (33) and (37)

Engine	$A'$	$A'_{pz}$	$B'$	$B'_{pz}$
J79-17A	185	42	870	199
J79-17C	100	31	-	-
F101	79	32	222	90
TF 41	46	13	228	634
TF 39	123	37	704	211
J85	213	64	597	179
TF 33	85	25.4	726	274
F100	65	23	483	170

## SECTION VII

### IGNITION

#### 1. The Ignition Process

For the proper interpretation of experimental data on lightup performance it is important to recognize that the ignition process is not a simple, single-step mechanism, but actually occurs in two or three distinct phases [9]. Phase 1 is the formation of a kernel of flame of sufficient size and temperature to be capable of propagation. Phase 2 is the subsequent propagation of flame from this kernel to all parts of the primary zone. Phase 3, which applies only to tubular and can-annular chambers, is the spread of flame from a lighted liner to an adjacent unlighted liner. Failure of any single phase is, of course, equivalent to failure to ignite.

The success or failure of Phase 1 depends mainly on whether or not the rate of heat release by combustion in the spark kernel exceeds the rate of heat loss to the surroundings by radiation, thermal conduction, and turbulent diffusion. The rate of heat release is governed mainly by the effective fuel/air ratio adjacent to the igniter plug, which should be close to stoichiometric, and by the size and temperature of the kernel, which are in turn determined by the energy and duration of the spark. The rate of heat loss from the kernel is largely dictated by the local conditions of velocity and turbulence and by the quantity of excess fuel present in the ignition zone.

The success of Phase 2 is governed partly by the location of the igniter, since this determines whether or not the hot kernel is entrained into the primary-zone reversal or is swept away downstream. It is also affected by all the factors that control flame stability. Thus, an increase in pressure and/or temperature, a reduction in primary zone velocity, or any change in fuel/air ratio toward the stoichiometric value, all of which are beneficial to stability, will also improve phase 2.

The location of the interconnector is of prime importance in phase 3. Ideally, each tube entrance should coincide with the region of highest gas temperature in the liner, whereas the tube exit should be sited so as to ensure that the issuing hot gas flows directly into the recirculation zone of the adjacent liner. Phase 3 is enhanced by the use of interconnectors in which the flow area is made large to facilitate the passage of flame, and whose length is kept short to minimize heat loss.

Although ignition of a combustible mixture may be accomplished in a variety of ways, in the gas turbine it is usually effected by means of an electric spark, and large amounts of energy are needed to ignite the heterogeneous and highly turbulent mixture flowing at velocities of the order of 25 m/s.

In recent years a series of detailed experimental studies has been carried out on the influence of electrical and flow parameters on minimum spark energy in flowing mixtures of fuel drops and air. These studies have led to a better conceptual understanding of the basic ignition process and have provided a useful theoretical foundation for relating ignition characteristics to all the operating variables involved. They confirm practical experience in showing that ignition is made easier by increases in pressure, temperature and spark energy, and is impeded by increases in velocity and turbulence intensity. They also emphasize that ignition performance is markedly affected by fuel properties through the way in which they influence the concentration of fuel vapor in the immediate vicinity of the igniter plug. These influences arise mainly through the effect of volatility on evaporation rates, but also through the effects of surface tension and viscosity on mean fuel drop size. The amount of energy required for ignition is very much larger than the values normally associated with gaseous fuels at stoichiometric fuel/air ratio. Much of

this extra energy is absorbed in the evaporation of fuel droplets, the actual amount depending on the distribution of fuel throughout the primary zone and on the quality of atomization.

## 2. Theory

One model for the ignition of fuel sprays is based on the assumption that chemical reaction rates are infinitely fast and that the onset of ignition is limited solely by the rate of fuel evaporation [15]. Support for this notion may be found in the literature on the ignition of turbojet combustors. For example, the reports by Foster and Straight [16] and Wigg [17] contain ample evidence that various fuel spray characteristics, such as mean drop size and volatility, can appreciably affect the energy required for ignition. These effects are due to their influence on fuel evaporation rates that govern the mixture strength in the ignition zone. Further confirmation of the importance of fuel vapor concentration to ignition is provided in the more basic studies conducted by Rao and Lefebvre [18] on the ignition of heterogeneous, flowing kerosine/air mixtures. They found that for mixtures weaker than stoichiometric the main factor limiting ignition is a deficiency of fuel vapor in the ignition zone.

The process of ignition is envisaged to occur in the following manner. Passage of the spark creates a small, roughly spherical, volume of air (the spark kernel) whose temperature is sufficiently high to initiate rapid evaporation of the fuel drops contained within the volume. It is assumed that reaction rates and mixing times are infinitely fast so that any fuel vapor created within the spark kernel is instantly transformed into combustion products at the stoichiometric flame temperature. If the rate of heat release by combustion exceeds the rate of heat loss at the surface of the inflamed volume, then the spark kernel will

grow in size to fill the entire combustion volume. If, however, the rate of heat release is less than the rate of heat loss, the temperature within the spark kernel will fall steadily until fuel evaporation ceases altogether. This concept leads to the definition of 'quenching distance' as the critical size that the inflamed volume must attain in order to propagate unaided, while the amount of energy required from an external source to attain this critical size is termed the "minimum ignition energy."

Analysis of the relevant heat transfer and evaporation processes [19] yields the following expression for the quenching distance of quiescent or slow-moving monodisperse mists:

$$d_q = \left[ \frac{\rho_F D_o^2}{\rho_A \phi \ln(1 + B_{st})} \right]^{0.5} \quad (34)$$

It should be noted that the above equation was derived directly from basic considerations of the mechanisms of heat generation within the kernel and heat loss from its surface and contains no experimental or arbitrary constants.

Equation (34) and similar expressions for polydisperse sprays of the type provided by most practical atomizing devices, provide simple relationships between quenching distance and the key spray properties. Essentially, they state that quenching distance is directly proportional to drop size and is inversely proportional to the square root of gas pressure. An increase in  $\phi$  and reduction in  $\rho_F$  both reduce  $d_q$  because they promote evaporation by increasing the surface area of the fuel. Similarly, an increase in  $B$  will also accelerate evaporation and thereby decrease  $d_q$ . Values of  $E_{min}$  may be obtained by inserting the calculated values of  $d_q$  from Eq. (34) into the following expression

$$E_{min} = c_{pA} \rho_A \Delta T_{st} (\pi/6) d_q^3 \quad (35)$$

Subsequently, Ballal and Lefebvre [19] extended the model described above to include (1) the effects of finite chemical reaction rates, which are known to be significant for very well-atomized fuels at low pressures and low equivalence ratios, and (2) the effect of heat loss from the spark kernel by turbulent diffusion. Thus the model has general application to both quiescent and flowing mixtures of air with either gaseous, liquid or evaporated fuel, or any combination of these fuels.

From a gas turbine viewpoint, the value of the type of model described above lies not so much in its ability to predict minimum ignition-energy requirements, since the available spark energy is determined by the specifications of the igniter plug and the high-energy unit; rather, its importance is in highlighting the key parameters that control ignition and in providing quantitative relationships or "rates of exchange" between these parameters.

Consider, for example, a combustor that normally operates on kerosine fuel. It is required to know what improvement in atomization quality would be needed to achieve the same ignition performance when diesel oil is burned. Now the relevant fuel properties are density and volatility, the latter being represented in the quenching-distance equations by the mass-transfer number  $B$ . From Eq. (34) we have

$$d_q \propto \left[ \frac{\rho_F D_o^2}{\ln(1 + B_{st})} \right]^{0.5}$$

Thus, for unchanged ignition performance, i.e., unchanged  $d_q$ , we can write

$$\frac{(D_o)_{\text{diesel}}}{(D_o)_{\text{ker}}} = \left[ \frac{[\ln(1 + B_{st})/\rho_F]_{\text{diesel}}}{[\ln(1 + B_{st})/\rho_F]_{\text{ker}}} \right]^{0.5} \quad (36)$$

Now for diesel oil,  $\rho_F = 900$  and  $B_{st} = 2.80$ ; for kerosine,  $\rho_F = 775$  and  $B_{st} = 3.75$ . Substituting these values into Eq. (36) gives

$$\frac{(D_o)_{\text{diesel}}}{(D_o)_{\text{ker}}} = 0.86$$

which suggests that for diesel oil the SMD should be reduced by about 20 percent to retain the ignition performance obtained with kerosine.

### 3. Data Analysis

Application of the theoretical concepts described above to the analysis of the experimental data on ignition contained in references 1 to 6 was inhibited, as for the lean blowout data, by lack of accurate information on mean drop size. So again recourse was made to relationships in which the key fuel properties are not expressed in absolute terms but in values relative to those of the baseline fuel, JP4. This approach leads to the following equation for lean lightup fuel/air ratio.

$$q_{LL0} = \frac{B'_{pz} \dot{m}_A}{V_c P_3^{1.5} \exp(T_3/300)} \times \frac{D_r^2}{\lambda_r LCV_r} \times \left[ \frac{D \text{ at } T_F}{D \text{ at } 277.5K} \right]^2 \quad (37)$$

This equation is virtually identical to Eq. (13) except for a higher pressure dependence;  $P_3^{1.5}$  versus  $P_3^{1.3}$ .

The correlation of lightup data obtained with Eq. (37) is illustrated in Figs. 27 to 38. The level of agreement between predicted and experimental values is considered satisfactory, especially in view of the well known lack of consistency that usually characterizes experimental data on spark

ignition. The values of B' and B'f for the various combustors are listed in Table 5.

A curious anomaly exists in regard to the ignition data obtained from the J79 17C combustor. For this combustor the results, as shown plotted in Figs. 29 and 30, indicate a correlating parameter of the form

$$q_{LLO} = C_7 + \frac{C_8 f_{pz} \dot{m}_A}{V_c P_3^{1.5} \exp(T_3/300)} \times \frac{D_r^2}{\lambda_r LCV_r} \times \left( \frac{D \text{ at } T_F}{D \text{ at } 277.5K} \right)^2 \quad (38)$$

Assigning values to  $C_7$  and  $C_8$  of 3.92 and 200 respectively provides the excellent correlation illustrated in Figs. 31 and 32.

For the F101 combustor it was found that, in common with the lean blowout data discussed earlier, the reported lightoff fuel/air ratios were unusually high. Thus only the results obtained with the fuel having the highest number of test points (No. 12) are shown in Fig. 33 to illustrate the level of prediction attained. As for the lean blowout case, it was again assumed that a computational error had arisen in the calculation of fuel/air ratios due to tests being performed on a 54° sector rig, and a correction factor of (54/360) was again used to calculate the values of B and Bf shown in Table 5 for the F101 combustor.

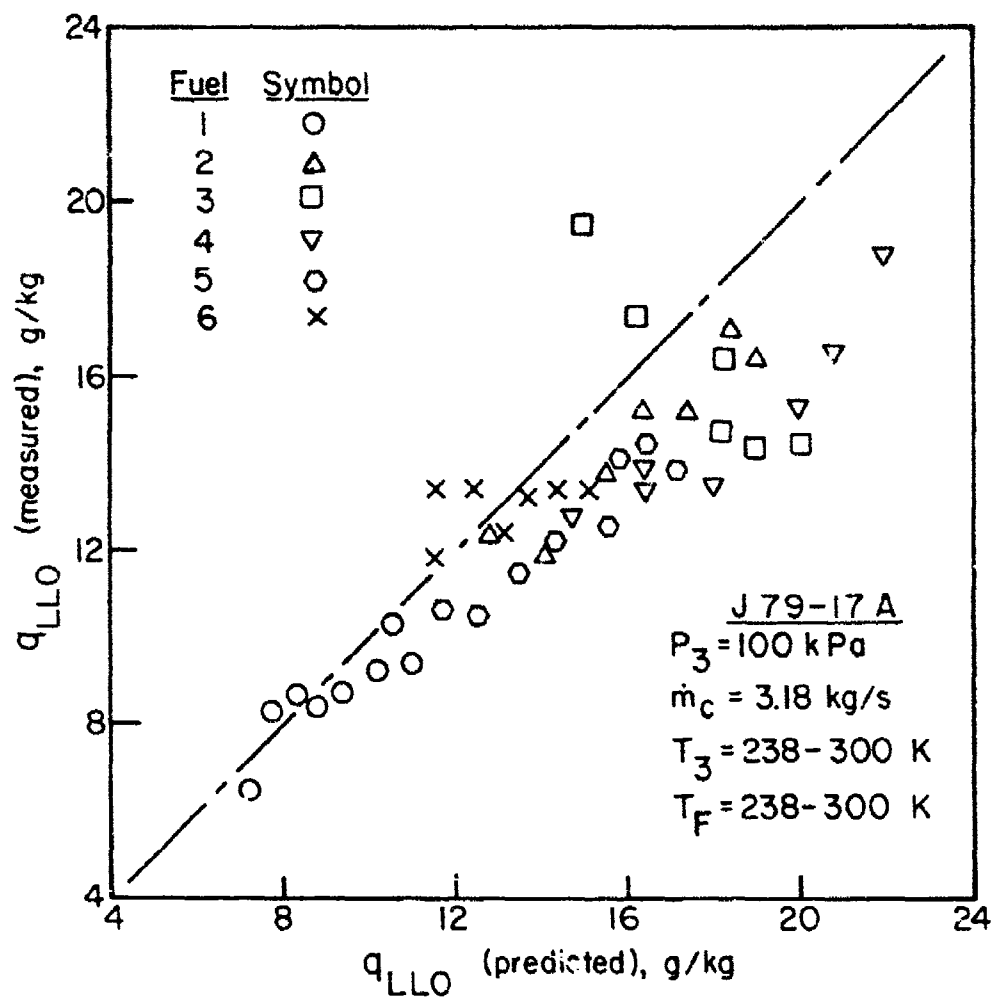


Figure 27. Comparison of Measured and Predicted Values of  $q_{LLO}$  for J79-17A Combustor. (Fuels 1 to 6).

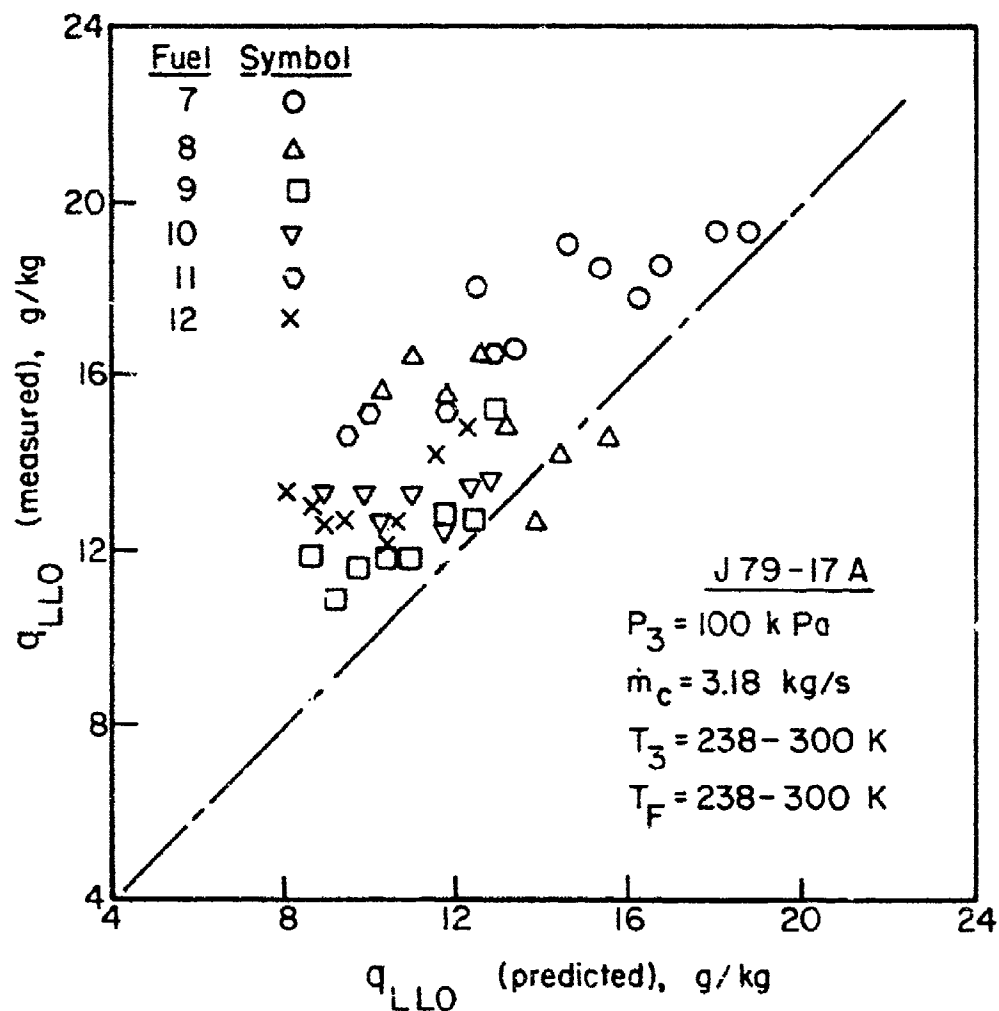
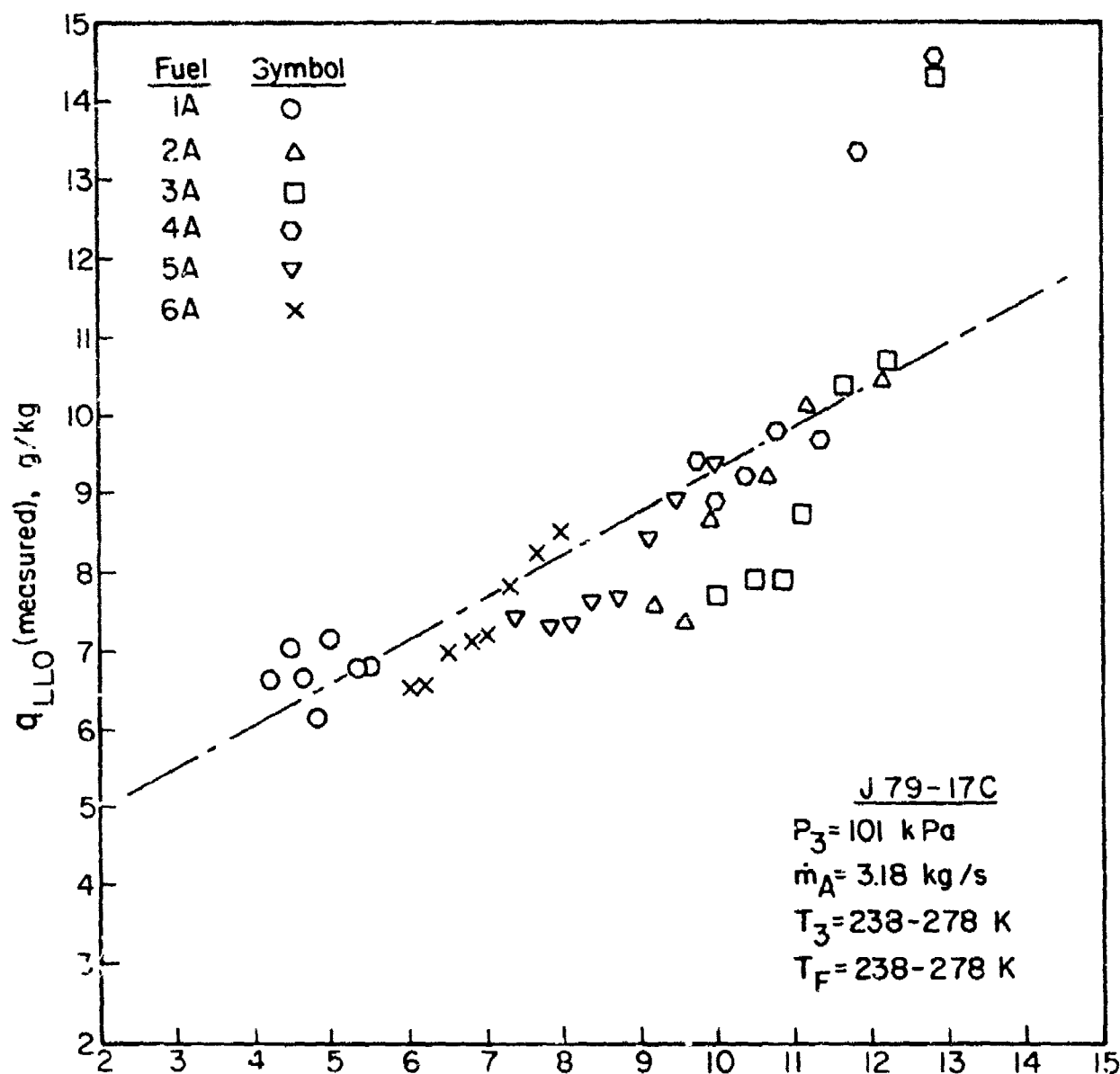


Figure 28. Comparison of Measured and Predicted Values of  $q_{LLO}$  for J79-17A Combustor. (Fuels 7 to 12).



$$\frac{200 f_{tz} \dot{m}_A}{V_c P_3^{1.5} \exp(T_3/300)} \times \frac{D_r^2}{\lambda_r LCV_r} \times \left( \frac{D \text{ at } T_F}{D \text{ at } 277.5K} \right)^2$$

Figure 29. Correlation of Experimental Data on  $q_{LLO}$  for J79-17C Combustor. (Fuels 1A to 6A).

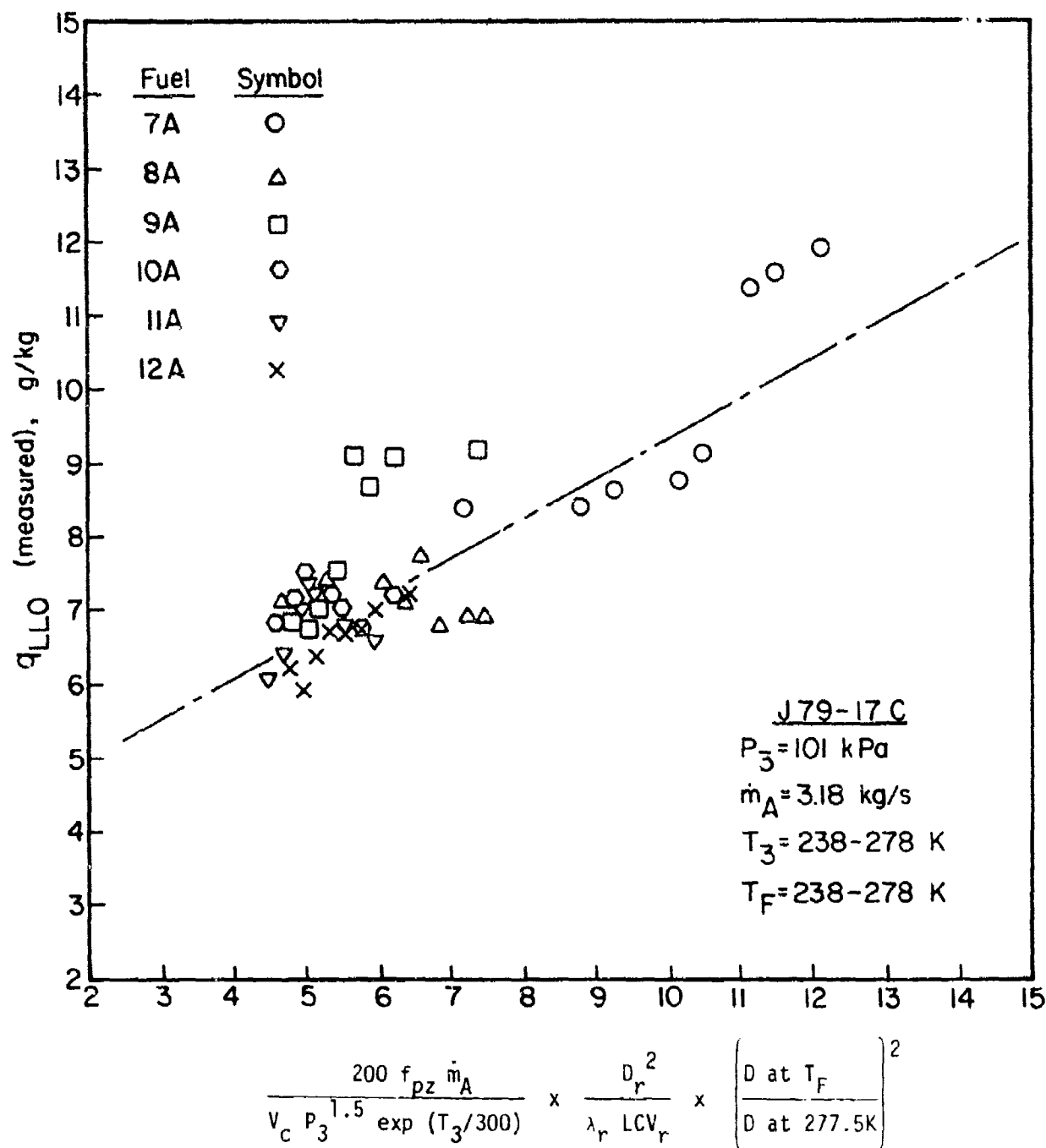


Figure 30. Correlation of Experimental Data on  $q_{LLO}$  for J79-17C Combustor. (Fuels 7A to 12A).

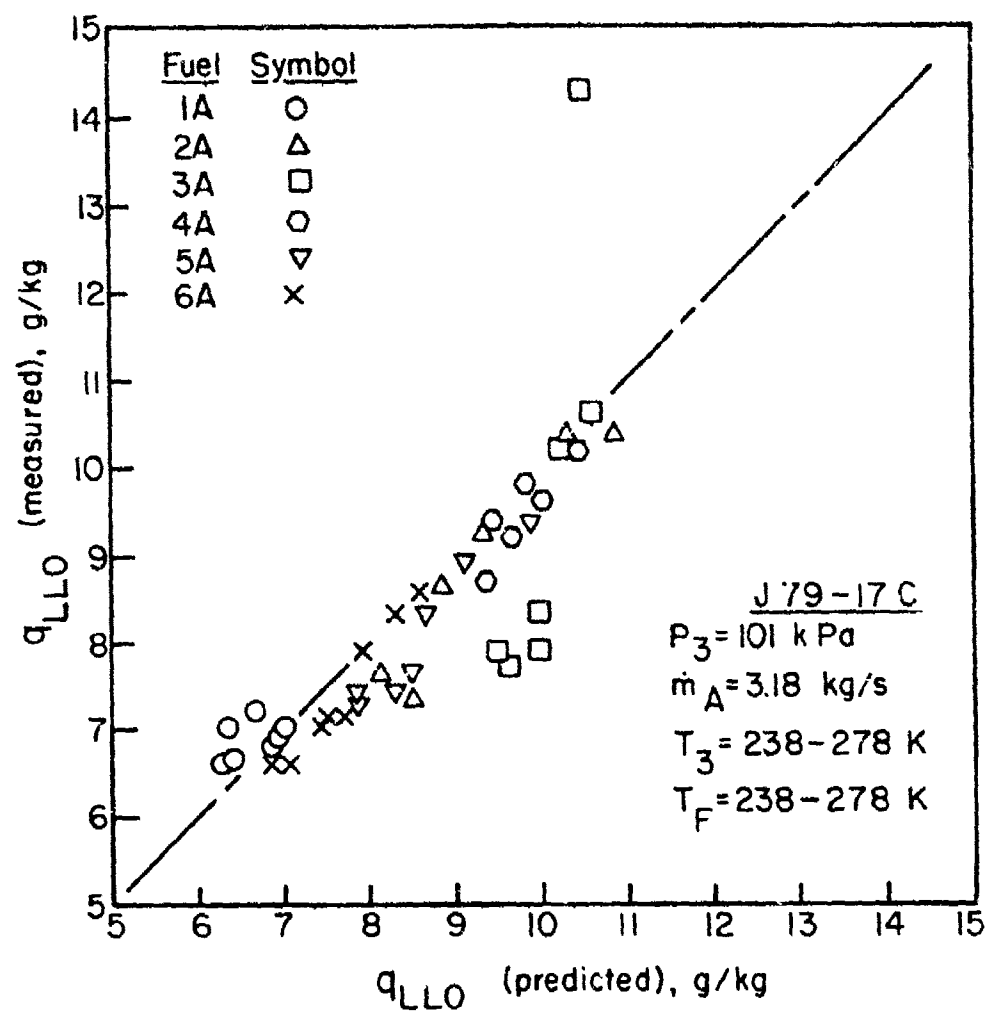


Figure 31. Comparison of Measured and Predicted Values of  $q_{LLO}$  for J79-17C Combustor. (Fuels 1A to 6A).

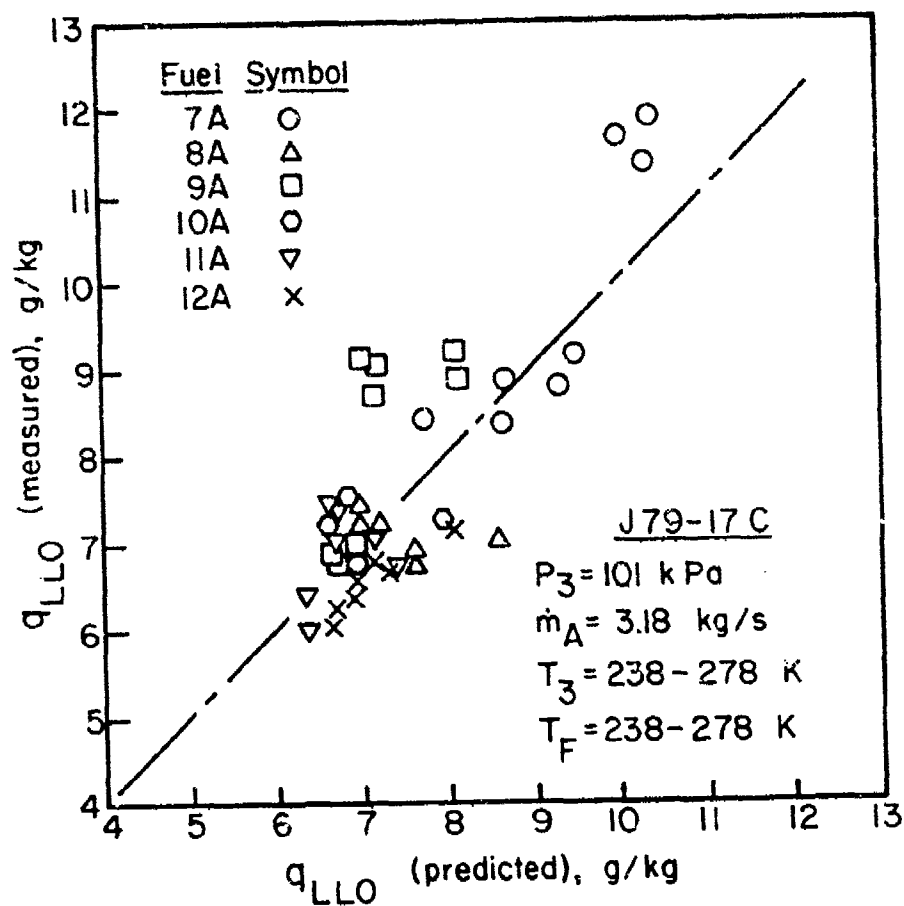


Figure 32. Comparison of Measured and Predicted Values of  $q_{LLO}$  for J79-17C Combustor. (Fuels 7A to 12A).

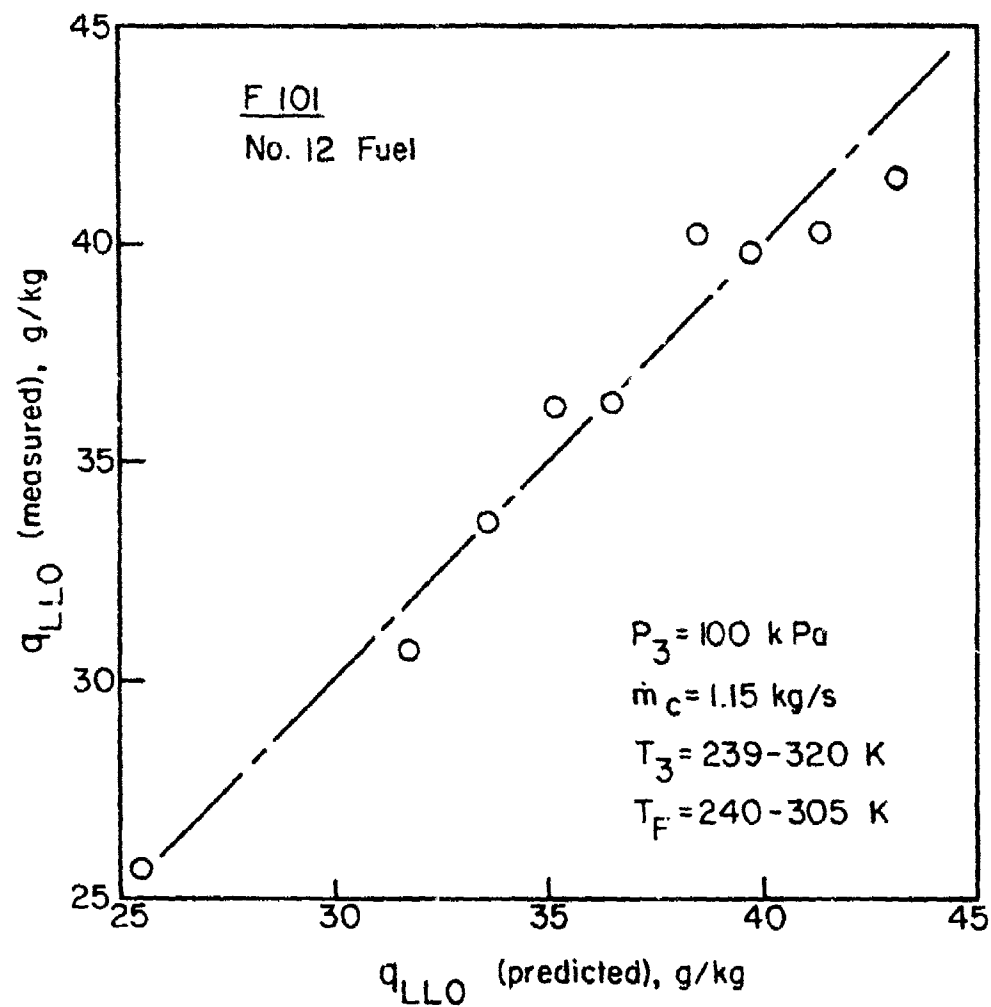


Figure 33. Comparison of Measured and Predicted Values of  $q_{LLO}$  for F101 Combustor.

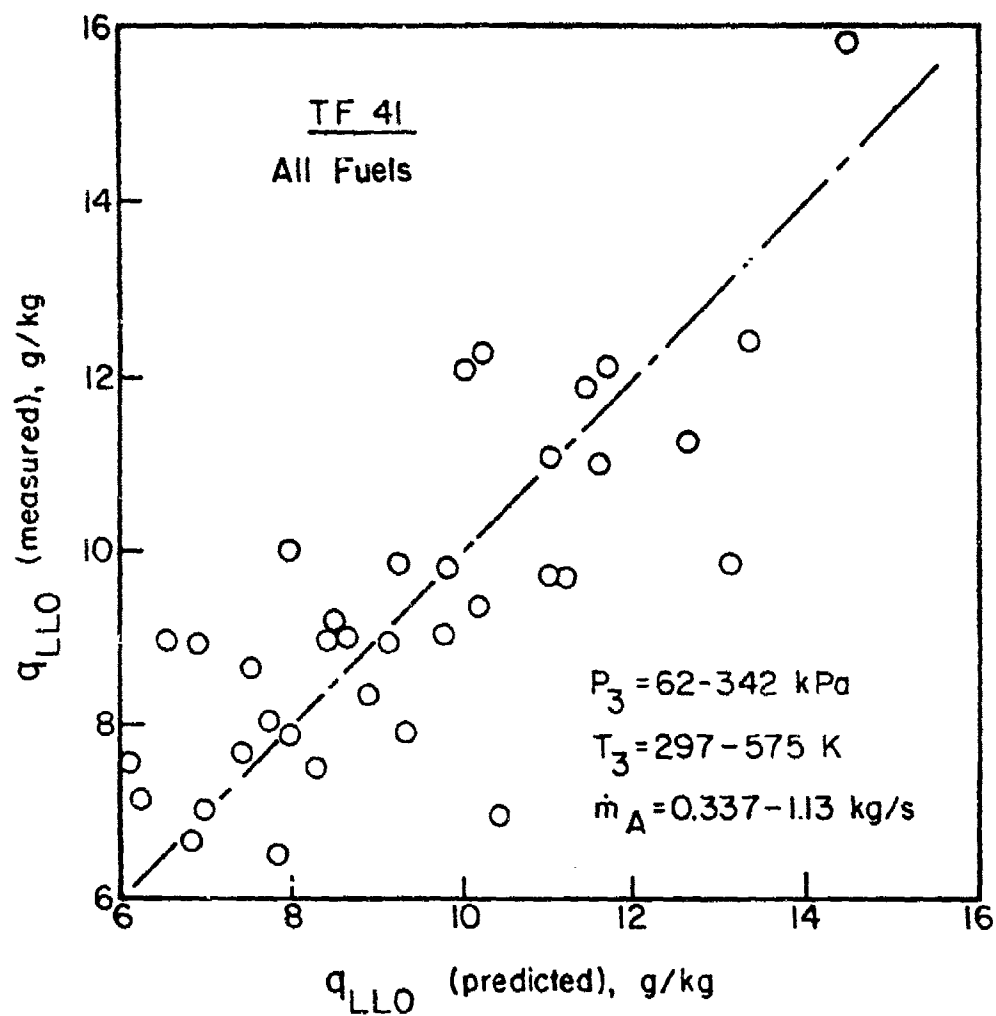


Figure 34. Comparison of Measured and Predicted Values of  $q_{LLO}$  for TF 41 Combustor.

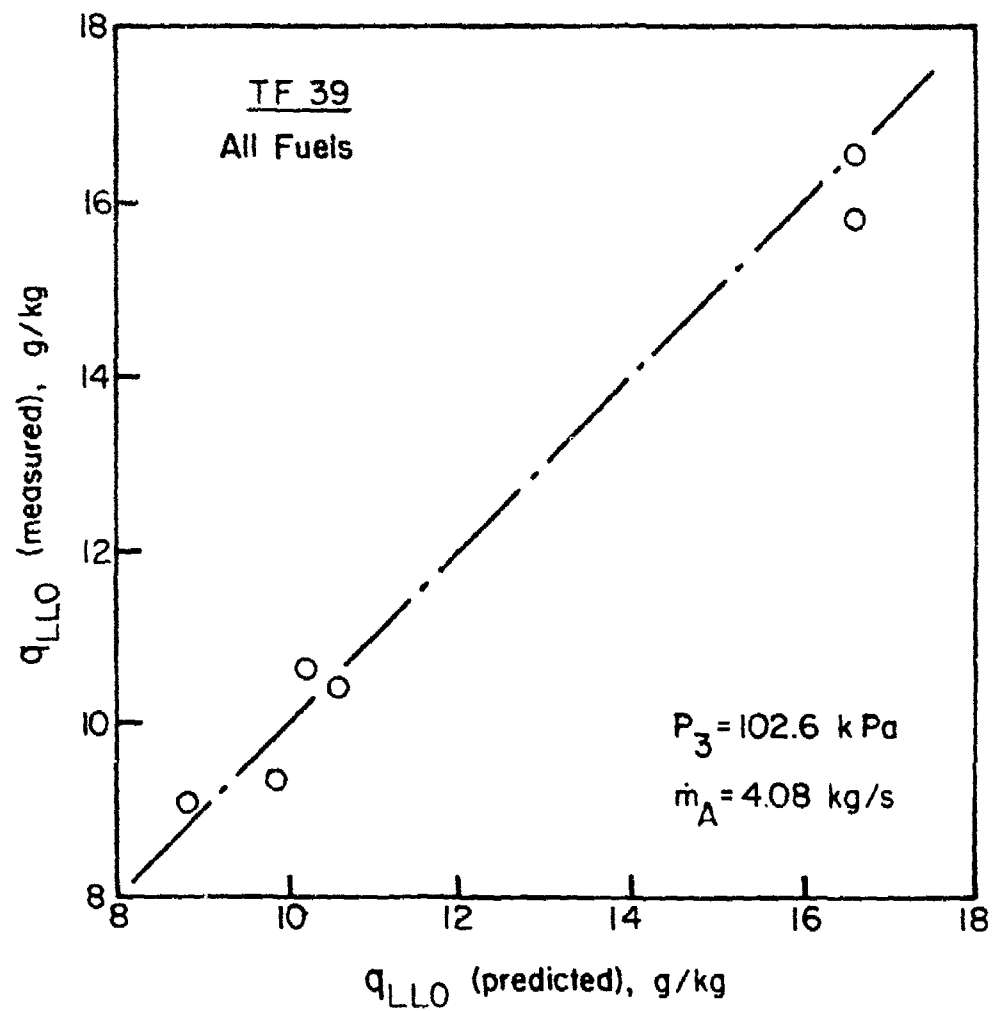


Figure 35. Comparison of Measured and Predicted Values of  $q_{LLO}$  for TF 39 Combustor.

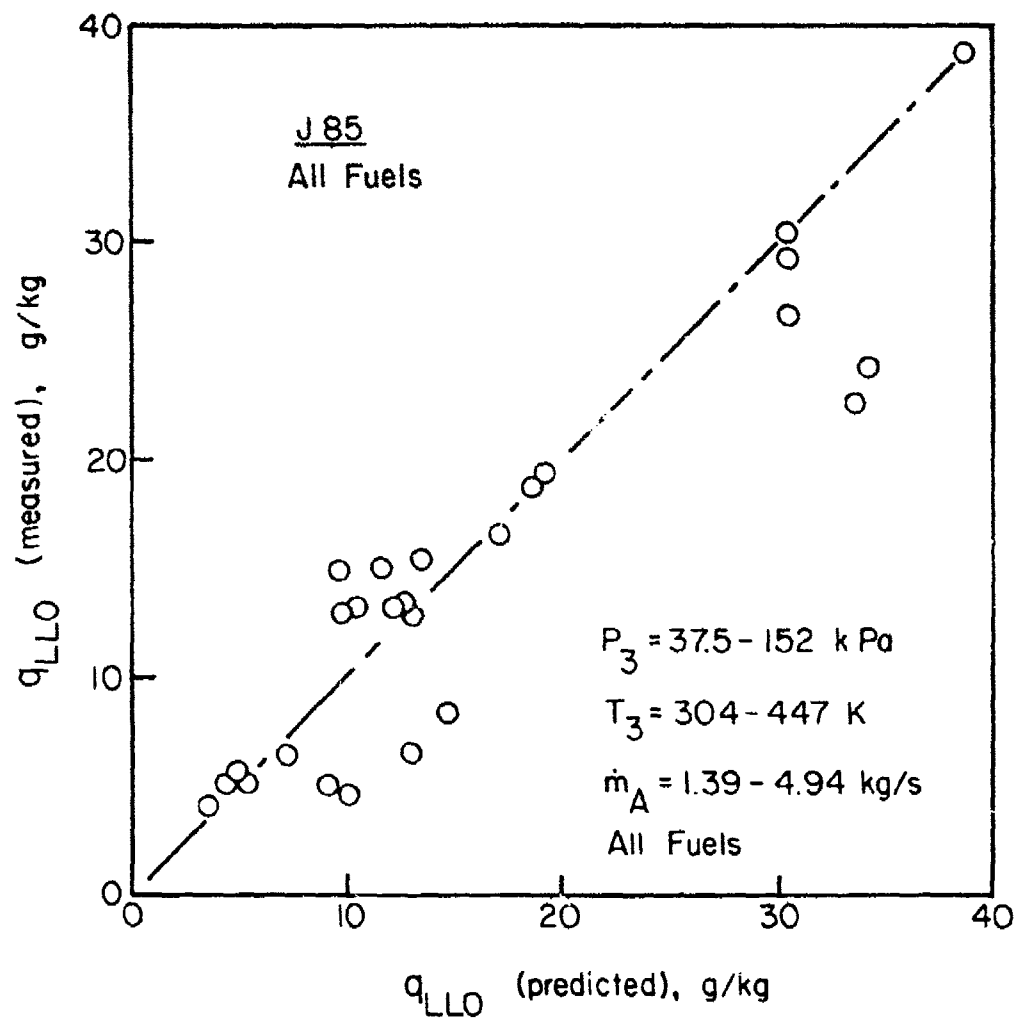


Figure 36. Comparison of Measured and Predicted Values of  $q_{LLO}$  for J85 Combustor.

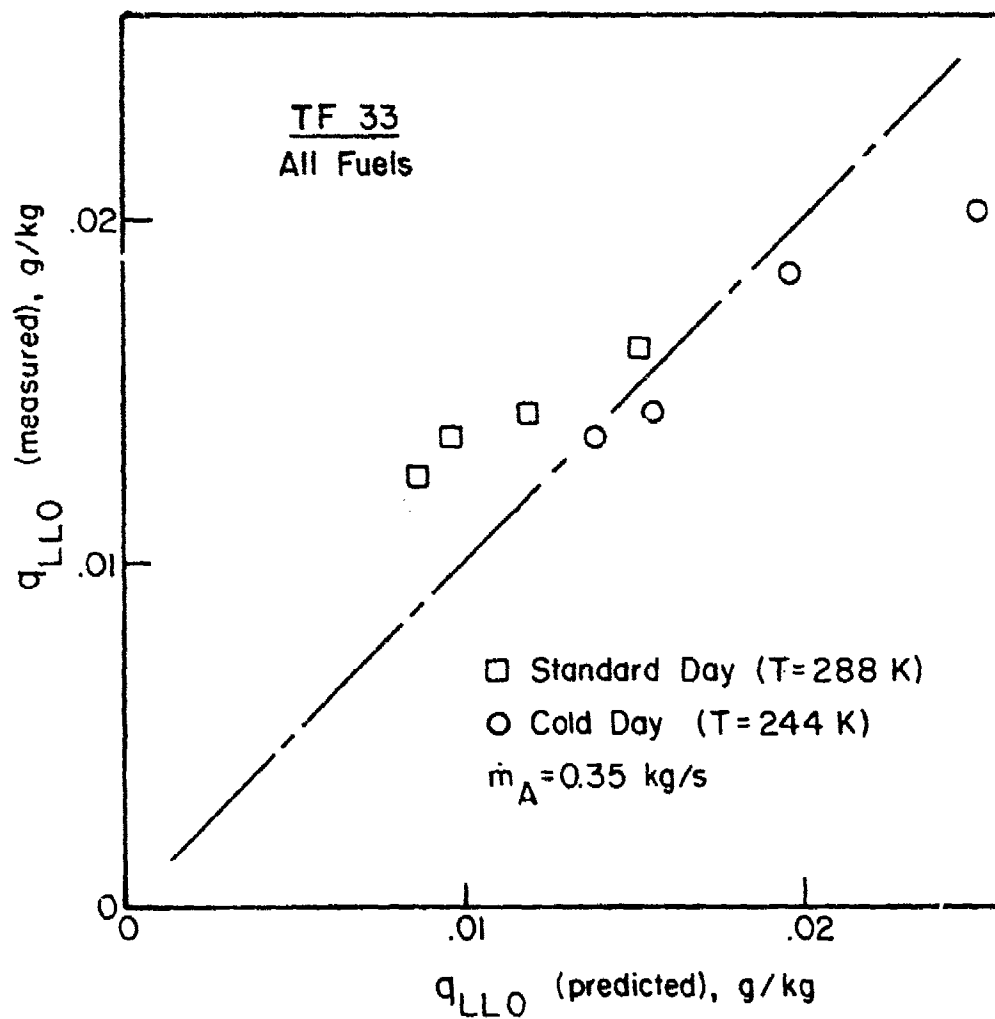


Figure 37. Comparison of Measured and Predicted Values of  $q_{LLO}$  for TF 33 Combustor.

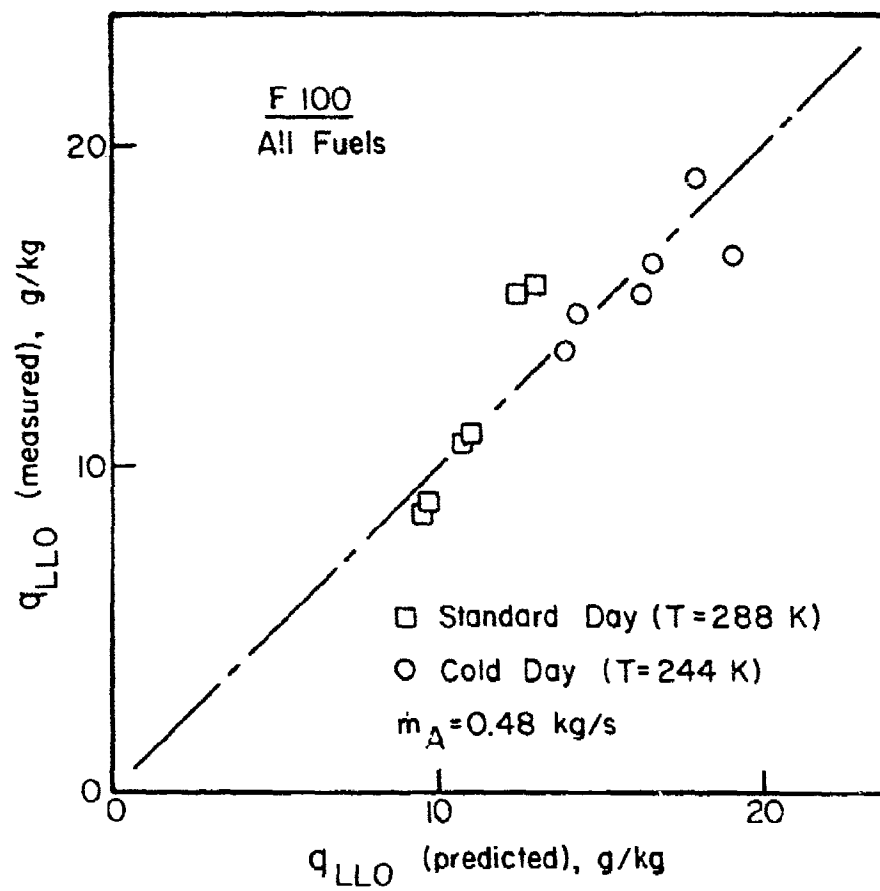


Figure 38. Comparison of Measured and Predicted Values of  $q_{LLO}$  for F100 Combustor.

## SECTION VIII LINER WALL TEMPERATURE

For the purpose of analysis a liner may be regarded as a container of hot flowing gases surrounded by a casing in which air is flowing between the container and the casing. Broadly, the liner is heated by radiation and convection from the hot gases inside it, and is cooled by radiation to the outer casing and by convection to the annulus air. The relative proportions of the radiation and convection components depend upon the geometry and operating conditions of the system. Under equilibrium conditions the liner temperature is such that the internal and external heat fluxes at any point are just equal. Loss of heat by conduction along the liner wall is comparatively small and usually may be neglected. Under steady-state conditions the rate of heat transfer into the wall must be balanced by the rate of heat transfer out. Thus, we have

$$R_1 + C_1 = R_2 + C_2 \quad (39)$$

### 1. Internal Radiation, $R_1$

This is the component of heat transfer that is most affected by a change in fuel type. It is given by [20]

$$R_1 = 0.5 \sigma (1 + \epsilon_w) \epsilon_g T_g^{1.5} (T_g^{2.5} - T_w^{2.5}) \quad (40)$$

where  $\sigma$  = Stefan Boltzmann constant

$\epsilon_w$  = liner wall emissivity

$\epsilon_g$  = gas emissivity

$T_g$  = gas temperature

$T_w$  = wall temperature

The 'bulk' or mean gas temperature,  $T_g$ , is obtained as the sum of the chamber entry temperature,  $T_3$ , and the temperature rise due to combustion,  $\Delta T_{\text{comb}}$ .

Thus:

$$T_g = T_3 + \Delta T_{\text{comb}}$$

$\Delta T_{\text{comb}}$  may be derived from standard temperature rise curves. The appropriate value of fuel/air ratio is the product of the local fuel/air ratio and the local level of combustion efficiency. Most heat transfer calculations are carried out at high pressure conditions where it is reasonable to assume a combustion efficiency of 100 percent.

For the luminous flames associated with the combustion of heterogeneous fuel-air mixtures, the value of  $\epsilon_g$  for insertion in Eq. (40) is obtained as [20]

$$\epsilon_g = 1 - \exp[-290 P_3 L (q \ell_b)^{0.5} T_g^{-1.5}] \quad (41)$$

where  $q$  is the local fuel/air ratio and  $\ell_b$  is the 'beam length' of the radiating gas. Beam length depends on the size and shape of the gas volume. For most practical purposes it is given to sufficient accuracy [20] by the expression

$$\ell_b = 3.4 (\text{volume/surface area})$$

The luminosity factor,  $L$ , is an empirical correction introduced to obtain reasonable agreement between experimental data on gas radiation and predictions from Eq. (40). Experiments have shown that luminosity factor depends largely on the carbon-to-hydrogen mass ratio of the fuel [9, 20, 21].

The original equation for L is [20]

$$L = 7.53(C/H - 5.5)^{0.84} \quad (42)$$

Later the following expression was suggested by Kretschmer and Odgers [21]

$$L = 0.0691 [C/H - 1.82]^{2.71} \quad (43)$$

Another correlation, which is simpler and probably no less accurate, is [9]

$$L = 3 (C/H - 5.2)^{0.75} \quad (44)$$

More recent investigations have tended to emphasize fuel hydrogen content, rather than carbon/hydrogen ratio, as the property most relevant to flame radiation. Figure 39 shows the correlation obtained by Blazowski and Jackson [22, 23] between hydrogen content and liner wall temperature for several engines. The data shown represent cruise conditions with combustor inlet temperatures ranging from 547 to 756 K. The parameter used to correlate the experimental data is

$$(T_{L_{\max}} - T_{L_0}) / (T_{L_0} - T_3)$$

in which the numerator represents the increase in maximum liner temperature over that obtained with a baseline fuel containing 14.5 percent hydrogen.

The excellent correlation of data exhibited in Fig. 39 could not be duplicated for the results contained in references 1 to 4, as shown in Figs. 40 to 43. This is believed to be due to the fact that the magnitude of the parameter  $(T_{L_{\max}} - T_{L_0}) / (T_{L_0} - T_3)$  is very sensitive to the value of  $T_{L_0}$ . Since maximum values of wall temperature are notoriously difficult



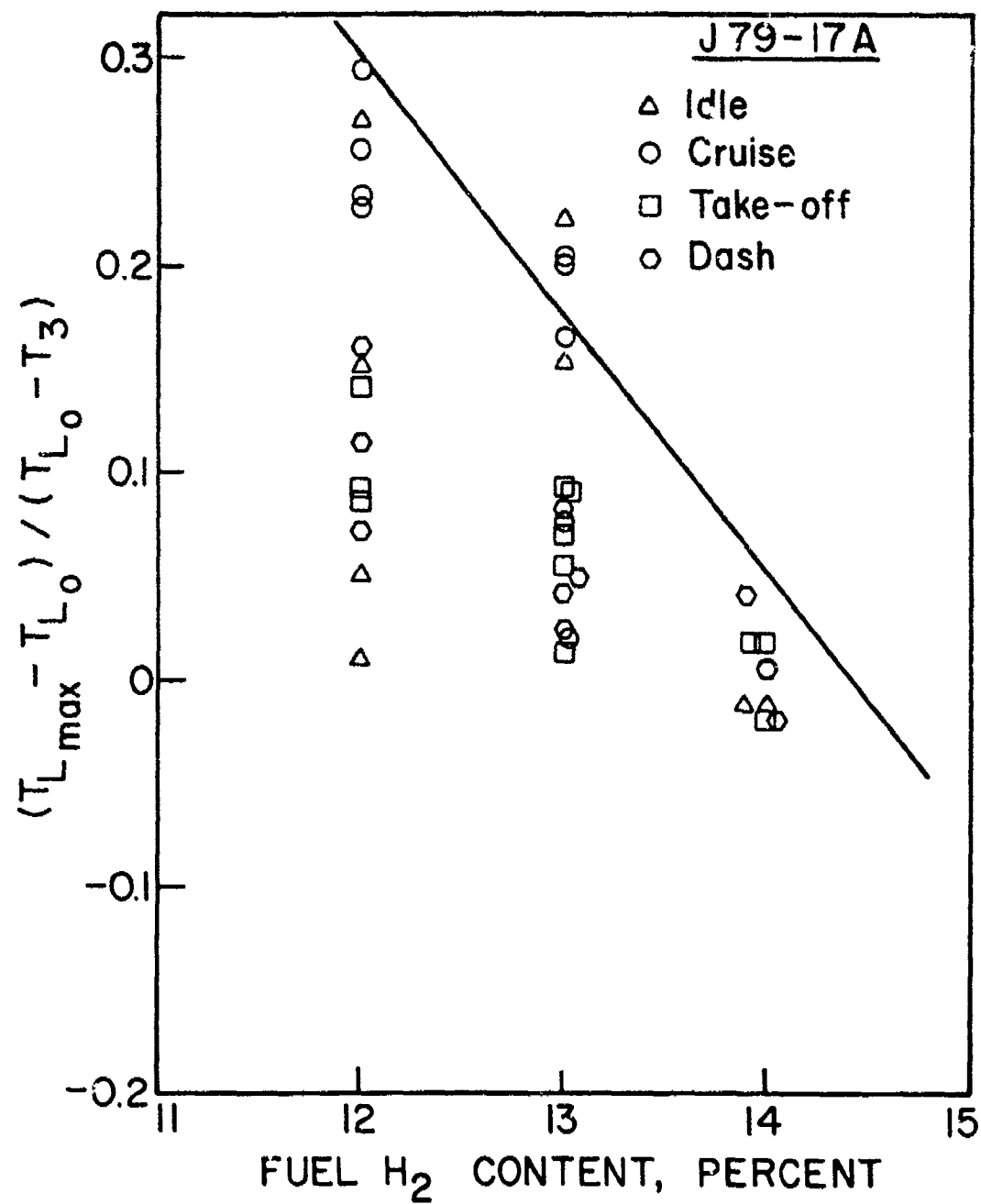


Figure 40. Effect of Fuel Hydrogen Content on Liner Temperature Parameter for J79-17A Combustor.

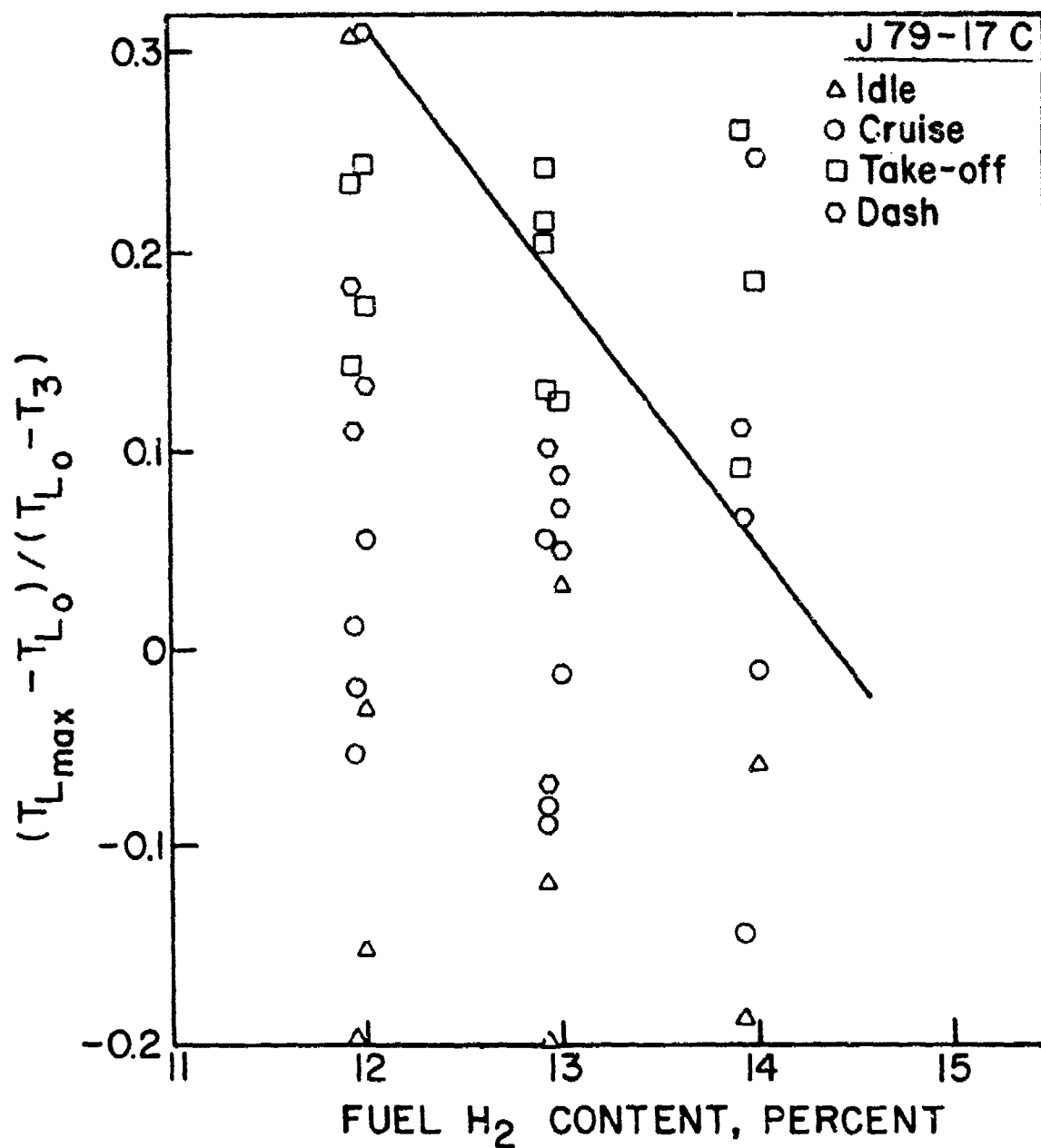


Figure 41. Effect of Fuel Hydrogen Content on Liner Temperature Parameter for J 79-17C Combustor.

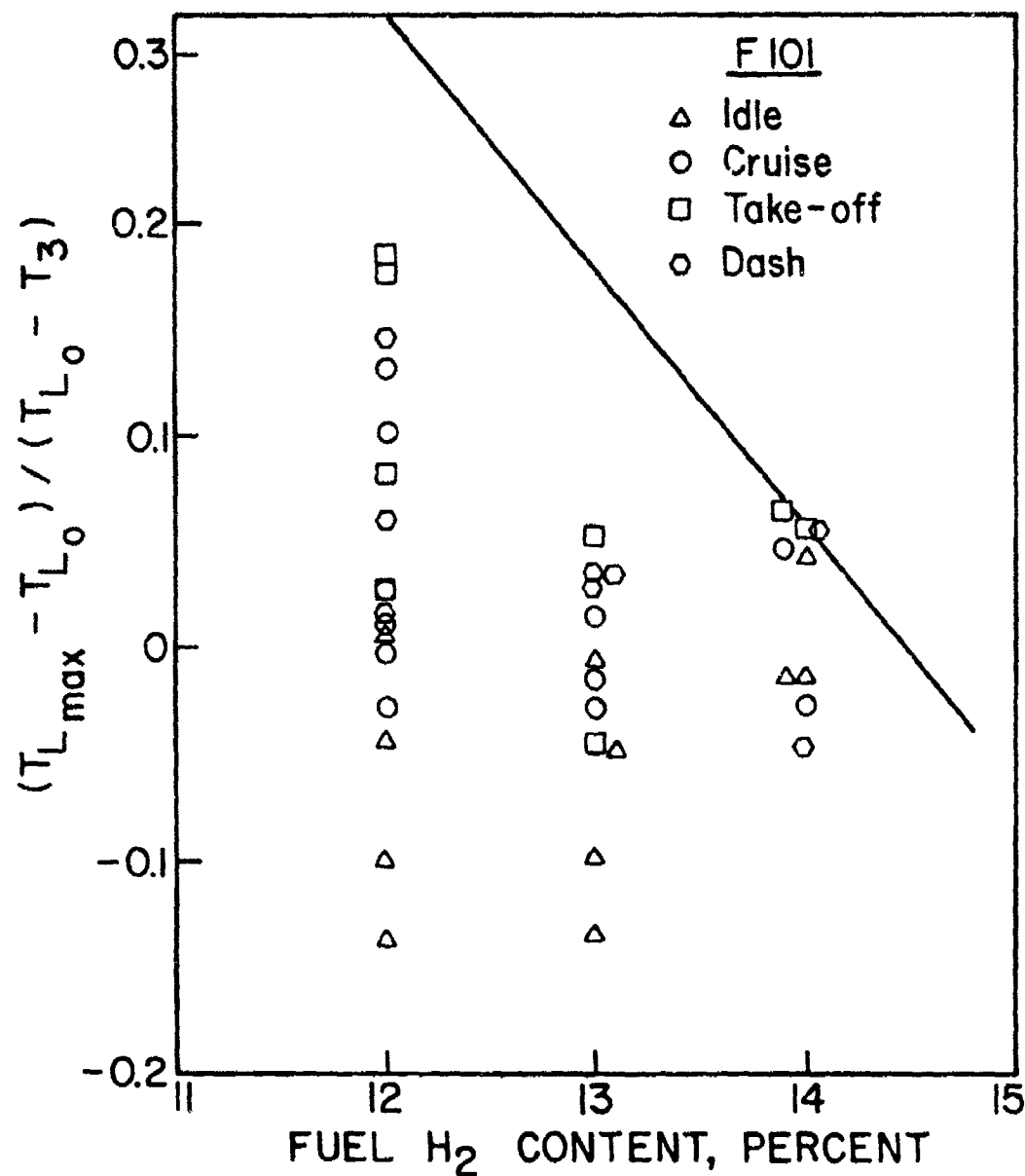


Figure 42. Effect of Fuel Hydrogen Content on Liner Temperature Parameter for F101-Combustor.

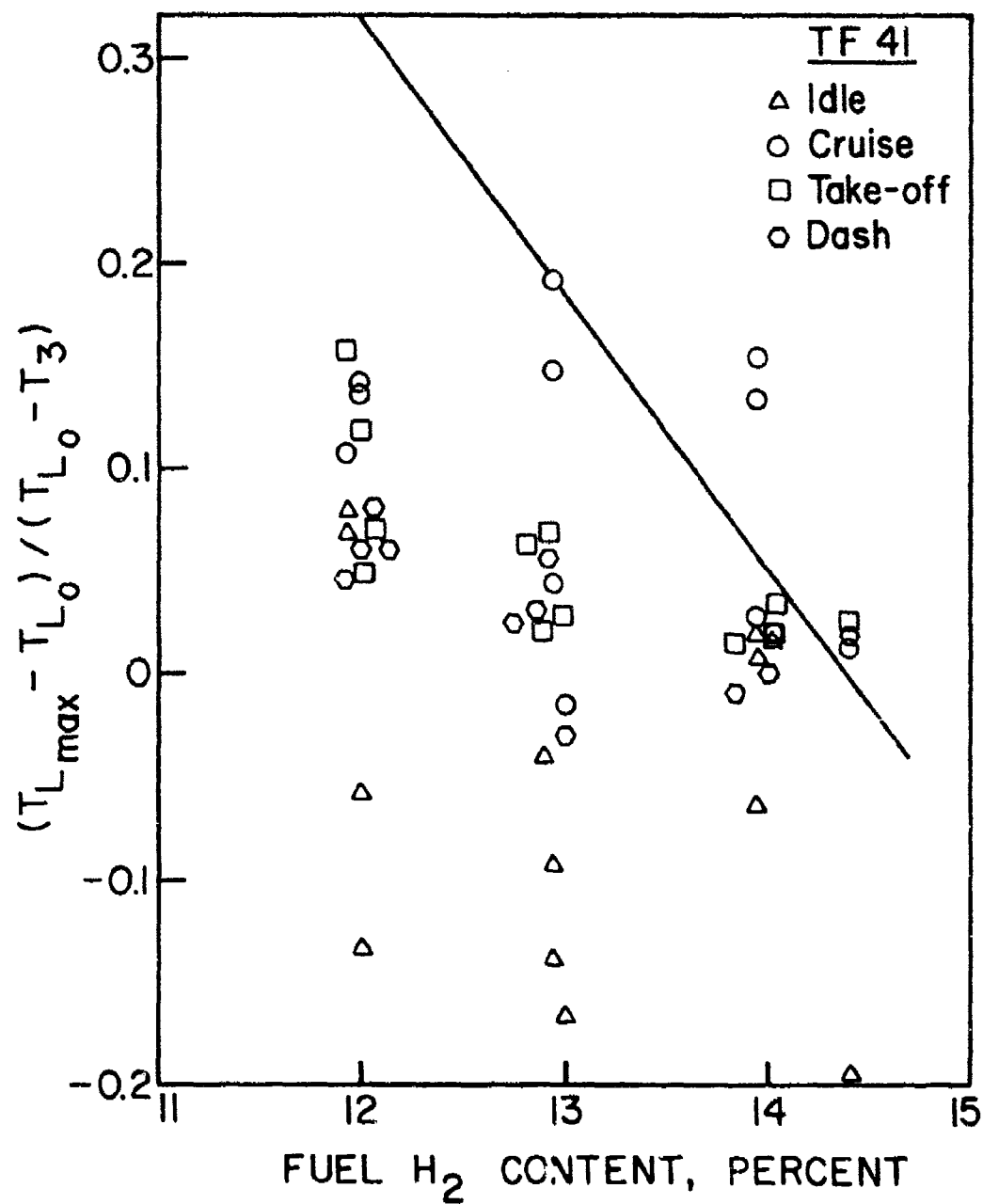


Figure 43. Effect of Fuel Hydrogen Content on Liner Temperature Parameter for TF 41 Combustor.

to determine, this would appear to be a serious drawback to the use of this type of temperature parameter.

An alternative approach attempted here was to find a relationship between fuel hydrogen content and luminosity factor. Analysis of the experimental data led to the following expression

$$L = 336/(\text{percent hydrogen})^2 \quad (45)$$

Substitution of this value of  $L$  into Eq. (4i) allows calculations of flame radiation to be carried out for all fuels over the entire range of test conditions.

## 2. External Radiation, $R_2$

The radiation heat transfer from the liner wall to the outer casing,  $R_2$ , can be approximated by assuming gray surfaces with emissivities  $\epsilon_w$  and  $\epsilon_c$ , and assuming that  $T_w$  and  $T_c$  are approximately uniform in the axial direction. The significance of  $R_2$  increases with liner wall temperature, and at low values it can often be neglected. It can be estimated only approximately because of lack of accurate knowledge of wall emissivities. For this reason it is sufficient to use the cooling-air temperature,  $T_3$ , in place of the unknown temperature of the outer air casing. Also, for radiation across a long annular space, the geometric shape factor can be assumed equal to unity. The expression for the net radiation flux, then reduces to

$$R_2 = \sigma \left[ \frac{\epsilon_w \epsilon_c}{\epsilon_c + \epsilon_w (1 - \epsilon_c)} \frac{A_w}{A_c} \right] (T_w^4 - T_3^4) \quad (46)$$

For a tubular chamber,  $(A_w/A_c)$  is equal to the ratio of liner to casing diameter at the section considered. For tubo-annular systems, where the depth of the annulus varies from point to point around the liner, an average value of 0.8 is used. For an annular chamber the ratio  $(A_w/A_c)$  is slightly greater than unity for the inner liner and slightly less than unity for the outer liner.

Accurate values of emissivity for various materials may be obtained from McAdams [24]. However, for most practical purposes the following expression, based on typical values of emissivity and diameter ratio, will suffice:

$$R_2 = 0.4 \sigma (T_w^4 - T_3^4) \quad (47)$$

### 3. Internal Convection, $C_1$

Of the four heat transfer processes which together determine the liner temperature, this component is the most difficult to estimate accurately. In the primary zone the gases involved are at high temperature and undergoing rapid physical and chemical change. Further difficulty is introduced by the existence within the primary zone of steep gradients of temperature, velocity and composition. Uncertainties regarding the airflow pattern, the state of the boundary-layer development and the effective gas temperature make the choice of a realistic model almost arbitrary.

In the absence of more exact data it is reasonable to assume that some form of the classical heat-transfer relation for straight pipes will hold for conditions inside a liner, using a Reynolds number index consistent with established practice for conditions of extreme turbulence. This leads to an expression of the form [20]

$$C_1 = 0.017 \left( \frac{k_g}{D_L^{0.2}} \right) \left( \frac{\dot{m}_{pz}}{A_L \mu_g} \right)^{0.8} (T_g - T_w) \quad (48)$$

#### 4. External Convection, $C_2$

This is obtained as [20]

$$C_2 = 0.020 \left( \frac{k_A}{D_{an}^{0.2}} \right) \left( \frac{\dot{m}_{an}}{A_{an} \mu_A} \right)^{0.8} (T_w - T_3) \quad (49)$$

The fluid properties are evaluated at the annulus air temperature,  $T_3$ . In practice the cooling-air temperature increases during its passage downstream, but normally this amounts to no more than a few degrees and can reasonably be neglected.

For equilibrium

$$R_1 + C_1 = R_2 + C_2 \quad (39)$$

Solution of this equation yields the wall temperature,  $T_w$ .

The value of  $T_w$  as determined by the method outlined above represents the liner wall temperature that would be obtained in the absence of internal wall cooling. Unfortunately references 1 to 6 do not contain the detailed information needed to estimate film-cooling effects on  $T_w$ . Thus, and bearing in mind the lengthy and tedious nature of the procedures involved, it was decided to calculate 'uncooled' wall temperatures for four combustors only, namely J79-17A, J79-17C, F101 and T41, in order to ascertain if the results obtained reflected anticipated trends in regard to the effect of fuel hydrogen content on liner wall temperature. The results of these calculations are shown in Figs. 44 to 47 for all fuels as plots of  $T_w$  versus hydrogen content.

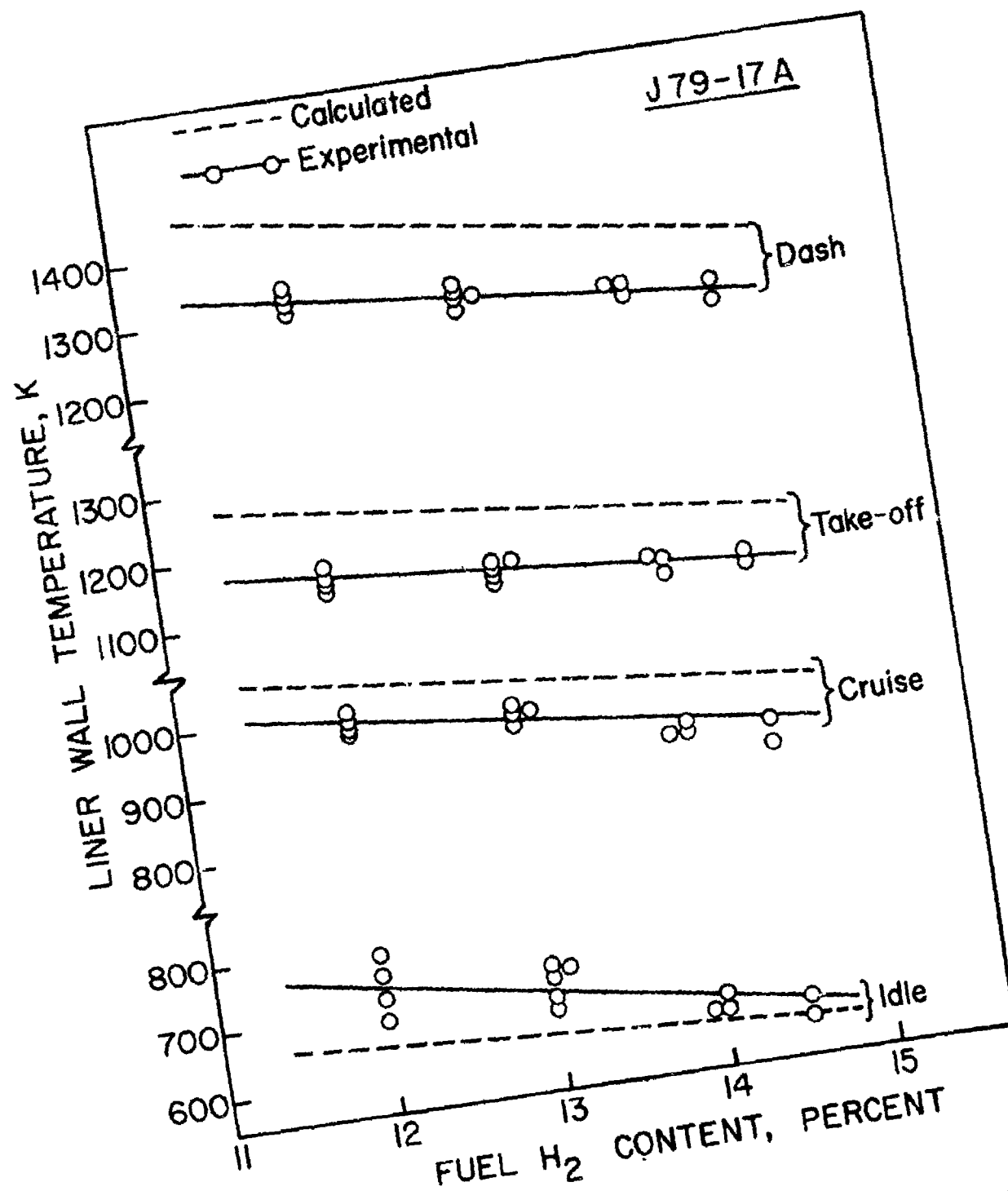


Figure 44. Comparison of Measured and Predicted Values on the Effect of H<sub>2</sub> Content on Liner Temperature for J79-17A Combustor.

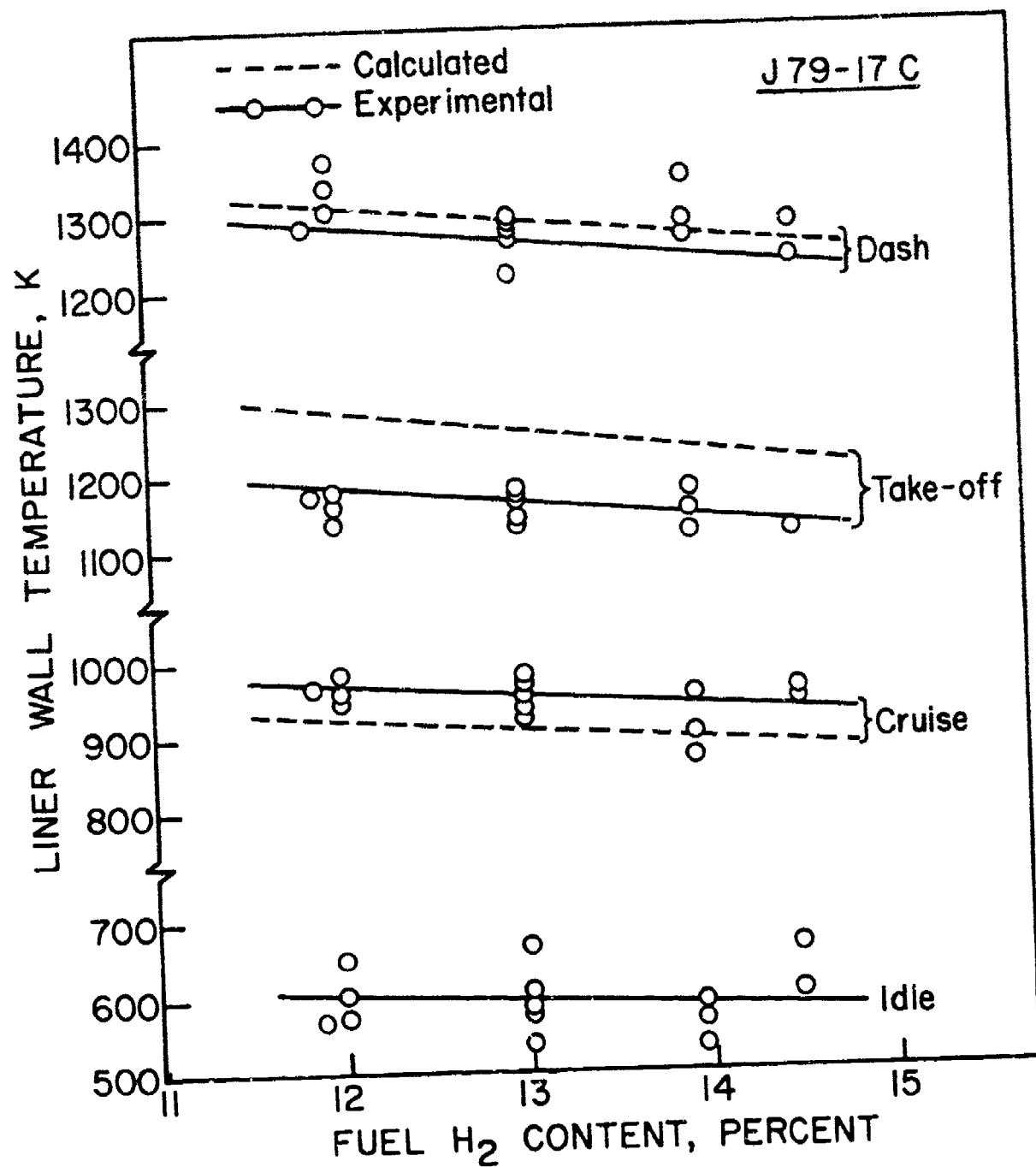


Figure 45. Comparison of Measured and Predicted Values on the Effect of H<sub>2</sub> Content on Liner Temperature for J79-17C Combustor.

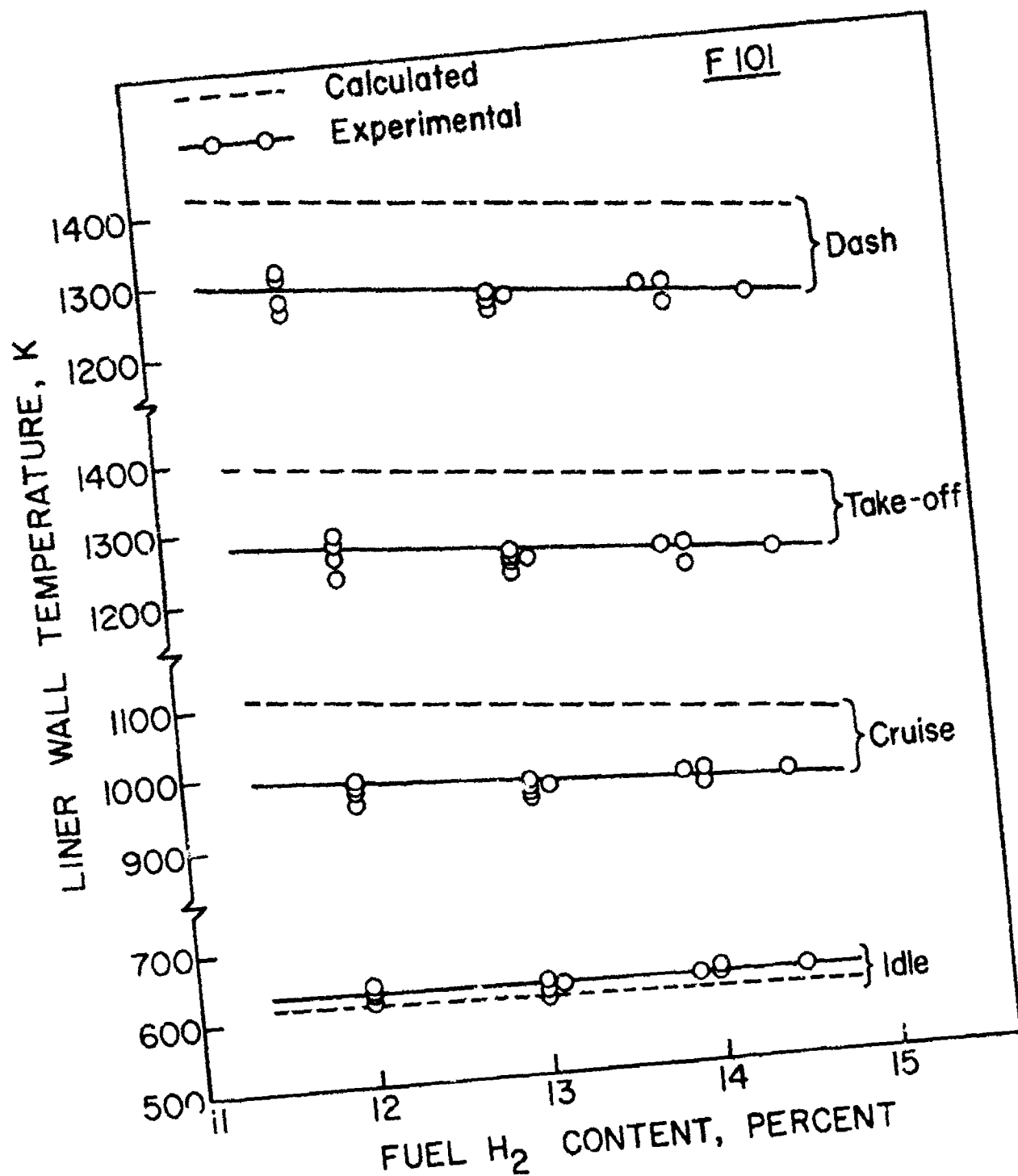


Figure 46. Comparison of Measured and Predicted Values on the Effect of H<sub>2</sub> Content on Liner Temperature for F101 Combustor.

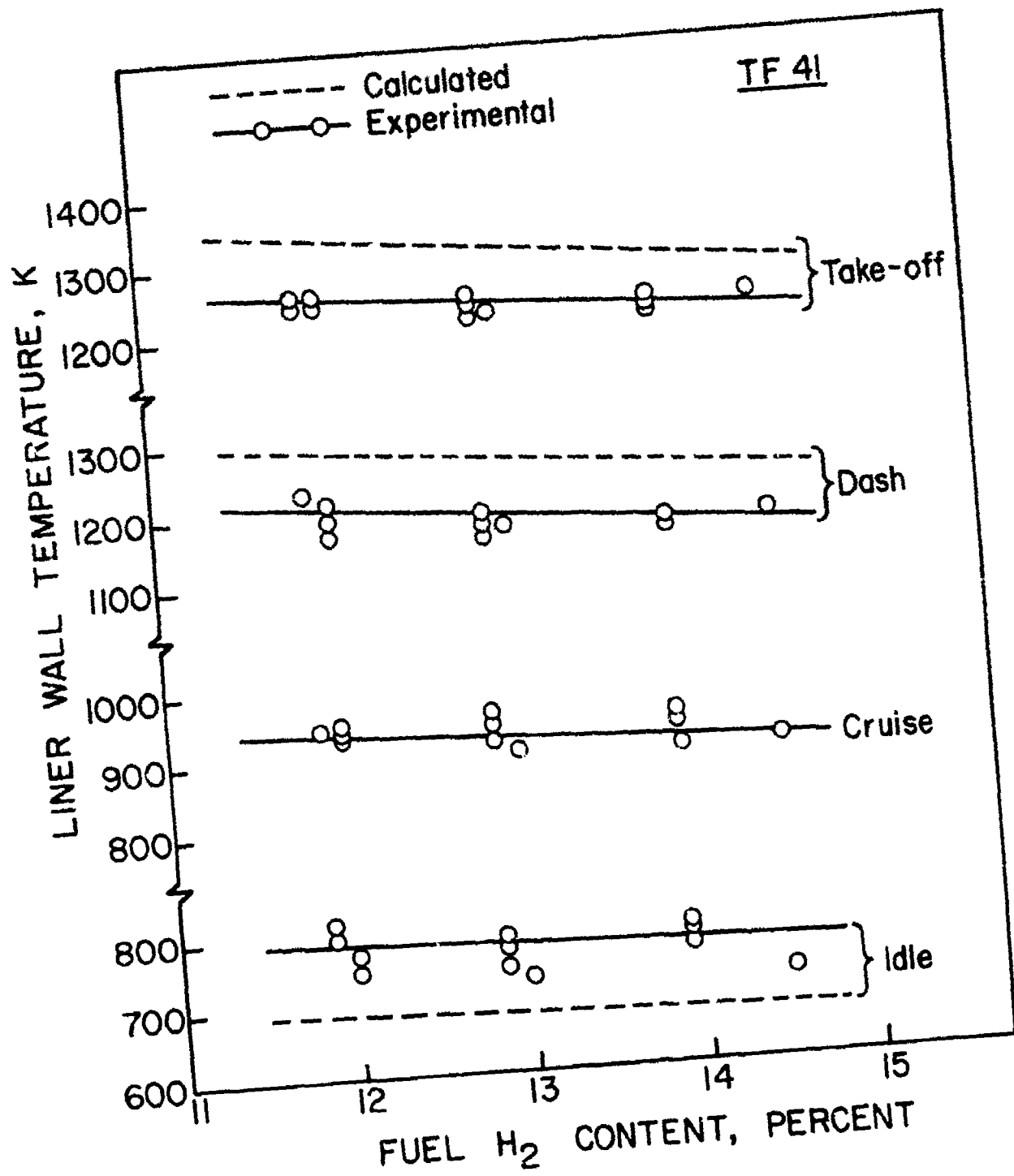


Figure 47. Comparison of Measured and Predicted Values on the Effect of H<sub>2</sub> Content on Liner Temperature for TF41 Combustor.

It may be noted in Figs. 44 to 47 that the calculated values of  $T_w$  are generally higher than the corresponding measured values due to neglect of internal wall cooling. Only at low power conditions, where the errors incurred through neglect of internal wall cooling are partially balanced by the assumption of 100 percent combustion efficiency in the combustion zone, do the measured and calculated wall temperatures roughly coincide.

These factors are not considered too serious in a study that is mainly concerned with fuel type, because they apply with equal force to all fuels. The fact that the measured and calculated values of  $T_w$  follow the same trend, as evidenced by Figs. 44 to 47, tends to support the validity of using the luminosity factor concept as a convenient means for incorporating fuel hydrogen content into the 'standard' equation for flame emissivity. Thus Eq. (41) may be rewritten as

$$\epsilon_g = 1 - \exp \left[ -97.44 P_3 (\%H_2)^{-2} (q \epsilon_b)^{0.5} T_g^{-1.5} \right] \quad (50)$$

## SECTION IX

### EMISSIONS

It is widely recognized that combustion-generated pollution is a threat to the environment, and regulative standards have been imposed to limit the pollutant emissions discharged by aircraft engines operating within or near airports [25, 26].

Smoke is the most obvious pollutant from gas turbine engines because it can be seen with the naked eye. Other pollutants of importance are carbon monoxide (CO), unburned hydrocarbons (UHC) and the oxides of nitrogen ( $\text{NO}_x$ ).

The concentration levels of most pollutants of interest in gas turbine exhausts can be related directly to the temperature, time and concentration histories that exist in the combustor. These histories vary from one combustor to another and, for any given combustor, with change in operating conditions. The nature of pollutant formation is such that the concentrations of carbon monoxide and unburned hydrocarbons are highest at low power conditions and diminish with increase in power. In contrast, oxides of nitrogen and smoke are fairly insignificant at lower power settings and attain maximum values at the highest power conditions.

#### 1. Carbon Monoxide

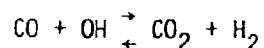
If the primary zone of a gas turbine combustor is designed to operate fuel rich, then large amounts of CO will be formed due to lack of the oxygen needed to complete the reaction to  $\text{CO}_2$ . If, however, the primary zone mixture strength is stoichiometric or moderately fuel lean, then significant amounts of CO will be present due to the dissociation of  $\text{CO}_2$ . In principle it should be possible to reduce this CO to a negligible level by the staged admission of additional air downstream

of the primary zone to achieve a gradual reduction in burned gas temperature.

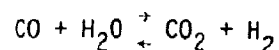
In practice, CO emissions are found to be much higher than predicted from equilibrium calculations, and to be highest at low power conditions, when peak temperatures are relatively low. This is in conflict with the predictions of equilibrium theory, and suggests that much of the CO arises from incomplete combustion of the fuel. This may be caused by one or more of the following:

1. Inadequate burning rates in the primary zone due to too low a fuel/air ratio and/or insufficient residence time.
2. Inadequate mixing of fuel and air, which produces some regions in which the mixture strength is too weak to support combustion, and others in which over-rich combustion yields high local concentrations of CO.
3. Quenching of the post-flame products by entrainment with the liner wall-cooling air. (Annular chambers, because of their lower surface/volume ratio, generally give lower CO emissions than tubular systems.)

CO is relatively resistant to oxidation, and in many practical systems its oxidation is 'rate determining' with respect to the minimum residence time and mean temperature needed for complete combustion. At high temperatures the major reaction removing CO is



This is a fast reaction over a broad temperature range. At lower temperatures the reaction



is important as a means of removing CO.

## 2. Unburned Hydrocarbons

Unburned hydrocarbons include fuel which emerges at the combustor exit in the form of droplets or vapor, and also the products of thermal degradation of the parent fuel into species of lower molecular weight, such as methane and acetylene. They are normally associated with poor atomization, inadequate burning rates, the chilling effects of film-cooling air, or any combination of these. Increase in engine power setting reduces the emission of unburned hydrocarbons, partly by improved fuel atomization, but mainly through the effects of higher inlet air pressure and temperature which together enhance chemical reaction rates in the primary combustion zone.

In general, the emissions of UHC parallel those of CO. Any factor that raises the level of CO emissions will tend to raise UHC emissions also. Conversely, any combustor/nozzle modifications carried out for the reduction of CO will usually reduce UHC also. For this reason no further consideration will be given to unburned hydrocarbons.

## 3. Oxides of Nitrogen

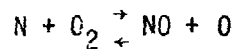
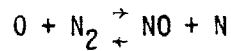
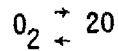
Oxides of nitrogen, of which the predominant compound at high emission levels is nitric oxide, are produced by the oxidation of atmospheric nitrogen in high-temperature regions of the flame. The process is endothermic and proceeds at a significant rate only at temperatures above around 1800 K. Thus, in contrast to CO and UHC, NO arises only in the hot central regions of the combustor, and levels are highest at full power conditions.

Nitric oxide can be produced by three different mechanisms:

1. "Thermal" NO - by oxidation of atmospheric nitrogen in the post-flame gases

2. "Prompt" NO - by high speed reactions at the flame front
3. "Fuel" NO - by oxidation of nitrogen contained in the fuel.

Thermal NO. It has been fairly well established that NO formation in combustion processes proceeds by the Zeldovich chain mechanism



The main fuel-air reaction proceeds quickly in the lean case, merely adding heat to the mixture and playing a minor role in NO formation. Free oxygen from the equilibrium dissociation of unburned oxygen molecules initiates the chain. A nitrogen atom is liberated which reacts with oxygen to form NO. Equilibrium dissociation of nitrogen molecules is not achieved at the temperatures encountered in a gas turbine combustor, and the only source of nitrogen atoms is the second reaction. The calculated equilibrium NO level rises continually as equivalence ratio is reduced at a fixed temperature, or as temperature is increased at a fixed equivalence ratio. In a practical system, temperature is not independent of equivalence ratio, and NO formation is then found to peak on the fuel-lean side of stoichiometric. This is a consequence of competition between fuel and nitrogen for the available oxygen. Although system temperature is a maximum at, or slightly on the rich side of stoichiometric, the available oxygen is then all consumed preferentially by the fuel (due to the higher rate of the exothermic fuel-oxygen reaction). At equivalence ratios below around 0.8 the fall-off in temperature is so great as to override the effect of increasing free oxygen concentration, and NO levels begin to fall.

The strong correlation between temperature and  $\text{NO}_x$  emissions was first demonstrated by Lipfert [27] for a large number of engines. Lipfert based his correlation on combustor inlet temperature, which is important only insofar as it influences the flame temperature. Roffe and Venkataramani [28] have examined the effects of combustion temperature and pressure on  $\text{NO}_x$  emissions, using propane/air mixtures. Their results conform well with the expression

$$\ln(\text{NO}_{EI}/t) = -72.28 + 2.80 \sqrt{T} - T/38 \quad (51)$$

where  $T$  is the adiabatic flame temperature, K, and  $t$  is the combustor residence time, ms. They found no effect of pressure over the range from 0.5 to 3 MPa. This is in accordance with expectations, since the reaction  $\text{N}_2 + \text{O}_2 = 2\text{NO}$  involves no volume change.

The effect of residence time on  $\text{NO}_x$  emissions was examined by Anderson [29] using a premixed/prevaporized combustor supplied with gaseous propane fuel. His results show that  $\text{NO}_x$  emissions increase with increase in residence time except for very lean mixtures ( $\phi \approx 0.4$ ) where the rate of formation is so low that it becomes fairly insensitive to time.

Prompt NO. Under certain conditions, and especially in low temperature, fuel-rich flames, NO is found very early in the flame region, which is in conflict with the idea of a kinetically slow overall process. The mechanisms involved are not yet fully understood, but it has been shown that the enhanced reaction rates are a result of interactions between the many intermediate species that are produced during the main hydrocarbon - CO -  $\text{CO}_2$  reactions [30].

Although prompt NO levels cannot be predicted with any degree of precision, for the conditions that exist in modern combustors it is likely

that they will be between 0 to 30 ppm V, with low values occurring at high temperature, lean combustion and the higher values at low temperature, fuel-rich conditions.

Fuel NO. If fuels contain organically bounded nitrogen, then some of this nitrogen will eventually form the so-called "fuel NO." The percentage of nitrogen undergoing this change depends on the nature of the combustion process. With light distillate fuels, the content of organic nitrogen is small, usually less than 0.06 percent. Only with heavy distillates is the content of organic nitrogen high enough to yield significant amounts of fuel NO.

#### 4. NO<sub>2</sub> Emissions

The NO produced in combustion is oxidized to NO<sub>2</sub> as soon as the low temperatures required for this reaction are reached after leaving the engine. The transformation from NO into NO<sub>2</sub> actually begins in the combustor in zones of considerable excess air. At full load the fraction of NO<sub>2</sub> formed within the combustor is very small but, at idle conditions the NO<sub>2</sub> level may be as much as 50 percent of the total NO<sub>x</sub> (NO + NO<sub>2</sub>) emissions [31, 32].

#### 5. Smoke

Exhaust smoke is caused by the production of finely-divided soot particles in fuel-rich regions of the flame, and may be generated in any part of the combustion zone where mixing is inadequate. With pressure atomizers the main soot-forming region lies inside the fuel spray at the center of the combustor. This is the region in which the recirculating burned products move upstream toward the fuel spray, and where local pockets of fuel vapor are enveloped in oxygen-deficient gases at high

temperature. In these fuel-rich regions soot may be produced in considerable quantities.

Most of the soot produced in the primary zone is consumed in the high temperature regions downstream. Thus from a smoke viewpoint a combustor may be considered to comprise two separate zones, first, the primary zone, which governs the rate of soot formation and, second, the intermediate zone (and, on modern high temperature engines, the dilution zone also) which determines the rate of soot consumption. The soot concentration actually observed in the exhaust gases is an indication of the dominance of one zone over the other.

Soot is not an equilibrium product of combustion except at mixture strengths far richer than those employed in the primary zones of combustors. Thus it is impossible to predict its rate of formation and final concentration from kinetic or thermodynamic data. In practice, the rate of soot formation tends to be governed more by the physical processes of atomization and fuel-air mixing than by kinetics.

Many specific mechanistic models for soot formation have been proposed. Current thinking tends to favor the notion that condensed ring aromatic hydrocarbons may produce soot via a different mechanism than do aliphatic hydrocarbons. Aromatic hydrocarbons can produce soot via two mechanisms: (1) condensation of the aromatic rings into a graphite-like structure, or (2) breakup to small hydrocarbon fragments which then polymerize to form larger, hydrogen-deficient molecules which eventually nucleate and produce soot. Based on his shock tube studies, Graham [33, 34] concludes that the condensation route is much faster than the fragmentation/polymerization route. According to this simple model, aliphatics produce soot via the fragmentation/polymerization mechanism only. As a result, these hydrocarbons

do not form the quantities of soot produced by the aromatics. Indeed, during the fuel-rich combustion of a fuel blend composed of aromatics and aliphatics, the aromatic hydrocarbons would produce the major quantity of soot. Combustion of the aliphatic portions of the fuel would influence temperature and hydrocarbon fragment concentration but soot formation via fragmentation/polymerization would be minimal.

Experimental data obtained by Blazowski [35] using various blends of iso-octane and toluene fuels were found to be consistent with this model. However, the results of an experimental study by Naegeli and Moses [36] suggest that the picture will be more complicated for fuels with high concentrations of polycyclic aromatics.

For gas turbine combustors the main controlling factors for soot formation and smoke have been determined experimentally as fuel properties, combustion pressure and temperature, fuel/air ratio, atomization quality and mode of fuel injection [37 to 50].

Influence of Fuel Properties. Fuel properties can influence smoke production in two ways: firstly, by inducing the formation of local over-rich fuel regions and, secondly, by exerting variable resistance to carbon formation. The former is controlled by physical properties such as viscosity and volatility which affect the mean drop size, penetration and rate of evaporation of the fuel spray, whereas the latter relates to molecular structure. It is well established that smoking tendency increases with reduction in hydrogen content [51]. However, it is of interest to note that Naegeli and Moses [36] found that fuels containing high concentrations of polycyclic aromatics produced more soot than would be expected from a correlation based solely on hydrogen content.

Influence of Pressure. Problems of soot and smoke are always most severe at high pressures. There are several reasons for this, some of which derive from chemical effects, while others stem from physical factors which affect spray characteristics and hence also the distribution of mixture strength in the soot-generating regions of the flame [38, 43-45]. For premixed kerosine-air flames it is found that no soot is formed at pressures below around 0.6 MPa, or at equivalence ratios below about 1.3 [42]. One adverse effect of increase in pressure is to extend the limits of flammability, so that soot is produced in regions which, at lower pressures, would be too rich to burn. Increase in pressure also accelerates chemical reaction rates, so that combustion is initiated earlier and a larger proportion of the fuel is burned in the fuel-rich regions adjacent to the spray. With pressure atomizers of the duplex or dual-orifice type, reduced spray penetration is one of the main causes of smoke at high pressures [45]. Thus whereas at low pressures the fuel is distributed across the entire combustion zone, at high pressures it tends to concentrate in the soot-forming region just downstream of the nozzle. Another adverse effect of an increase in pressure is to reduce the cone angle of the spray. This encourages soot formation, partly by increasing the mean drop size, but mainly by raising the mixture strength in the soot-forming zone. The total effect of all these factors is that smoke emission increases steeply with pressure. Airblast atomizers are spared these problems because the fuel drops they produce are always airborne and their distribution throughout the combustion zone is dictated solely by the liner airflow pattern which is not susceptible to changes in pressure.

Influence of Temperature. Combustor inlet temperature tends to influence many variables in the carbon formation process, so that the effect of a change in  $T_3$  on exhaust smoke is not always clear. However, it is well established that increase in combustor outlet temperature reduces smoke by extending the soot consumption region downstream into the dilution zone where there is ample air to burn up the soot, provided there is sufficient temperature also.

Influence of Fuel/Air Preparation. Soot is formed only in fuel-rich regions of the flame. Thus all that is needed to eliminate soot and smoke is to ensure that nowhere in the flame region does the equivalence ratio exceed around 1.3. However, even when the overall equivalence ratio in the primary zone is well below 1.3, imperfections in fuel-air mixing can create local regions in which pockets of fuel-rich mixture are enveloped in oxygen-deficient gases at high temperature, leading to high rates of soot formation. The superior performance of the airblast atomizer is due partly to better atomization but also to the thorough fuel-air mixing incurred in the atomization process prior to combustion, which effectively eliminates fuel-rich pockets from the combustion zone.

In practice it is found that, even at the worst conditions, only a very small fraction of the fuel carbon is converted to soot, and almost all of this is oxidized in the regions downstream of the primary combustion zone [44]. Appleton [52] has developed a method for calculating the size reduction experienced by a carbon particle as it travels through a mixture of known pressure, temperature and composition. For conditions typical of the gas turbine, this method predicts that all particles below  $0.04 \mu\text{m}$  will be oxidized, and that the maximum rate of oxidation proceeds at an equivalence ratio of approximately 0.75. A similar conclusion was

reached by Fenimore and Jones [53] who found evidence that as soot aggregates increase in size they become more resistant to oxidation. According to these workers a soot-bearing flame ought to burn smoke-free if the carbon aggregates are less than  $0.01\ \mu\text{m}$ , no matter how many are present.

#### 6. Prediction of Emissions Characteristics

Many attempts have been made to model gas turbine combustors with a view to predicting their emission characteristics. Most modeling has been concerned with  $\text{NO}_x$  emissions, but efforts have also been made to predict the formation of other important pollutant species. To be successful a model must accommodate the complex flow behavior and include a kinetic scheme of the important chemical reactions occurring within the combustor. The kinetics of some relevant combustion processes are, unfortunately, not well understood at the present time, particularly for the production of carbon, carbon monoxide and the hydrocarbon species that are intermediaries in the fuel oxidation process.

The primary requirement for a satisfactory emissions model for gas-turbine combustors is that it should represent an optimum balance between accuracy of representation, utility, ease of use, economy of operation, and capability for further improvement. In recent years considerable effort has been directed toward the development of relatively complex mathematical emissions models that can be applied to gas turbines. They have varied in level of sophistication from those with potential to yield a complete description of the relevant thermodynamic and chemical properties as a function of spatial location within the combustor, to others which merely assume that homogeneous conditions exist at all axial stations [54-63].

The high cost and complexity of the more sophisticated mathematical models, combined with the somewhat dubious value of the results obtained, have encouraged the development of semi-empirical models for  $\text{NO}_x$  and CO emissions. Hung's approach to the modeling of  $\text{NO}_x$  emissions places more emphasis on the physical processes considered to be important and delegates chemical kinetics to a relatively minor role [64]. His analysis includes a five-region combustor internal flowfield model, fuel distribution models for liquid and gaseous fuels, a single overall hydrocarbon complete combustion model, a nitric oxide formation model based on the Zeldovich mechanism, a diffusion-limited complete mixing model, and a model to account for the influence of ambient humidity. This model has been used successfully in predicting the influence on  $\text{NO}_x$  emissions of water injection and wide variations in fuel type [64-67].

Other successful semi-empirical models for predicting emissions have been developed by Fletcher and Heywood [55, 68] and by Hammond and Mellor [69-71]. Useful critical evaluations of both mathematical and semi-empirical prediction methods have been made by Rubins and Marchionna [72], Sullivan and Mas [73], and Odgers [74].

Empirical models can also play an important role in the design and development of low emission combustors. They may serve to reduce the complex problems associated with emissions to forms which are more meaningful and tractable to the combustion engineer, who often requires only an insight and a quick estimate of the levels attainable with the design variables at his disposal. They also permit more accurate correlations of emissions for any one specific combustor than can be achieved by the more general, analytical models discussed previously.

## 7. $\text{NO}_x$ and CO

In attempting to derive an empirical model for emissions, emphasis is placed on CO and  $\text{NO}_x$ . This is because the highly complex and unknown nature of the hydrocarbon oxidation reaction makes it impossible to derive satisfactory models for UHC and smoke. Moreover, it is known that reduction in CO and  $\text{NO}_x$  will also ensure lower levels of UHC and smoke, respectively.

It may be assumed for both nitric oxide and carbon monoxide that their exhaust concentration is proportional to the product of three terms which are selected to represent the following:

1. Mean residence time in the combustion zone.
2. Chemical reaction rates, and
3. Mixing rates.

Expressions for these three parameters may be derived in simplified form as:

$$1. \text{ Residence time} = \frac{L}{U} = \frac{L \rho A}{\dot{m}_A} = \frac{PV}{\dot{m}_A RT}$$

$$\text{i.e., residence time} \propto \left( \frac{PV}{\dot{m}_A T} \right)$$

2. It is assumed that reaction rates are a function of pressure and temperature only, i.e.

$$\text{reaction rate} \propto P^m \exp(zT) \text{ for } \text{NO}_x$$

$$\text{and reaction rate} \propto P^n \exp(cT) \text{ for CO.}$$

3. It is assumed that mixing rates are a function of liner pressure drop. Specifically we have

$$\text{mixing rate} \propto \left( \frac{\Delta P}{P} \right)^x$$

Thus  $NO_x = f(\text{residence time})(\text{reaction rate})(\text{mixing rate})$

or

$$NO_x = A \left( \frac{PV}{\dot{m}_A T} \right) \left( \frac{\Delta P}{P} \right)^x P^m \exp(zT)$$

$$= \frac{AV_C (\Delta P/P)^x P^y \exp(zT)}{\dot{m}_A T} \quad (52)$$

where  $y = 1 + m$ , and  $A$  is a constant.

Similarly, for CO we have

$$CO = f(\text{residence time})^{-1}(\text{reaction rate})(\text{mixing rate})$$

or

$$CO = C \left( \frac{\dot{m}_A T}{PV_C} \right) \left( \frac{\Delta P}{P} \right)^a P^n \exp(-cT)$$

$$= C V_C^{-1} \dot{m}_A T (\Delta P/P)^a P^b \exp(-cT) \quad (53)$$

where  $b = n - 1$ , and  $C$  is a constant.

It is recognized that the above equations have no strong theoretical foundation. However, they do embody the main variables of combustor size, pressure loss, flow proportions and operating conditions of inlet pressure, temperature and air mass flow. The effect of variations in overall combustor fuel/air ratio is also included via its influence on primary-zone temperature. Fuel type affects both flame temperature and mean drop size. For  $NO_x$  drop size is unimportant since, at the high pressure conditions where  $NO_x$  emissions are most prominent, the fraction of the total combustion volume employed in fuel evaporation is so small that wide variations in fuel drop size have a negligible

effect on  $\text{NO}_x$  emissions. However, at low pressure operation where CO emissions attain their highest concentrations, a significant proportion of the primary-zone volume is needed to evaporate the fuel. Under these conditions, any factor that influences fuel evaporation rates, such as evaporation constant, or mean drop size, will have a direct effect on the volume available for chemical reaction and, therefore, on the emissions of CO and UHC. Thus, for the correlation of CO data the effects of fuel type cannot be ignored. The manner in which they may be introduced conveniently into the equation for CO emissions is illustrated below. From analysis of the experimental data contained in references [1 to 6] it was found for Eq. (52) that

$$A = 9 \times 10^{-8}, x = 0, y = 1.25, z = 0.01.$$

For Eq. (53) the results show that

$$C = 86, a = -0.5, b = -1.5, c = 0.00345$$

Substituting these values into Eqs. (52) and (53) gives

$$\text{NO}_x = \frac{9 \times 10^{-8} p_3^{1.25} v_c \exp(0.01 T_{st})}{\dot{m}_A T_{pz}} \quad \text{g/kg} \quad (54)$$

$$\text{CO} = \frac{86 \dot{m}_A T_{pz} \exp(-0.00345 T_{pz})}{\left( v_c - 0.55 \frac{f_{pz} \dot{m}_A D_o^2}{\rho_{pz} \lambda_{eff}} \right) \left( \frac{\Delta P_L}{p_3} \right)^{0.5} p_3^{1.5}} \quad \text{g/kg} \quad (55)$$

From Eq. (54) it may be noted that the only influence of fuel type on  $\text{NO}_x$  formation is via the two temperature terms  $T_{pz}$  and  $T_{st}$ . The former is calculated as

$$T_{pz} = T_3 + \Delta T_{pz}$$

where  $\Delta T_{pz}$  is the temperature rise due to combustion corresponding to the inlet temperature,  $T_3$ , and fuel/air ratio,  $(q_{ov}/f)$ .  $T_{st}$  is the stoichiometric flame temperature corresponding to the inlet temperature,  $T_3$ . Equation (54) suggests that in the combustion of heterogeneous fuel-air mixtures it is the stoichiometric flame temperature that determines the formation of  $NO_x$ . However, for the residence time in the combustion zone, which is also significant to  $NO_x$  formation, the appropriate temperature term is the bulk value,  $T_{pz}$ , as indicated in the denominator of Eq. (54).

Equation (54) is suitable for conventional spray combustors only. For lean premix/prevaporize combustors, in which the maximum attainable temperature is  $T_{pz}$ , Eq. (54) may still be used, provided that  $T_{pz}$  is substituted for  $T_{st}$ . It should also be noted that predictions of  $NO_x$  based on Eq. (54) tend to be too high when the overall combustor air/fuel ratio exceeds a value of around 100. This is because with diminishing fuel/air ratio the flame shrinks back toward the fuel nozzle and no longer occupies the entire combustion volume,  $V_c$ . However, this is not considered a serious drawback since, in practice, interest is normally focused on conditions of high fuel/air ratio, where  $NO_x$  formation rates attain their highest values.

The excellent correlation of experimental data on  $NO_x$  provided by Eq. (54) is illustrated in Figs. 48 to 58. These figures include all combustors except the J85 for which the measured values are too low for satisfactory correlation.

The formation of CO in the primary combustion zone takes appreciably longer than the time required to produce  $NO_x$ . In consequence, the relevant temperature is not the local peak value adjacent to the evaporating

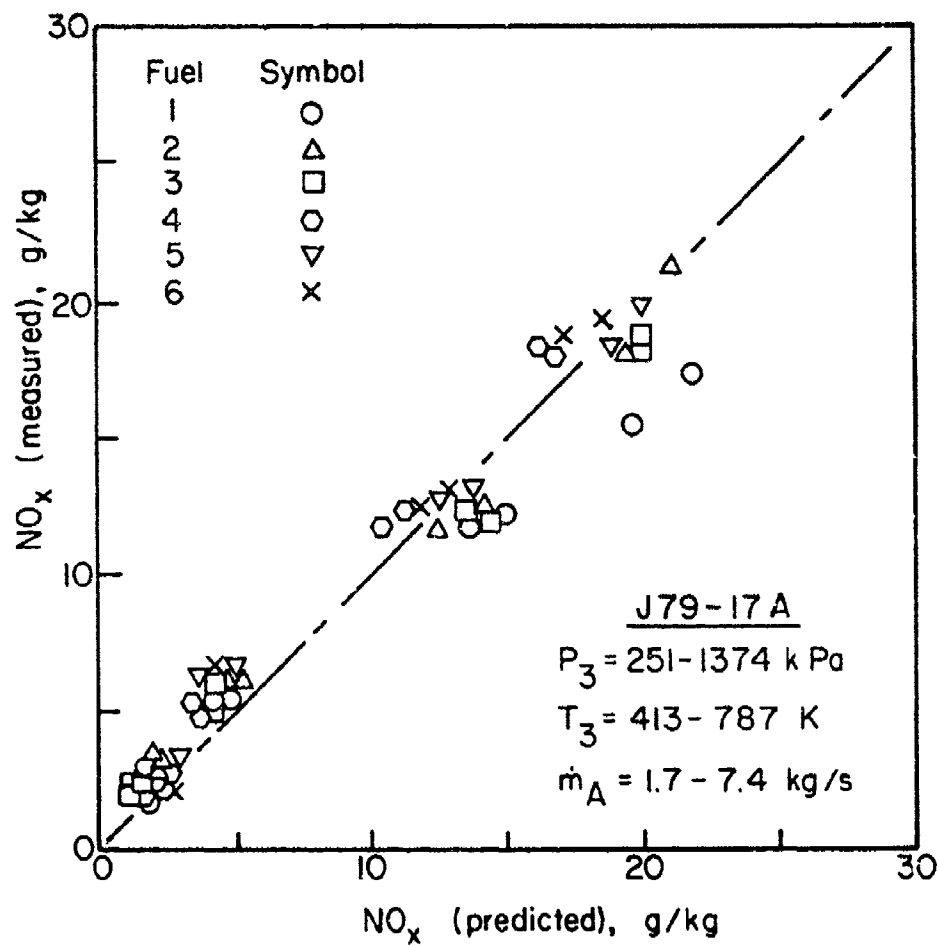


Figure 48. Comparison of Measured and Predicted Values of  $\text{NO}_x$  Emissions for J79-17A Combustor. (Fuels 1 to 6).<sup>x</sup>

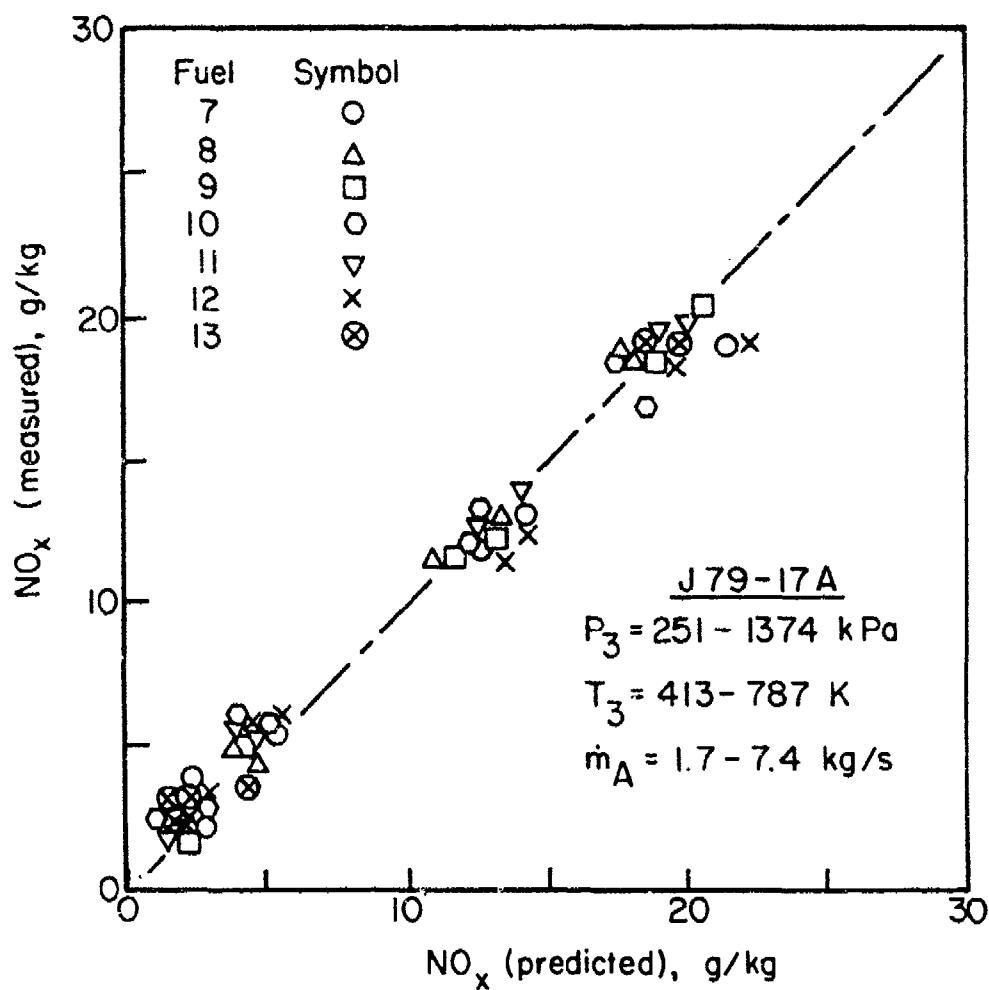


Figure 49. Comparison of Measured and Predicted Values of  $\text{NO}_x$  Emissions for J79-17A Combustor. (Fuels 7 to 13).

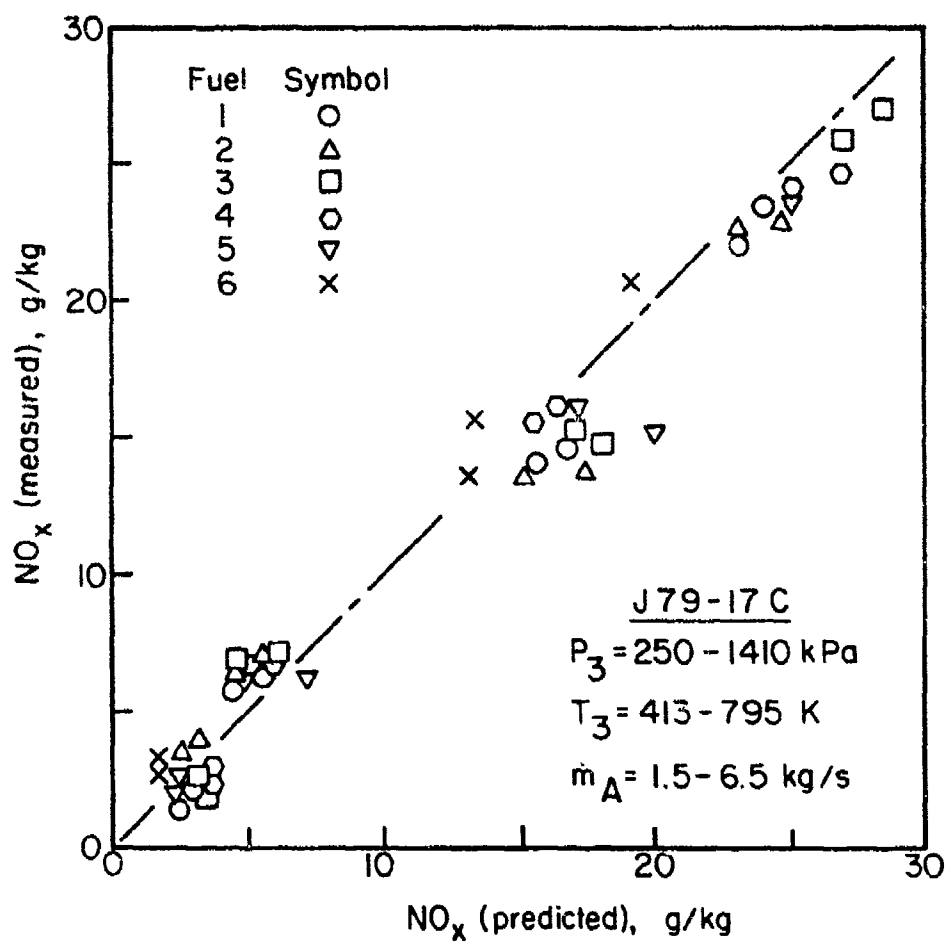


Figure 50. Comparison of Measured and Predicted Values of NO<sub>x</sub> Emissions for J79-17C Combustor. (Fuels 1A to 6A).

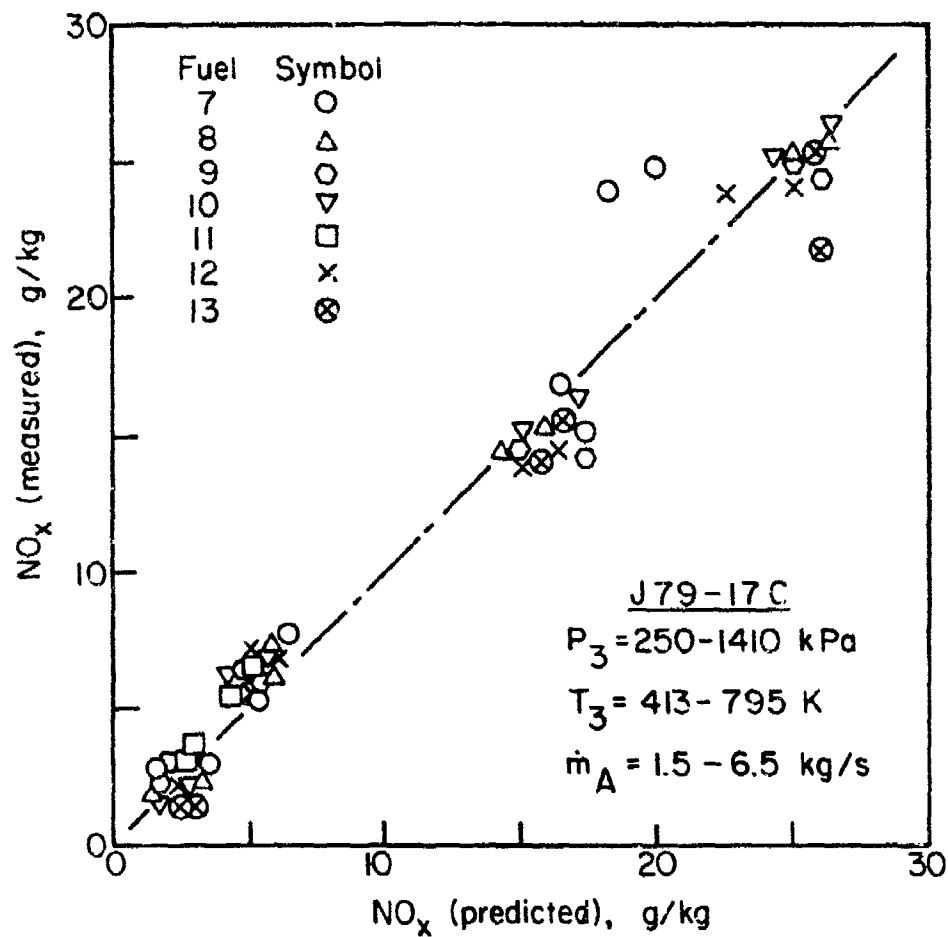


Figure 51. Comparison of Measured and Predicted Values of NO<sub>x</sub> Emissions for J79-17C Combustor. (Fuels 7A to 13A).

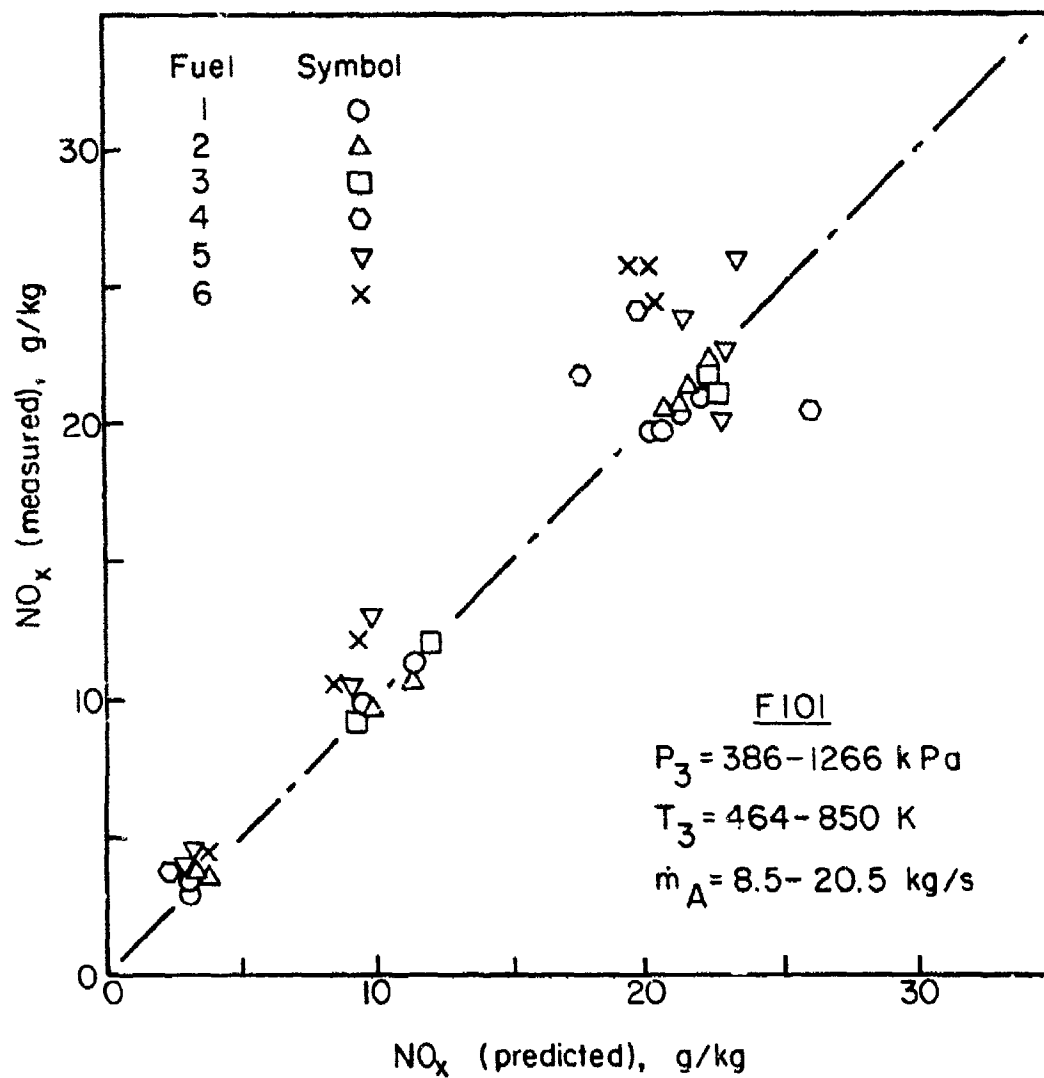


Figure 52. Comparison of Measured and Predicted Values of  $\text{NO}_x$  Emissions for F101 Combustor. (Fuels 1 to 6).

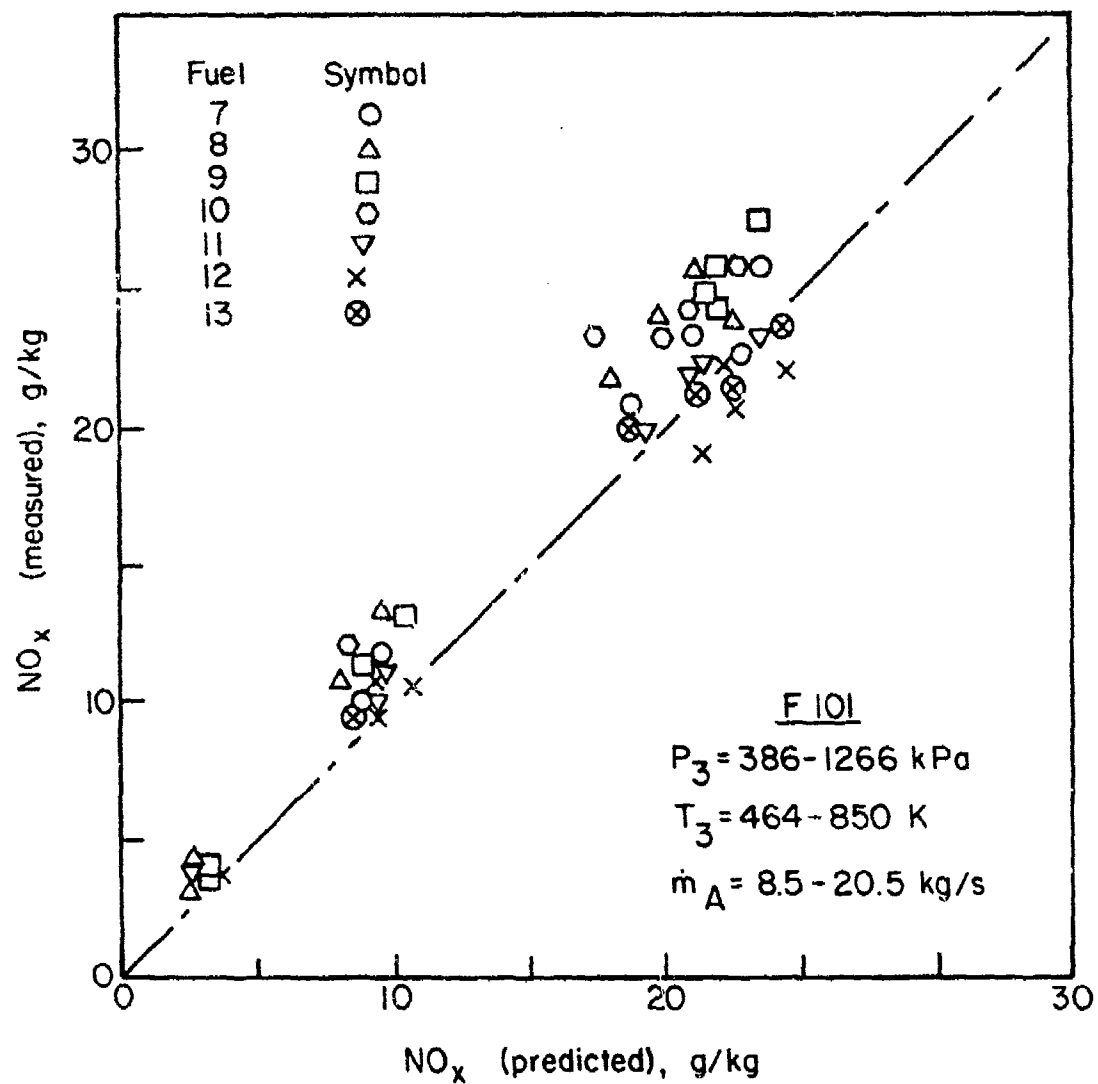


Figure 53. Comparison of Measured and Predicted Values of NO<sub>x</sub> Emissions for F101 Combustor. (Fuels 7 to 13).

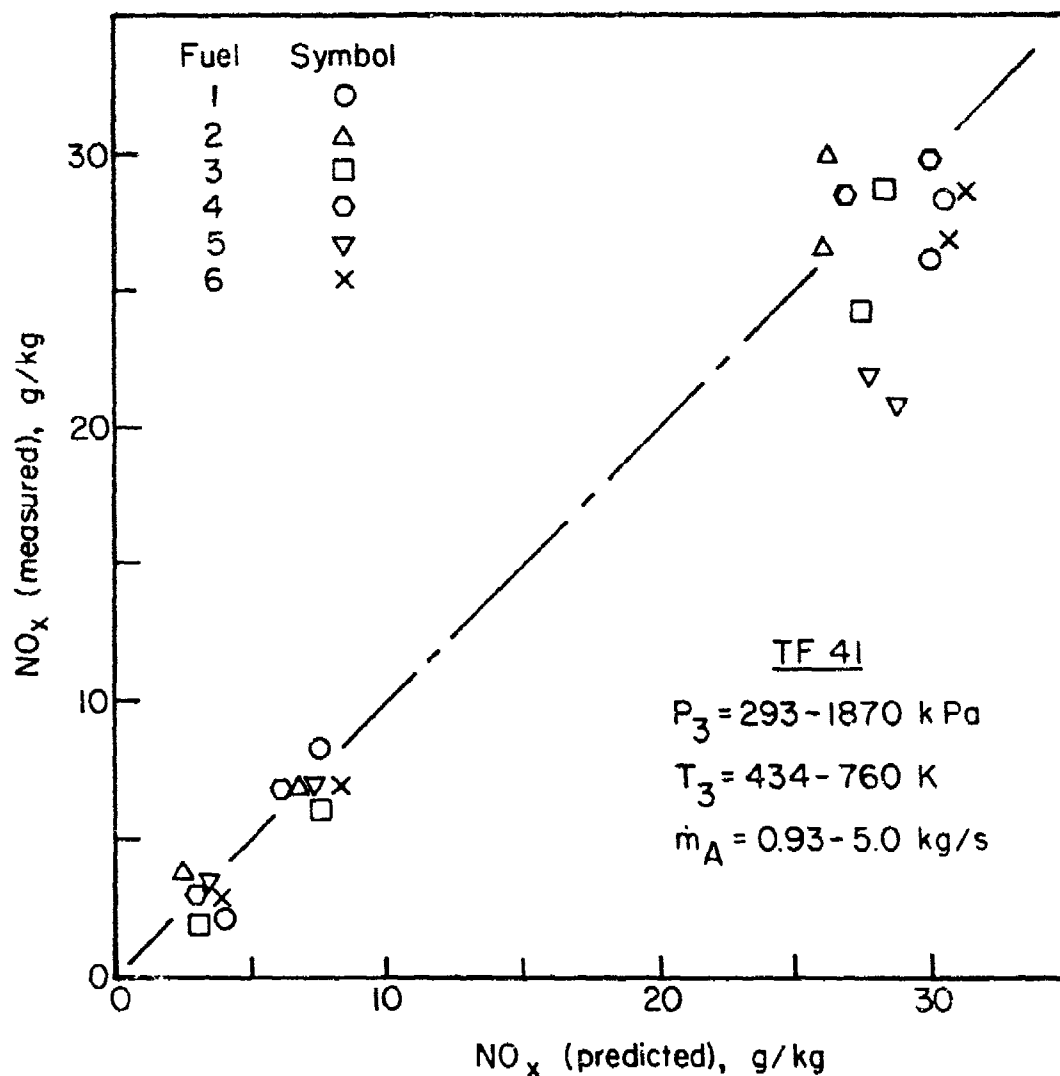


Figure 54. Comparison of Measured and Predicted Values of  $\text{NO}_x$  Emissions for TF 41 Combustor. (Fuels 1 to 6).<sup>x</sup>

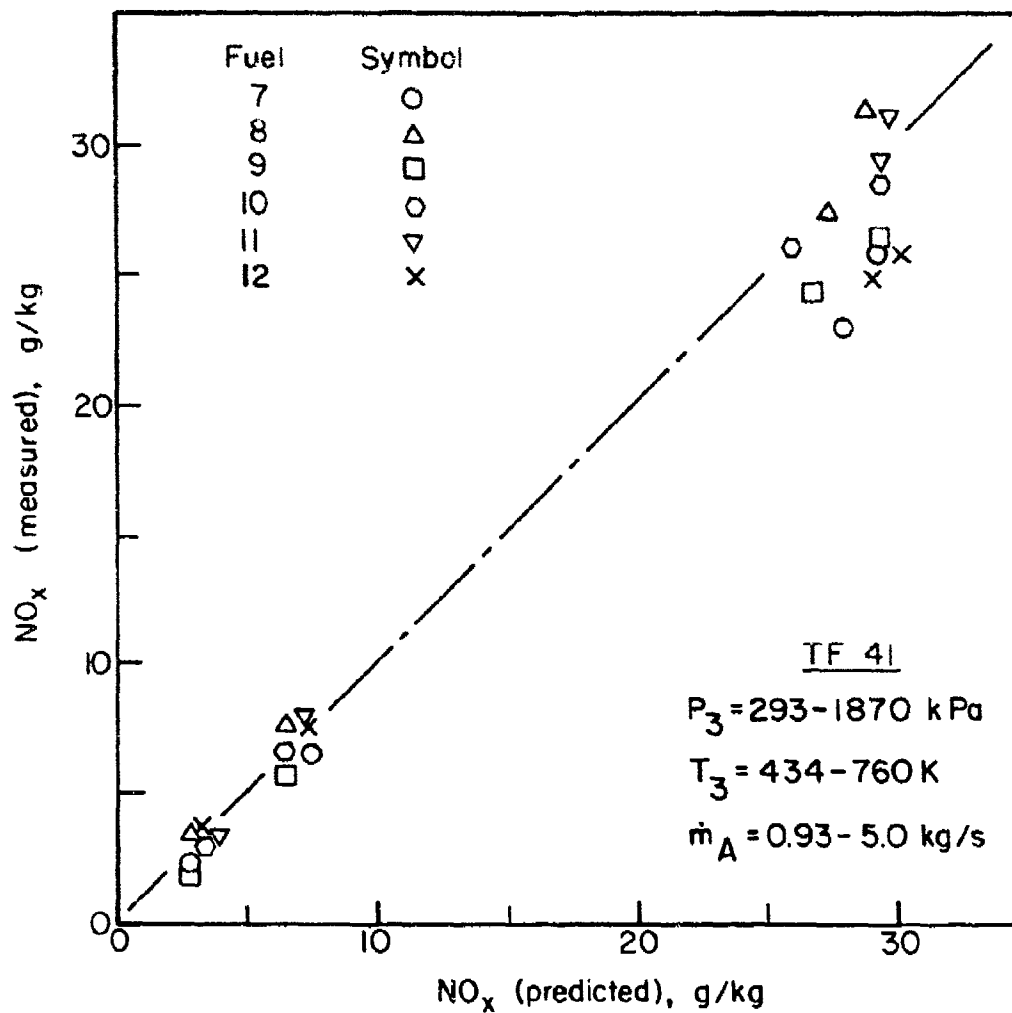


Figure 55. Comparison of Measured and Predicted Values of  $\text{NO}_x$  Emissions for TF 41 Combustor. (Fuels 7 to 12).<sup>x</sup>

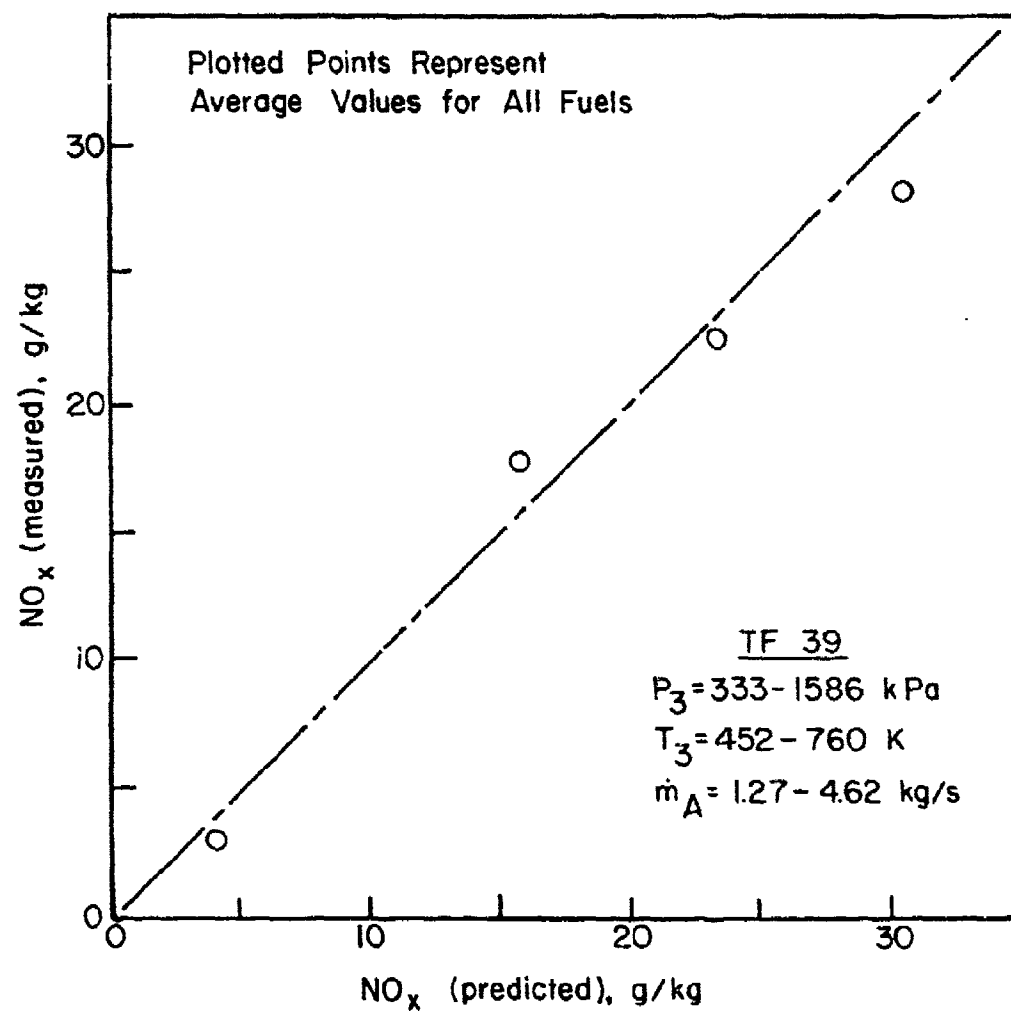


Figure 56. Comparison of Measured and Predicted Values of NO<sub>x</sub> Emissions for TF39 Combustor.

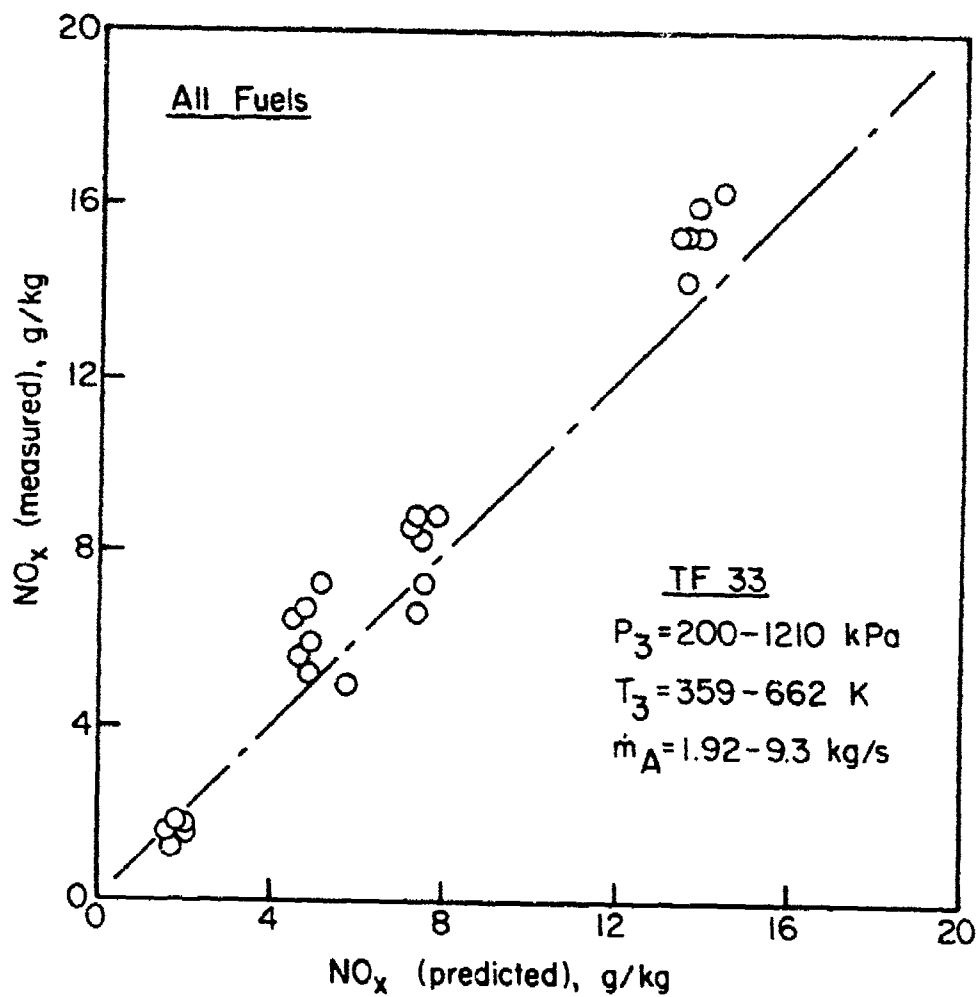


Figure 57. Comparison of Measured and Predicted Values of  $\text{NO}_x$  Emissions for TF 33 Combustor.

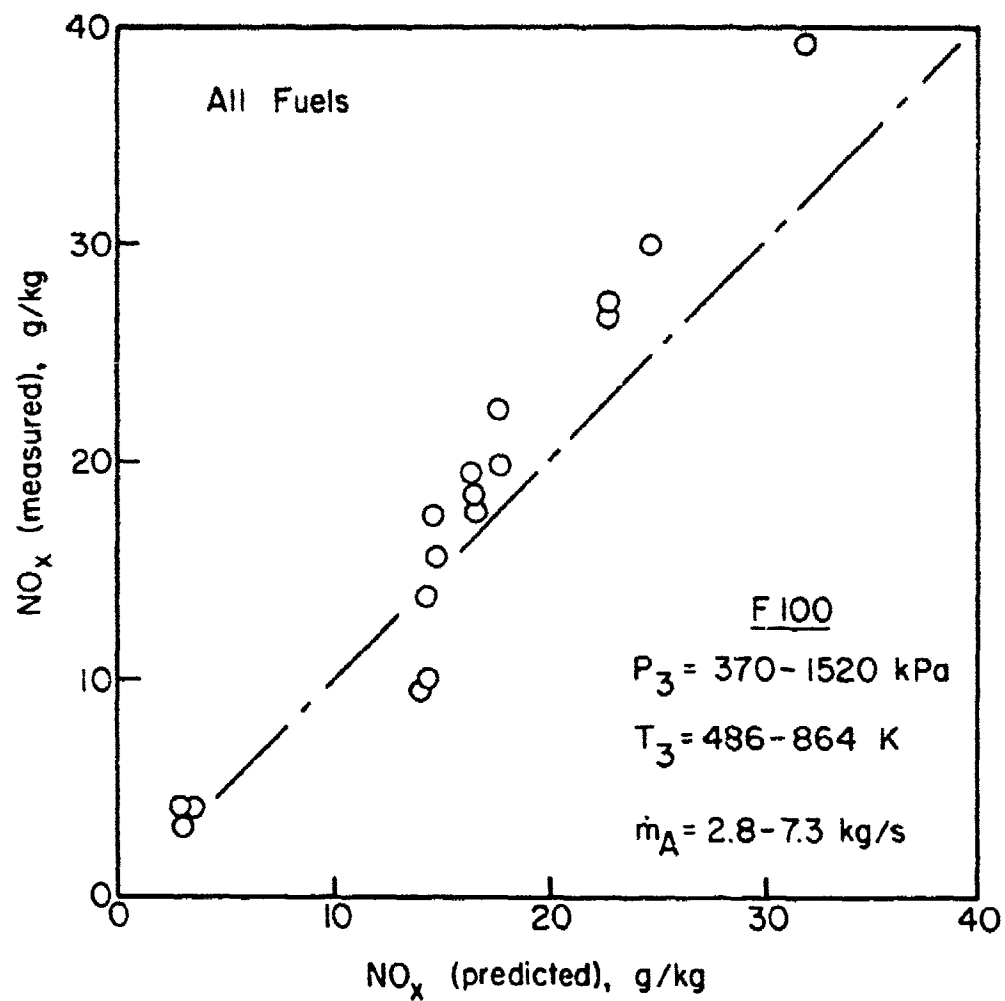


Figure 58. Comparison of Measured and Predicted Values of NO<sub>x</sub> Emissions for F100 Combustor.

fuel drops, but the average value throughout the primary zone, namely  $\bar{T}_{pz}$ . Also, because CO emissions are most important at low pressure conditions, where evaporation rates are relatively slow, it is necessary to reduce the combustion volume,  $V_c$ , by the volume occupied in fuel evaporation,  $V_e$ . This is given by (see Pattern Factor Section)

$$V_e = 0.55 f_{pz} \dot{m}_A D_0^2 / \rho_{pz} \lambda_{eff} \quad (56)$$

It is of interest to note the inclusion of a pressure loss term in Eq. (55). This suggests that the higher turbulence created by an increase in liner pressure drop promotes better mixing in the combustion zone and helps to eliminate the rich and weak pockets of fuel-air mixture, both of which are conducive to high rates of CO formation.

The very satisfactory correlation of experimental data on CO emissions obtained with Eq. (55) is illustrated in Figs. 59 to 63, for J79-17A, J79-17C, F101, TF41 and F100 combustors respectively.

#### 8. Smoke

In order to express smoke emissions in the same basic units as those employed for  $NO_x$  and CO, the first step must be to convert the smoke numbers (SN) quoted in references [1 to 6] to soot concentrations ( $X_c$ ) expressed in mg/kg. This conversion was accomplished using the following different factors for different levels of smoke number [75].

SN = 0 to 1	$X_c = 0.1$ (SN)
SN = 1 to 5	$\log X_c = 0.136$ (SN) - 1.136
SN = 5 to 10	$\log X_c = 0.06265$ (SN) - 0.769
SN = 10 to 20	$\log X_c = 0.03187$ (SN) - 0.4614
SN = 20 to 30	$\log X_c = 0.0301$ (SN) - 0.426
SN > 30	$\log X_c = 0.02538$ (SN) - 0.2845

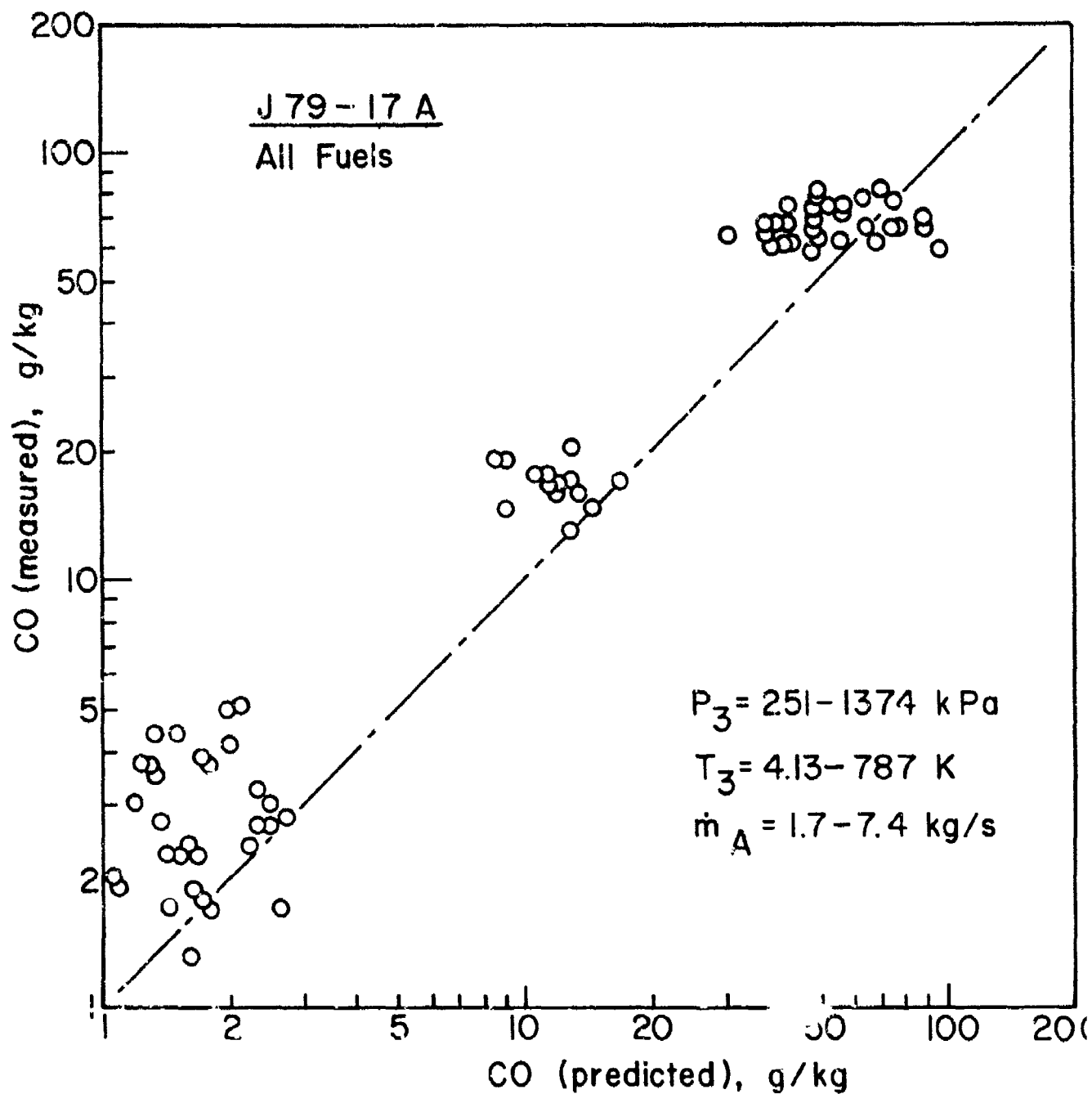


Figure 59. Comparison of Measured and Predicted Values of CO Emissions for J79-17A Combustor.

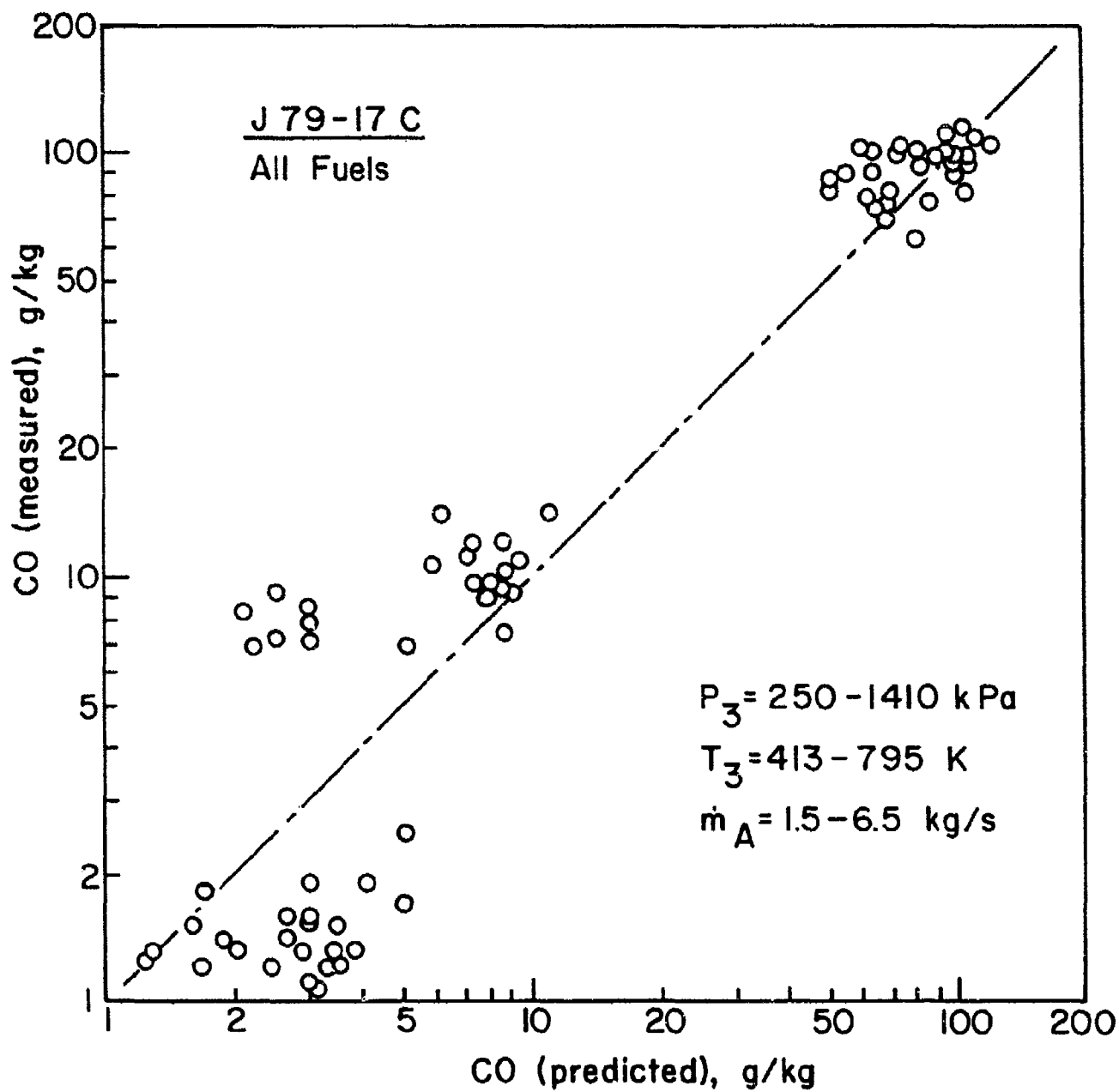
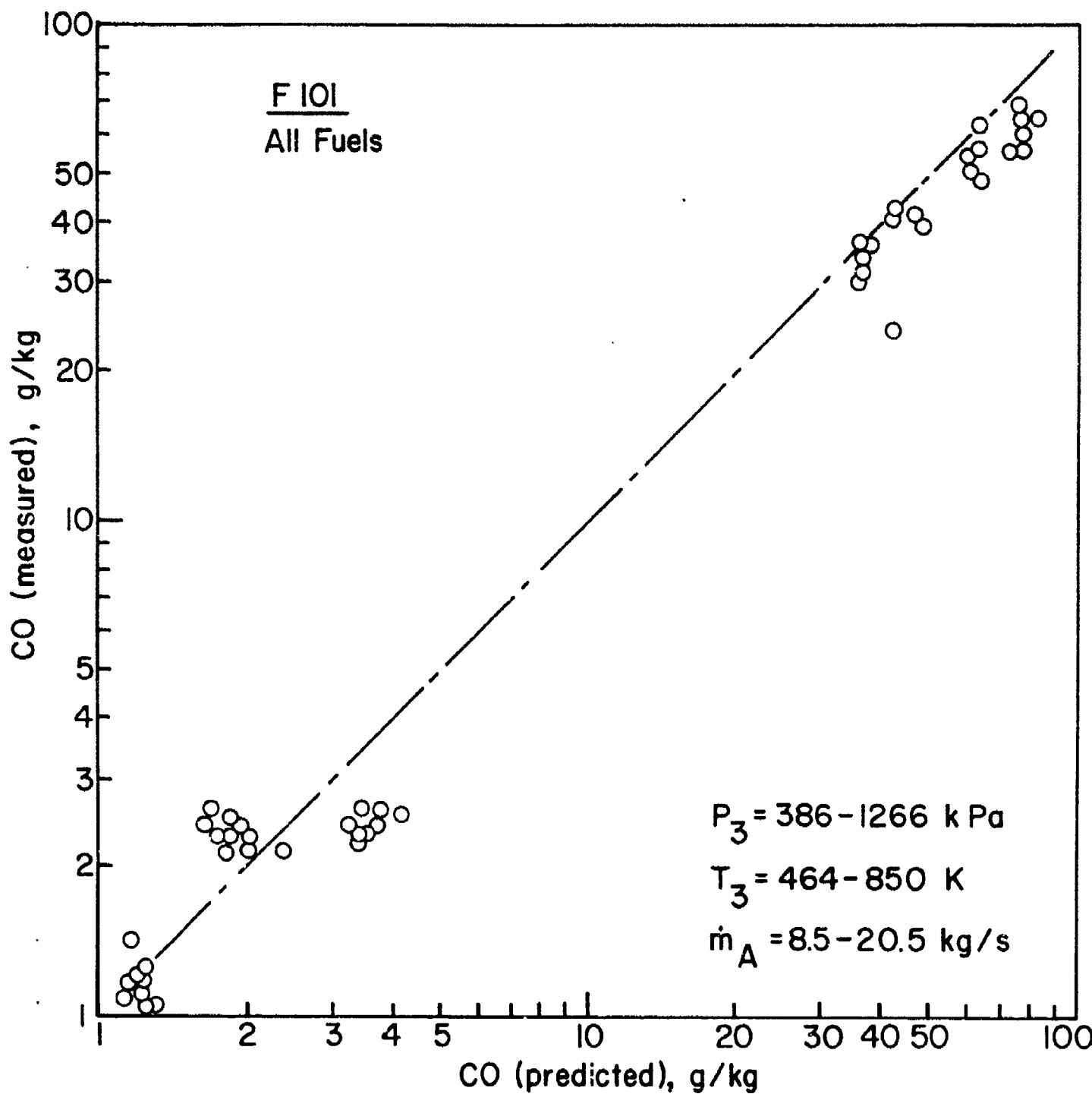


Figure 60. Comparison of Measured and Predicted Values of CO Emissions for J79-17C Combustor.



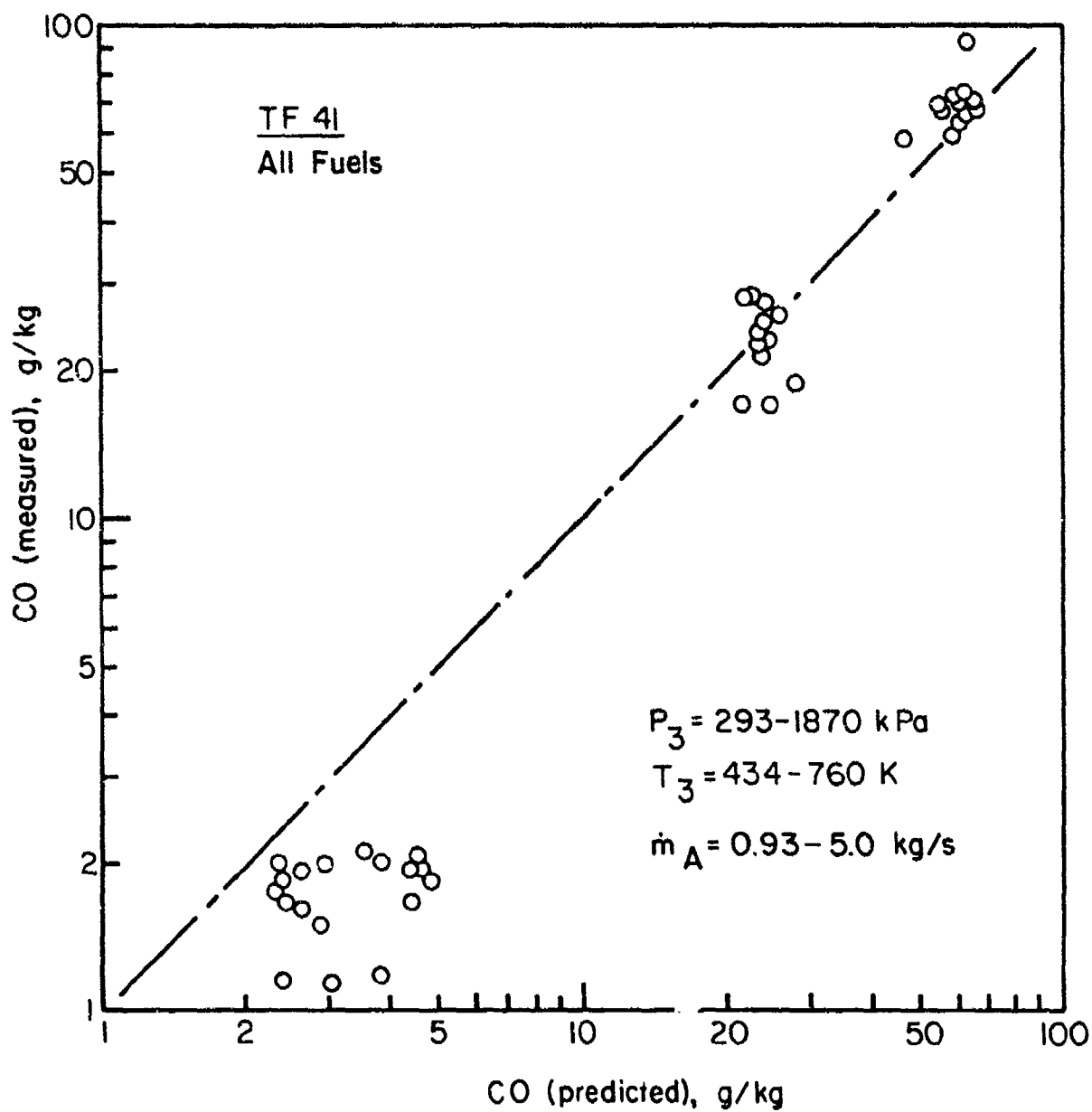


Figure 62. Comparison of Measured and Predicted Values of CO Emissions for TF 41 Combustor.

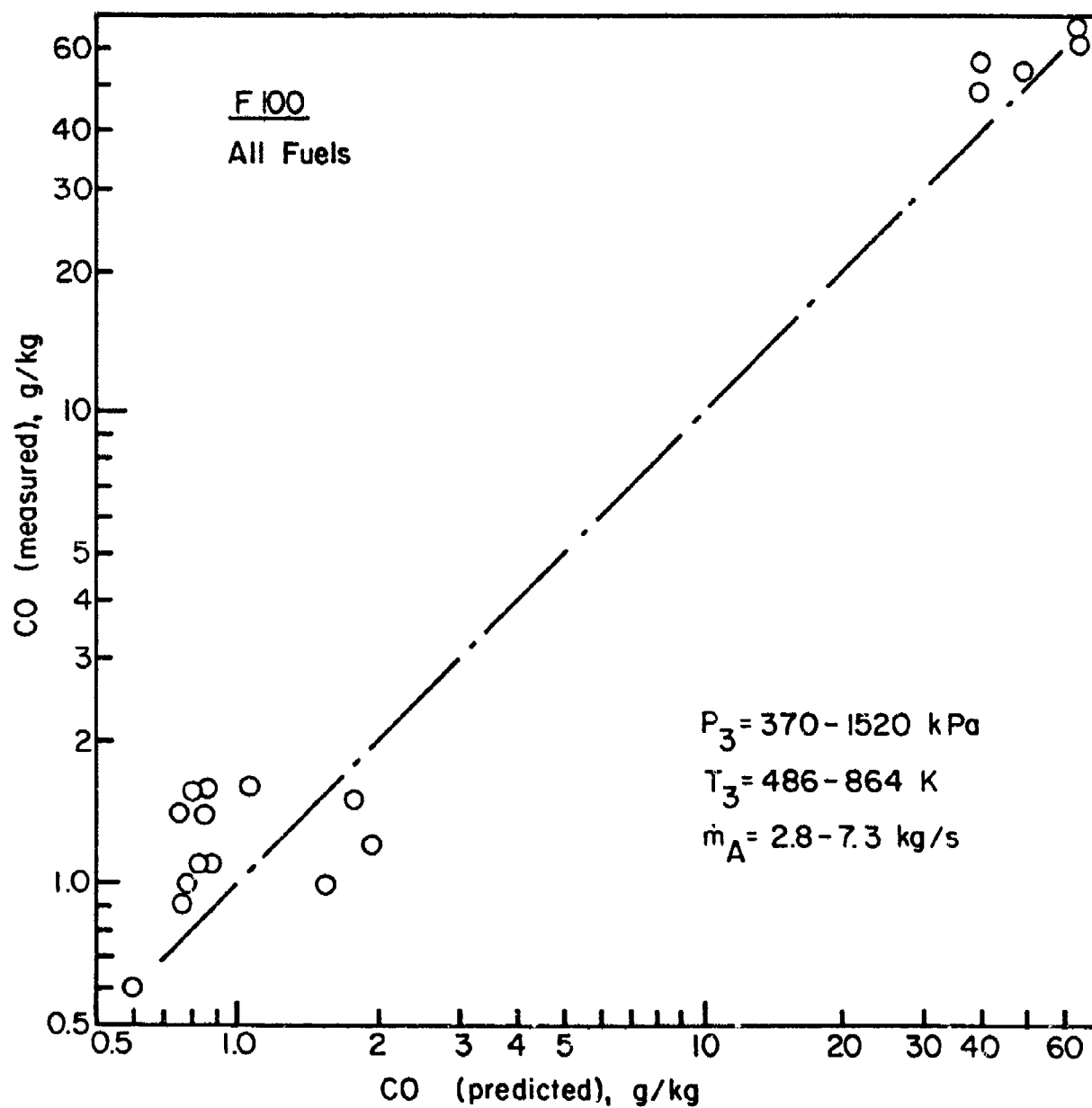


Figure 63. Comparison of Measured and Predicted Values of CO Emissions for F100 Combustor.

The following equation was used to convert engine exhaust soot concentrations into corresponding combustor exit values.

$$X_{c4} = X_{c8} \left( \frac{q_4}{q_8} \right) \left( \frac{1 + q_8}{1 + q_4} \right) \quad (57)$$

For the purpose of analysis, it is convenient to consider two separate zones (a) a soot-forming zone, and (b) a soot oxidation zone. The soot concentration measured at the combustor exit represents the difference in effectiveness between these two competing processes. Unfortunately, any attempt to derive suitable expressions to represent rates of soot-formation and soot-oxidation is seriously hampered by lack of knowledge of the basic mechanisms involved, so that, in practice, there is little alternative except to resort to an empirical approach. Useful guidance is provided by the knowledge gained from past experience in attempting to alleviate the problems of smoke and soot formation in gas turbine combustors. Thus, for example, the work of Macfarlane [42] has shown that soot formation increases rapidly with increase in pressure, and is appreciably diminished by increase in AFR. Moreover, sufficient is known to indicate that soot oxidation proceeds most rapidly in regions of high temperature containing excess air. These considerations, in conjunction with analysis of the experimental data, lead to the following expressions for the soot formation and soot oxidation processes.

$$X_F = \frac{A P_3^2 q_{pz} (\text{Aromatic Content} + B)}{f_{pz} \dot{m}_A T_{pz}} \quad (58)$$

$$X_o = \frac{[C q_{pz} p_3^2 \exp (0.0014 T_{sz})] (\text{Aromatic Content} + B)}{f_{pz} \dot{m}_A q_{sz} T_{pz}} \quad (59)$$

$$X_c = X_F - X_o$$

$$= \frac{p_3^2 q_{pz}}{f_{pz} \dot{m}_A T_{pz}} \left[ A - \frac{C}{q_{sz}} \exp (0.0014 T_{sz}) \right] [\text{Aromatic Content} + B] \quad (60)$$

Application of this equation to the correlation of experimental data on soot concentrations contained in references 1 to 4 yields the results shown in Figs. 64 to 67. The values of A, B and C associated with these figures are listed in Table 6.

If allowance is made for the difficulties involved in the sampling and measurement of soot concentrations, and the poor measurability of fuel aromatics content, the level of agreement between measured and predicted values of soot concentration, as exhibited in Figs. 64 to 67, is clearly very reasonable. However, if these results are accepted at face value they could also be very misleading. Although Eq. (60) predicts quite well the influence of combustor operating conditions on smoke output, and also demonstrates that soot concentrations rise with increase in aromatic content of the fuel, it also shows that the extent of this increase varies from one combustor to another in a manner that cannot be predicted a priori. Thus Eq. (60) offers no guidance whatsoever on the likely smoke emissions to be anticipated from any new type of combustor. Only if the values of A, B and C remained sensibly constant for all combustors would it be reasonable to regard Eq. (60) as completely satisfactory for the prediction of smoke emissions. In this context it is of interest to note that the values of A and C for the J79-17C and TF41 combustors are almost identical. However,

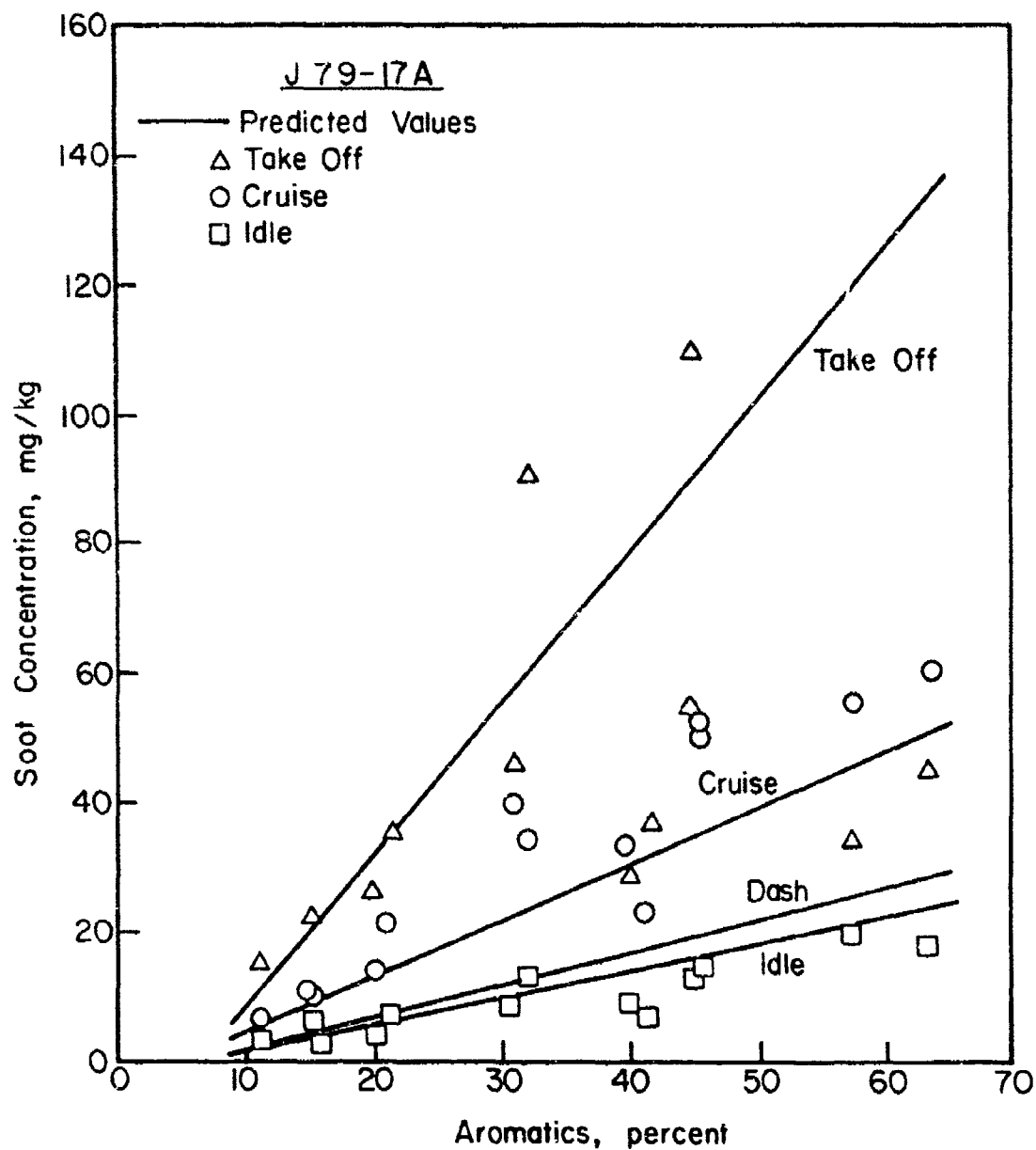


Figure 64. Graphs Illustrating Influence of Aromatics Content and Engine Operating Conditions on Soot Emissions for J79-17A Combustor.

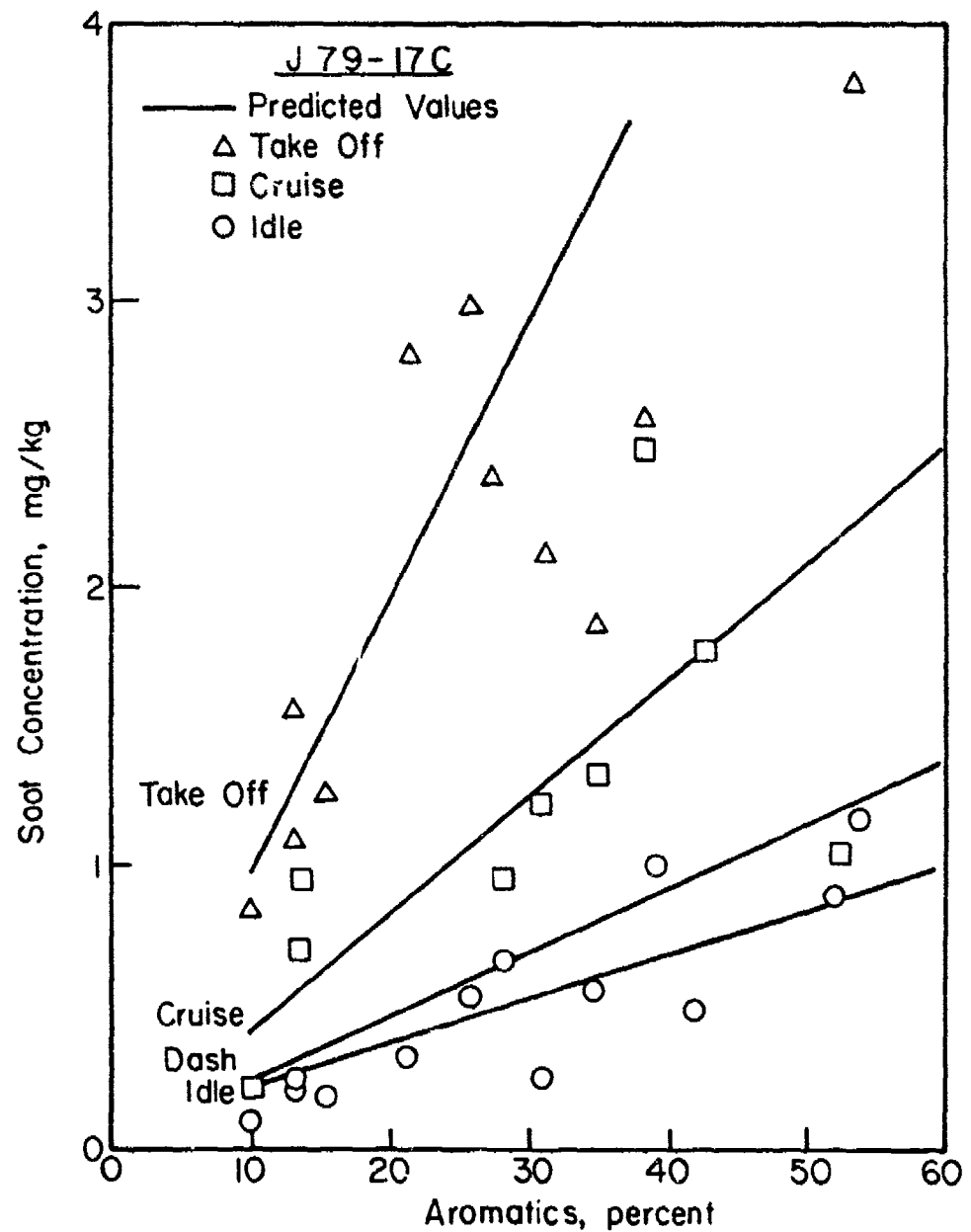


Figure 65. Graphs Illustrating Influence of Aromatics Content and Engine Operating Conditions on Soot Emissions for J79-17C Combustor.

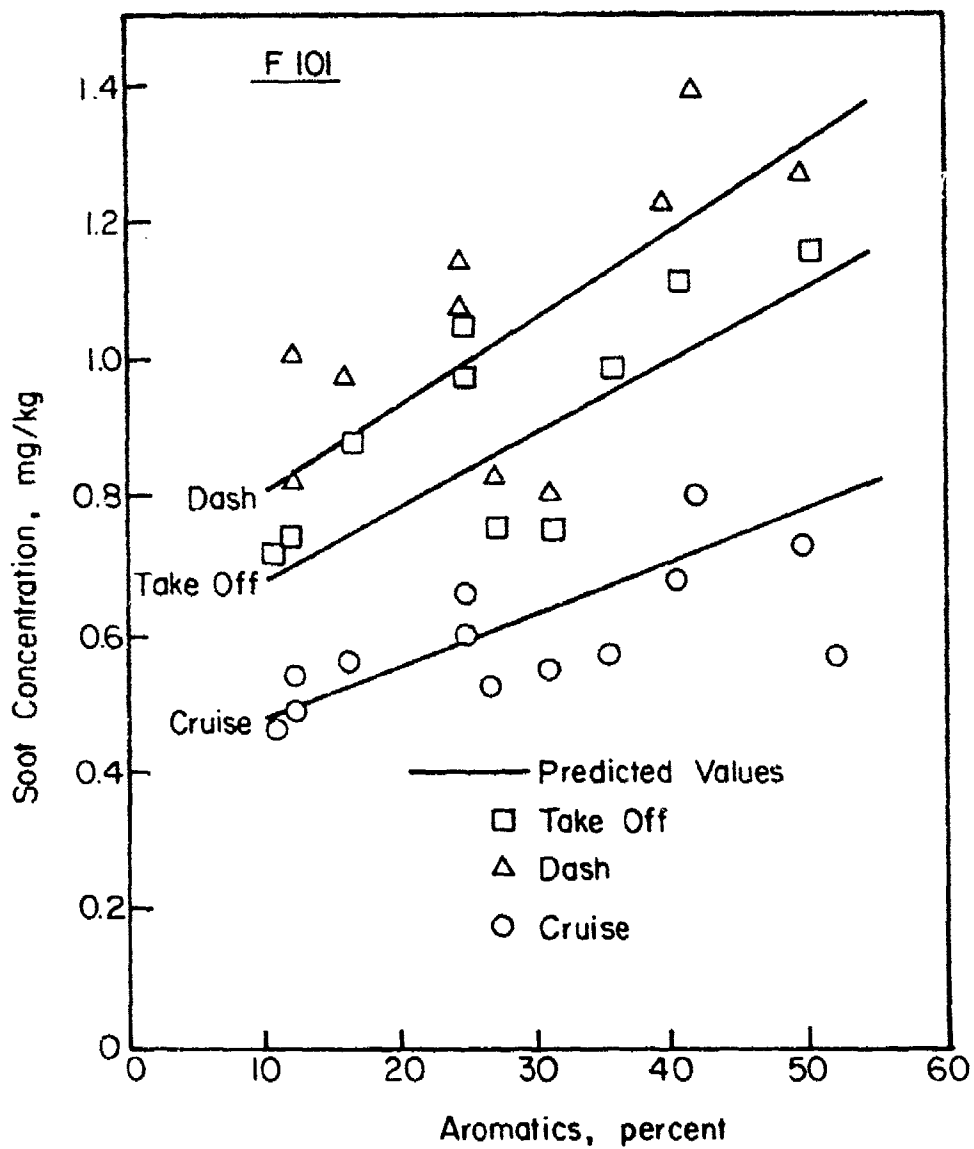


Figure 66. Graphs Illustrating Influence of Aromatics Content and Engine Operating Conditions on Soot Emissions for F101 Combustor.

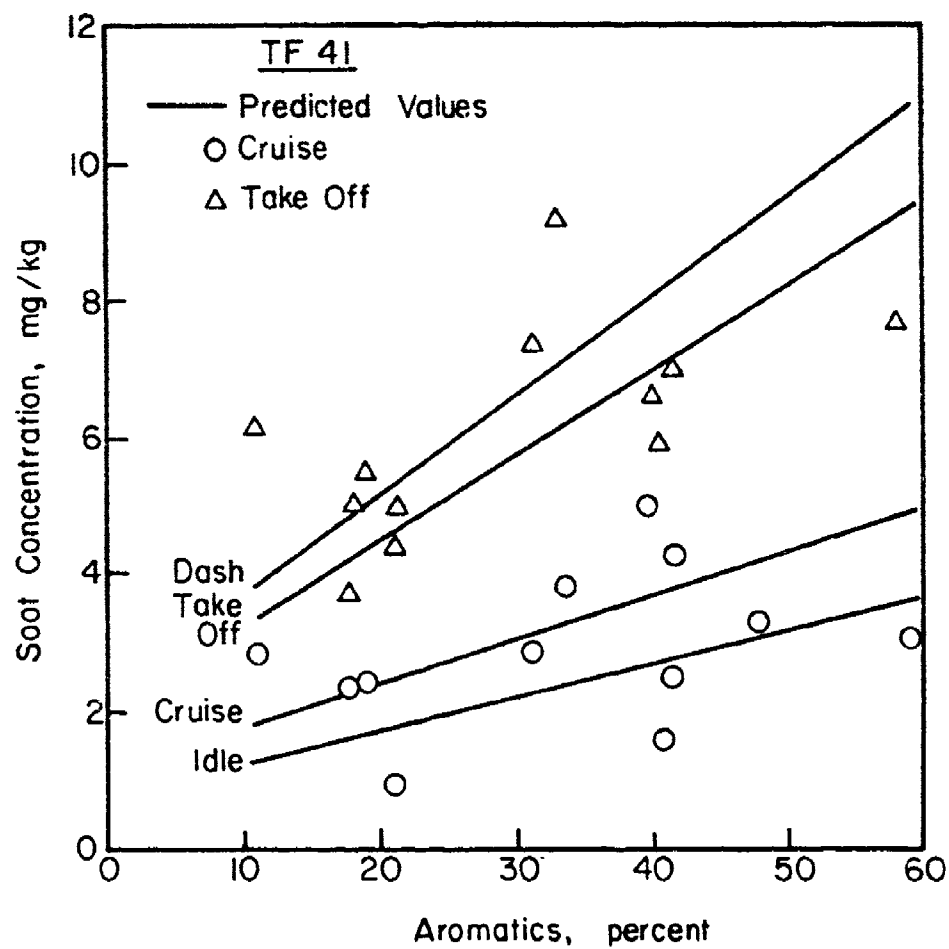


Figure 67. Graphs Illustrating Influence of Aromatics Content and Engine Operating Conditions on Soot Emissions for TF41 Combustor.

TABLE 6. Values of A, B and C employed in Eq. (60).

ENGINE	A	B	C
J79-17A	32.9	-0.06	0.08
J79-17C	3.22	-0.02	0.0078
F101	0.72	+0.55	0.001
TF41	3.2	+0.16	0.007

for the other two combustors examined the corresponding values are widely different, indicating that Eq. (60) fails to take into account one or more processes of great importance to soot formation. One obvious omission is a term to describe the degree of mixing of fuel and air prior to combustion. This is known to have a strong influence on smoke output; for example, the very large difference in smoke output between the J79-17A and J79-17C combustors, as reflected in the ten-fold difference in the value of A, is known to be due in large measure to the steps taken to improve the premixing of fuel and air in the latter case. Thus Eq. (60) contains some serious deficiencies, but little improvement in the prediction of smoke emission can be expected until more quantitative information is available on the influences of fuel-air preparation and fuel chemistry on soot formation.

## SECTION X

### PATTERN FACTOR

Perhaps the most important and, at the same time, most difficult problem in the design and development of gas turbine combustion chambers, is that of achieving a satisfactory and consistent distribution of temperature in the efflux gases discharging into the turbine. In the past, experience has played a major role in the determination of dilution-zone geometry, and trial and error methods have been widely used in developing the temperature-traverse quality of individual combustor designs to a satisfactory standard. Experimental investigations into dilution-zone performance carried out on actual chambers have provided useful guidance, but very often it has proved difficult or impossible to distinguish the separate influences of all the variables involved. Thus although it is now generally accepted that a satisfactory temperature profile is dependent upon adequate penetration of the dilution jets, coupled with the correct number of jets to form sufficient localized mixing regions, the manner in which the total dilution-hole area is utilized in terms of number and size of holes is still largely a matter of experience. Unfortunately, more basic studies of jet mixing do not usually yield results that can readily be expressed in terms of the parameters most familiar to those concerned with combustion-chamber design. However, some of these investigations can provide a useful guide to the relationships involved.

The temperature obtained by an elemental volume of gas at the chamber outlet is dependent on the history it undergoes from the time it emerges from the compressor. During its passage through the combustor its temperature and composition changes rapidly under the influence of various combustion, heat transfer and mixing processes, none of which are perfectly understood. Considering only the final mixing process, this is affected

in a complicated manner by the dimensions, geometry, and pressure drop of the liner, the size, shape and discharge coefficients of the liner holes, the airflow distribution to various zones of the chamber, and the temperature distribution of the hot gases entering the dilution zone. For any given combustor, the latter is strongly influenced by fuel spray characteristics such as drop size, spray angle and spray penetration, since these control the pattern of burning and hence the distribution of temperature in the primary-zone efflux. It is known that spray characteristics are strongly influenced by pressure, especially with atomizers of the simplex or dual-orifice type, and it is to be expected therefore that temperature traverse will also vary with pressure, although the extent of this variation will vary from one chamber to another depending on design and, in particular, on length.

The most important temperature parameters are those that affect the power output of the engine and the life and durability of the hot sections downstream. As far as the overall engine performance is concerned the most important temperature is the turbine inlet temperature,  $T_4$ , which is the mass flow weighted mean of the combustor exit temperature. Since the nozzle guide vanes are fixed relative to the combustor they must be designed to withstand the maximum temperature found in the traverse. Thus, the parameter of most relevance to the design of nozzle guide vanes is the overall temperature distribution factor, which highlights this maximum temperature. It is normally defined as: -

$$\text{Pattern factor} = \frac{T_{\max} - T_4}{T_4 - T_3} \quad (61)$$

The temperatures of most significance to the turbine blades are those that constitute the average radial profile. This is obtained by adding together the temperature measurements around each radius of the liner and then dividing by the number of locations at each radius, i.e., calculating the arithmetic mean at each radius. The expression used to describe the radial temperature distribution factor, also known as the profile factor, is

$$\text{Profile factor} = \frac{T_{mr} - T_4}{T_4 - T_3} \quad (62)$$

In Eqs. (61) and (62)

$T_{max}$  = maximum recorded temperature

$T_{mr}$  = maximum circumferential mean temperature

$T_3$  = mean inlet air temperature

$T_4$  = mean exit temperature

#### 1. Correlation of Data

Two parameters of crucial importance to pattern factor are liner length, which controls the time and distance that are available for mixing, and the pressure drop across the liner, which governs the penetration of the dilution jets and their rate of mixing with the products of combustion. From analysis of experimental data on tubular, tubo-annular and annular combustors, it is found that [9]

$$\frac{T_{max} - T_4}{T_4 - T_3} = f \left[ \frac{L_L}{D_L} \right] \left[ \frac{\Delta P_L}{q_{ref}} \right] \quad (63)$$

where  $\Delta P_L/q_{ref}$  = liner pressure loss factor

$L_L$  = total liner length

$D_L$  = liner diameter, or height

The data correlations obtained for tubular and annular liners are shown in Figs. 68 and 69 respectively. In connection with these figures it should be noted that the correlation is based not on the  $L/D$  ratio of the dilution zone, but on that of the complete liner. This is found to provide a better fit to the data.

For tubular and tubo-annular combustors it is found that

$$(T_{max} - T_4)/(T_4 - T_3) = 1 - \exp - \left[ 0.070 (L_L/D_L)(\Delta P_L/q_{ref}) \right]^{-1} \quad (64)$$

while for annular combustors

$$(T_{max} - T_4)/(T_4 - T_3) = 1 - \exp - \left[ 0.050 (L_L/D_L)(\Delta P_L/q_{ref}) \right]^{-1} \quad (65)$$

Comparison of Figs. 68 and 69 reveals that, for any given value of  $(L_L/D_L)$ , the pattern factor of the tubular system is superior to that of an annular system. This is because tubo-annular combustors tend to have lower annulus velocities than annular combustors, a property that is conducive to better jet penetration and mixing. Moreover, with tubo-annular combustors the pressure distributions in the annulus are less susceptible to changes in inlet velocity profile. This is because the longitudinal gap between liners ensures automatic radial balancing of pressure along the entire combustor length. In marked contrast, in the annular combustor the pressure difference between the inner and outer annuli is determined by

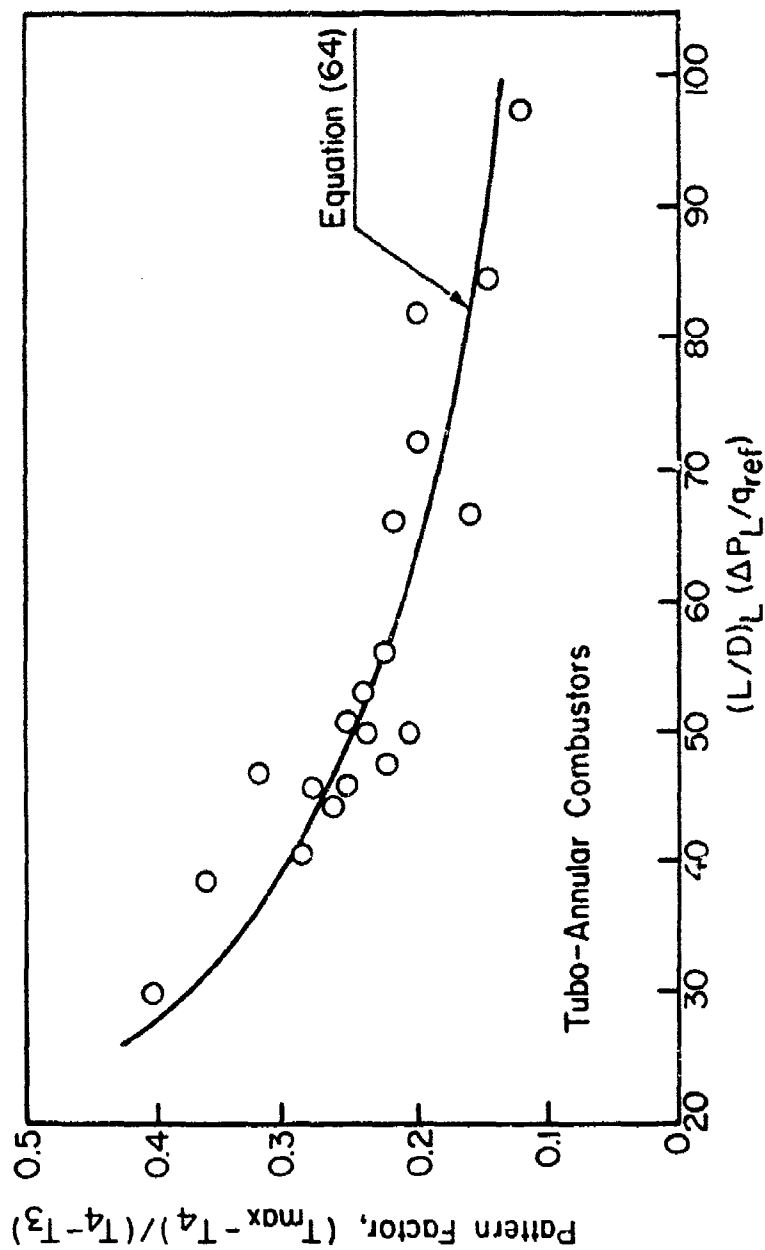


Figure 68. Pattern Factor Correlation for Tubo-Annular Combustors.

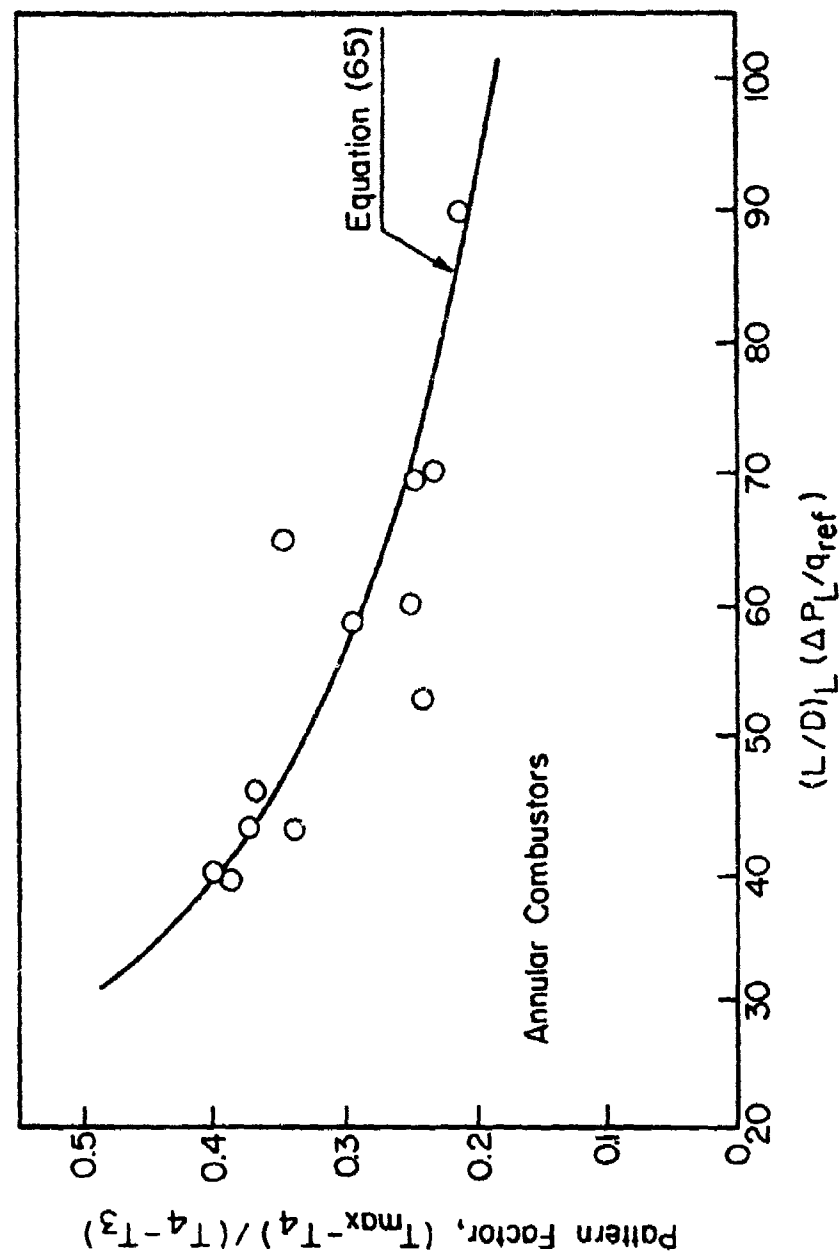


Figure 69. Pattern Factor Correlation for Annular Combustors.

the shape of the total pressure profile in the flow when it reaches the snout.

## 2. Data Analysis

As no information on liner pressure loss factor is contained in references 1 to 6 this might appear to rule out the use of Eqs. (64) and (65) in the present analysis. Another drawback to these equations is the inherent assumption that all the liner length is utilized in mixing and combustion and that the length occupied by evaporation processes is essentially zero. Although this assumption is not unreasonable for highly volatile fuels of low viscosity, such as JP4, it is difficult to justify for some of the alternative fuels employed in this program. These deficiencies may be remedied to a large extent by rewriting Eqs. (64) and (65) in following form

$$\frac{T_{max} - T_4}{T_4 - T_3} = 1 - \exp - Q \left[ \left( \frac{\Delta P_L}{q_{ref}} \right) (L_L - L_e) \right]^{-1} \quad (66)$$

where  $Q = 0.070$  for tubular liners

or,  $Q = 0.050$  for annular liners

$L_e$  is the liner length required to evaporate the fuel spray. This is obtained as the product of the average predilution liner velocity and the evaporation time.

$$\begin{aligned} \text{i.e. } L_e &= U_g \times t_e \\ &= \left( \frac{0.6 \dot{m}_A}{\rho_g A_L} \right) \times \left( \frac{D_o^2}{\lambda_{eff}} \right) \end{aligned} \quad (67)$$

The constant of 0.6 in Eq. (67) stems from the assumption that 60 percent of the total combustor airflow enters the liner upstream of the liner. A more accurate assessment of this constant for each individual liner design would not be justified at this stage due to the larger uncertainty surrounding the value of  $D_o$ . In practice it was found that correlation of experimental data could be improved by reducing the value of this constant from 0.6 to 0.33. This may be justified on the grounds that the combustion process does not wait until the fuel has fully evaporated; instead burning commences as soon as sufficient fuel has evaporated to produce a flammable mixture. Thus Eq. (66) may be rewritten as

$$\frac{T_{\max} - T_4}{T_4 - T_3} = 1 - \exp - Q' \left[ \frac{\Delta P_L}{q_{\text{ref}}} \left( \frac{L_L}{D_L} - \frac{0.33 \dot{m}_A D_o^2}{\rho_g A_L D_L \lambda_{\text{eff}}} \right) \right]^{-1} \quad (68)$$

where  $\rho_g$  is the average gas density upstream of the dilution zone. It is calculated at a temperature  $T_g$  which is obtained as

$$T_g = T_3 + \Delta T_g$$

where  $\Delta T_g$  is the temperature rise due to combustion for a fuel/air ratio of 0.6  $q_{ov}$ .  $A_L$  is the average cross-sectional area of the liner. It is estimated by dividing the volume of the liner by its maximum length.  $D_L$  is the average diameter or height of the liner. For a tubular liner it is readily obtained as  $D_L = (4 A_L / \pi)^{0.5}$ .

Mean drop sizes for insertion into Eq. (68) were calculated using either Eq. (1) or Eq. (2). Values of  $\lambda_{\text{eff}}$  were read off Figs. (2), (3) or (4) assuming a relative velocity between the fuel drop and the surrounding gas of twenty-five percent of the gas velocity,  $U_g$ .

For the three tubular combustors examined, namely the J79-17A, J79-17C, and TF41, values of  $Q'$  of 0.99, 1.03 and 1.35 respectively provided excellent correlations of the experimental data, as demonstrated in Figs. 70, 71 and 72. These values of  $Q'$  correspond to liner pressure loss factors for these combustors of 14, 15 and 19 respectively, all of which seem quite reasonable. It is of interest to note that the improvement in pattern factor with increase in engine power, as predicted by Eq. (68), (due to reduction in evaporation time), is fully borne out by the results contained in Figs. 70, 71 and 72.

The influence of fuel type on pattern factor is manifested through the effects of mean drop size (via viscosity and surface tension) and effective evaporation constant (via  $T_{bn}$ ) on droplet evaporation time. Over the range of fuels examined the effect of fuel type on pattern factor is relatively small, at least at high power conditions where the evaporation time is always a small fraction of the total combustor residence time, regardless of fuel type. However, if measurements of pattern factor are conducted at operating conditions where the evaporation time constitutes a significant proportion of the total residence time, then a strong effect of fuel type on pattern factor should be expected. This, in fact, was precisely the result obtained with the F101 combustor when the effect of fuel type on pattern factor was examined at various simulated engine operating conditions, but using air supplied at normal atmospheric pressure. The results of these tests are shown in Fig. 73, where it is of interest to note that the measured values of pattern factor are well correlated by Eq. (68) using a value for  $Q'$  of 2.0. Figure 73 demonstrates a clear effect of fuel type on pattern factor but it would be erroneous to assume that these data have any relevance to the real engine. If

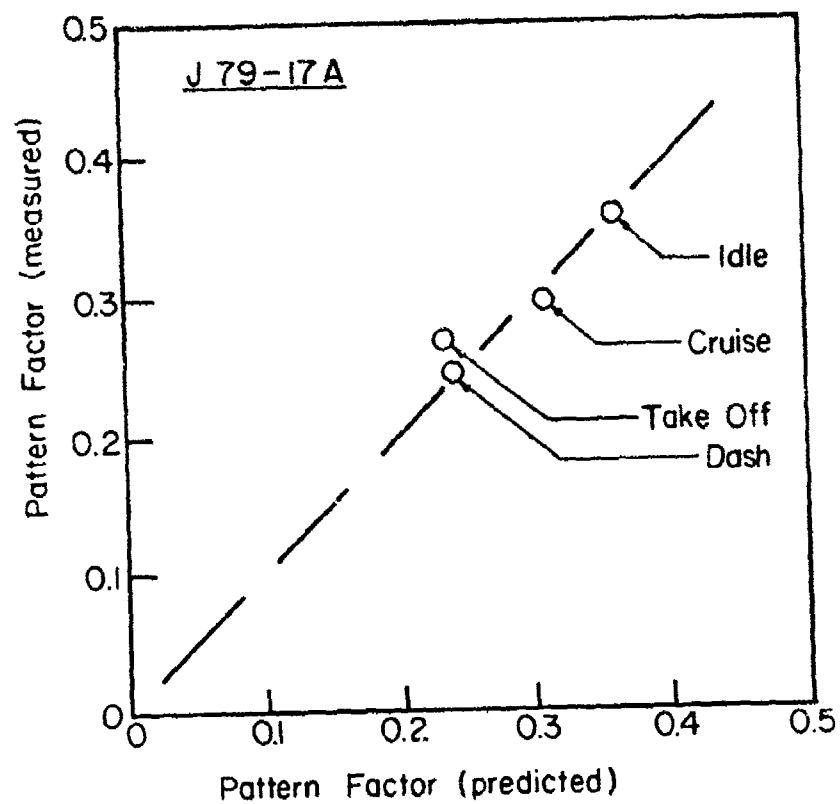


Figure 70. Comparison of Measured and Predicted Values of Pattern Factor for J79-17A Combustor.

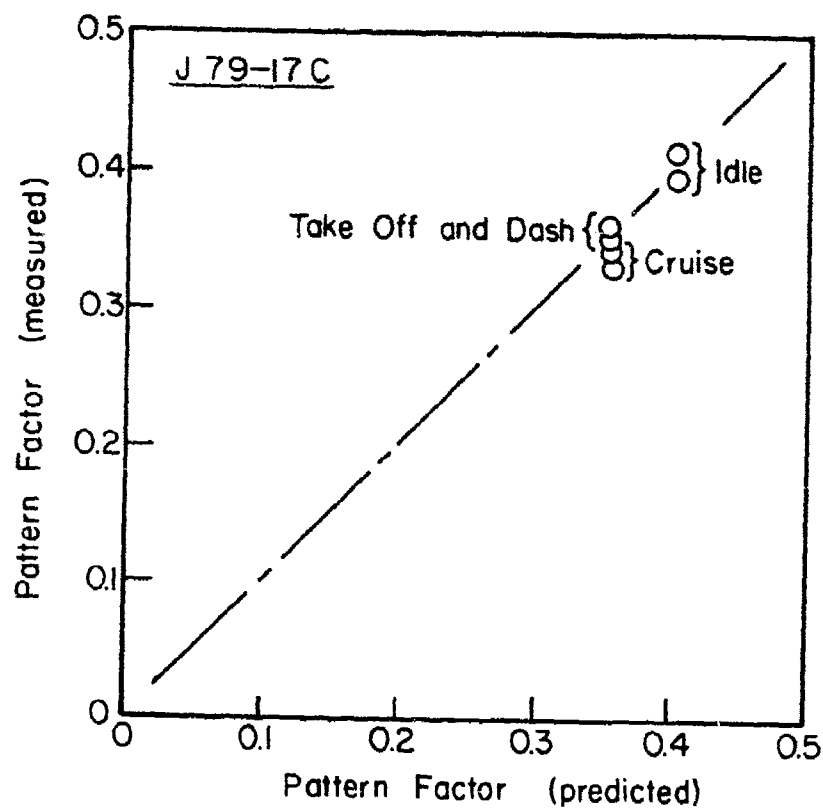


Figure 71. Comparison of Measured and Predicted Values of Pattern Factor for J79-17C Combustor.

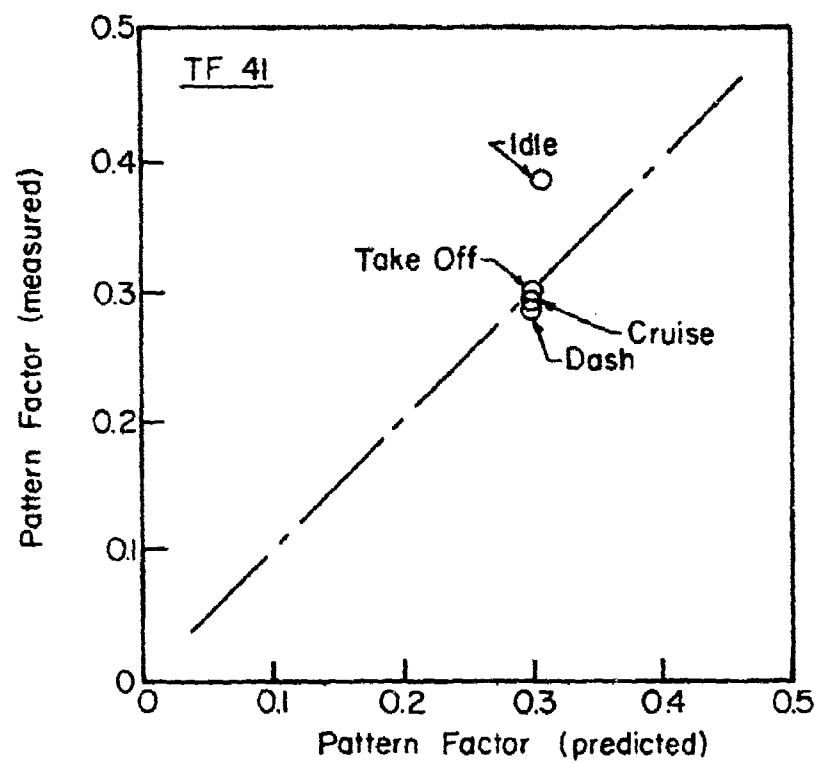


Figure 72. Comparison of Measured and Predicted Values of Pattern Factor for TF 41 Combustor.

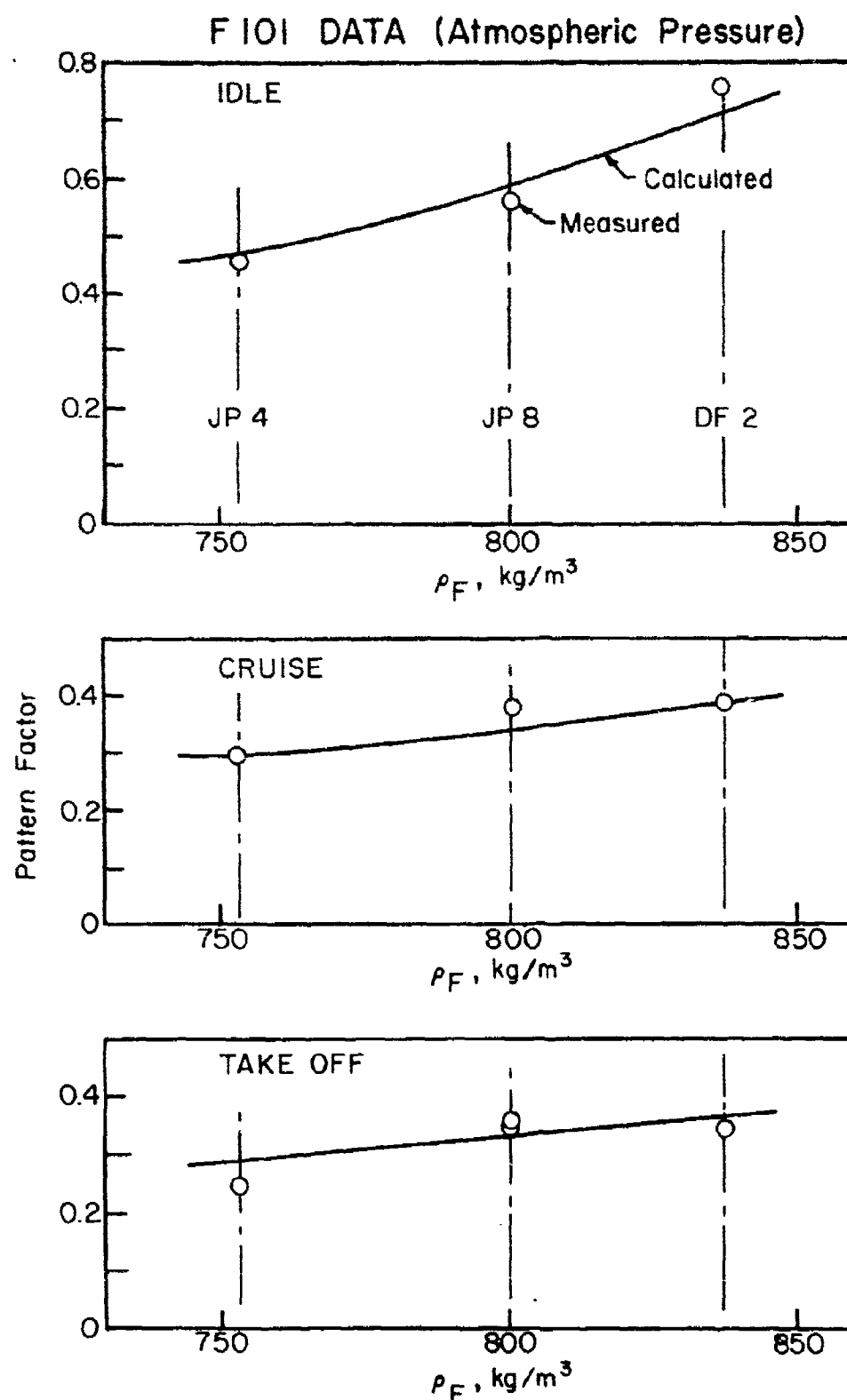


Figure 73. Comparison of Measured and Predicted Values of Pattern Factor for F101 Combustor.

Eq. (68) is used to calculate values of pattern factor at actual take-off conditions, including  $P_3$ , it is found that pattern factor is virtually independent of fuel type, as shown in Fig. 74. Thus, from a practical viewpoint, the results of the F101 tests are fully consistent with those of the J79-17A, J79-17C, and the TF41. They all confirm that, at the high power conditions where pattern factor is most important to engine durability, variation in fuel type has a negligible effect.

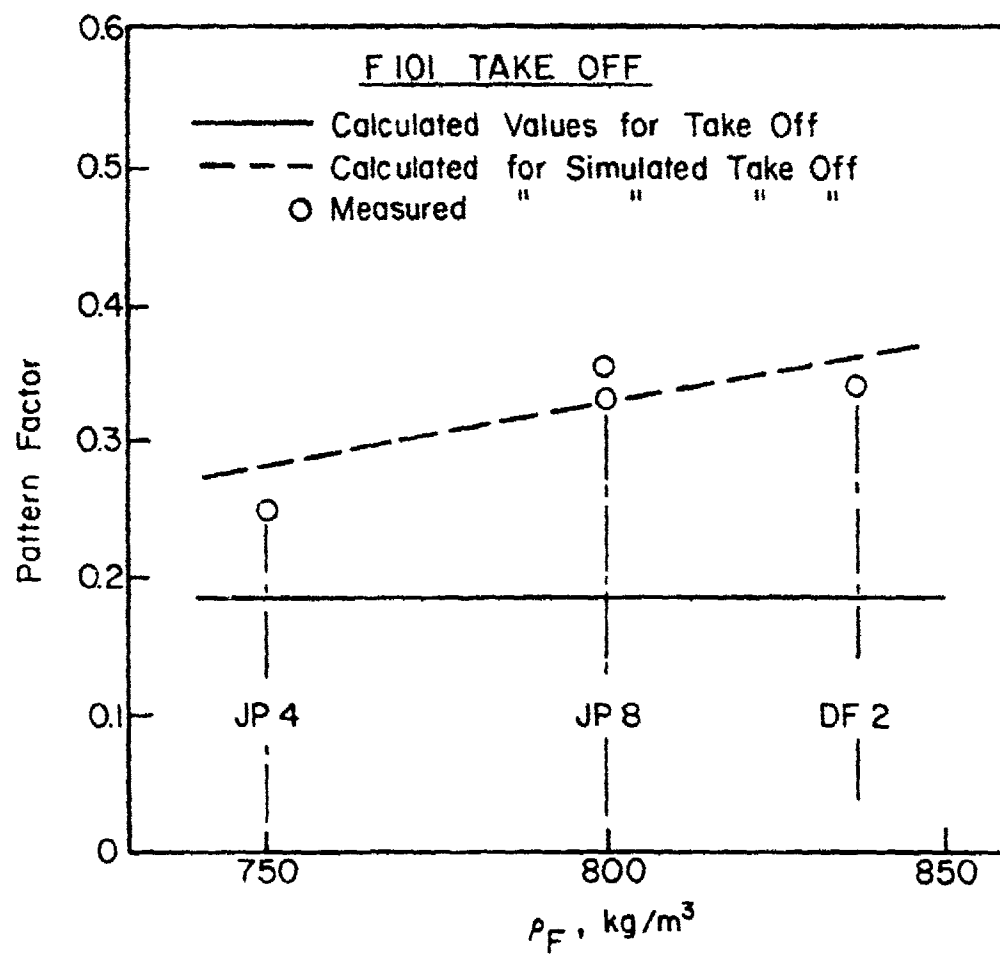


Figure 74. Graphs Illustrating the Effects of Fuel Density and Combustor Operating Conditions on Pattern Factor.

# SECTION XI

## DISCUSSION AND SUMMARY

Analysis of the key processes occurring within gas turbine combustors, along with examination of the experimental data contained in references 1 to 6, shows that although the impact of fuel type on combustion performance and liner durability is usually small in comparison with the effects of liner geometry and combustor operating conditions, it is nevertheless of sufficient magnitude to warrant serious consideration. For some performance parameters, such as liner wall temperature and exhaust smoke, it is found that fuel chemistry plays an important role. For others, the effects of fuel type are manifested through the physical properties that govern atomization quality and evaporation rates.

In the following sections the effects of liner size, liner pressure drop, combustor operating conditions, and fuel type on various aspects of combustion performance are briefly reviewed in turn.

### 1. Combustion Efficiency

For reaction-rate-controlled systems

$$\eta_{c,r} = f \left[ \frac{p_3^{1.75} v_c \exp(T_3/300)}{\dot{m}_A} \right] \quad (5)$$

For mixing-controlled systems

$$\eta_{c,m} = f \left[ \frac{p_3 A_L}{\dot{m}_A T_3^{0.5}} \right] \left[ \frac{A_P L}{p_3} \right]^{0.5} \quad (8)$$

For evaporation-rate-controlled systems

$$\eta_{c,e} = \lambda_{eff} v_g v_c \left[ f_c \dot{m}_A D_o^2 \right]^{-1} \quad (14)$$

From analysis of the experimental data contained in references 1 to 6 it was found that combustion efficiency is obtained as the product of the  $\theta$  efficiency,  $\eta_{c_\theta}$ , and the evaporation efficiency,  $\eta_{c_e}$ , i.e.

$$\eta_c = \eta_{c_\theta} \times \eta_{c_e}$$

$$\text{where } \eta_{c_\theta} = 1 - \exp \left[ \frac{-0.022 P_3^{1.3} V_c \exp(T_c/400)}{f_c \dot{m}_A} \right] \quad (22)$$

$$\text{and } \eta_{c_e} = 1 - \exp \left[ \frac{-36 \times 10^3 P_3 V_c \lambda_{\text{eff}}}{T_c D_o^2 f_c \dot{m}_A} \right] \quad (23)$$

Inspection of these equations reveals that combustion efficiency is enhanced by increases in  $P_3$ ,  $T_3$  (via  $T_c$ ), and  $V_c$ , and by reduction in combustor air flow rate. There is a very slight effect of fuel chemistry on  $\eta_c$ , via  $T_c$ , but the main influence of fuel type on combustion efficiency stems from the physical properties  $\mu_F$ ,  $\sigma_F$  and  $T_{bn}$  that govern the values of  $D_o$  and  $\lambda_{\text{eff}}$  in Eq. (23).

## 2. Lean Blowout

Weak extinction values of fuel/air ratio are obtained as

$$q_{\text{LBO}} = \frac{A' f_{pz} \dot{m}_A}{V_c P_3^{1.3} \exp(T_3/300)} \times \frac{D_r^2}{\lambda_r \text{LCV}_r} \times \left( \frac{D \text{ at } T_F}{D \text{ at } 277.5 \text{ K}} \right)^2 \quad (33)$$

In this equation it is of interest to note that the dependence of weak extinction limits on combustor volume and operating conditions is identical to that for combustion efficiency. Also in common with combustion efficiency is the slight effect of fuel chemistry (via  $LCV_r$ ), whereas physical properties are important due to their influence on  $D_r$  and  $\lambda_r$ .

### 3. Lean Lightup

The equation for lean lightup fuel/air ratio is virtually identical to that for lean blowout fuel/air ratio, except for a slightly stronger dependence on  $P_3$ . We have

$$q_{LLO} = \frac{B' f_{pz} \dot{m}_A}{V_c P_3^{1.5} \exp(T_3/300)} \times \frac{D_r^2}{\lambda_r LCV_r} \times \left[ \frac{D \text{ at } T_F}{D \text{ at } 277.5K} \right]^2 \quad (37)$$

Thus the observations made above on the influence of combustor operating conditions, and the relative importance of physical and chemical fuel properties, on combustion efficiency and lean blowout limits, apply with equal force to ignition performance.

### 4. Liner Wall Temperature

The most important factor governing liner wall temperature is the combustor inlet temperature,  $T_3$ . Inlet pressure is also significant due to its influence on the concentration of soot particles in the flame, and hence on the magnitude of the luminous radiation flux to the liner wall. At max power conditions, where liner wall temperatures are of most concern, evaporation rates are so high that the physical properties of the fuel appear to have a negligible influence on  $T_w$ . Chemical

effects are also quite small, as shown in Figs. 44 to 47. However, even small increases in maximum values of liner wall temperature can seriously curtail liner life. Thus, for the range of fuels covered in this investigation, fuel type must be considered of significance to liner durability.

In the calculation of liner wall temperatures the effect of fuel type can be accommodated quite conveniently by introducing the fuel hydrogen content into the existing equation for gas emissivity. This approach leads to the following equation for  $\epsilon_g$ .

$$\epsilon_g = 1 - \exp \left[ -97.44 P_3 (\%H_2)^{-2} (q \epsilon_b)^{0.5} T_g^{-1.5} \right] \quad (50)$$

#### 5. NO<sub>x</sub> Emissions

It is found that NO<sub>x</sub> emissions are very dependent on combustor operating conditions, and also on the size of the combustion zone which governs the time available for NO<sub>x</sub> formation. The key factor controlling NO<sub>x</sub> is the stoichiometric flame temperature which, in turn, is almost solely dependent on combustor inlet temperature. As far as fuel type is concerned, physical properties are of little consequence except at low power conditions where NO<sub>x</sub> emissions are always quite small due to the correspondingly low values of  $T_{st}$ . Fuel chemistry also has little influence on NO<sub>x</sub> because it affects only slightly the values of bulk gas temperature ( $T_{pz}$ ), and stoichiometric flame temperature ( $T_{st}$ ), in the following equation for NO<sub>x</sub>.

$$NO_x = \frac{9 \times 10^{-8} P_3^{1.25} V_c \exp(0.01 T_{st})}{m_A T_{pz}} \text{ g/kg} \quad (54)$$

## 6. CO Emissions

These are correlated by the expression: -

$$CO = \frac{86 \dot{m}_A T_{pz} \exp(-0.00345 T_{pz})}{\left[ V_c - 0.55 \frac{f_{pz} \dot{m}_A D_o^2}{\rho_{pz} \lambda_{eff}} \right] \left( \frac{\Delta P_L}{P_3} \right)^{0.5} P_3^{1.5}} \text{ g/kg} \quad (55)$$

It is again observed that combustor size and operating conditions play a prominent role in determining the level of CO emissions. Special importance is attached to inlet temperature and primary-zone fuel/air ratio, due to their combined effect in resolving the primary-zone temperature. As in the case of  $NO_x$  emissions, the influence of fuel chemistry is small and is manifested through slight variations in  $T_{pz}$  with changes in lower calorific value. However, since CO emissions attain their maximum values at low power conditions, where a sizeable proportion of the total residence time in the combustion zone is occupied by evaporation processes, the influence of those physical properties which affect evaporation rates, namely  $\nu_F$ ,  $\sigma_F$  and  $T_{bn}$ , becomes important. On this basis it would be anticipated that fuels of high viscosity would be characterized by slightly higher levels of CO emissions, and the experimental data generally confirm this expectation.

## 7. Smoke

Of all the parameters studied, smoke emissions is the one that is most affected by changes in fuel type. The physical properties of the fuel are important insofar as they influence the mean drop size in the spray and the penetration of the spray across the combustion zone. Spray penetration is of considerable importance from a smoke viewpoint because inadequate penetration leads to enhanced fuel enrichment of the soot-forming regions just downstream of the fuel injector. Unfortunately, present knowledge of

spray characteristics is insufficient to allow these effects to be described quantitatively. However, as mean drop size and spray penetration (especially for swirl pressure atomizers) are both dependent on pressure, their combined effect can be embodied into a pressure term such as that contained in the following equation for soot concentration in the combustor exhaust gas.

$$X_c = \frac{P_3^2 q_{pz}}{f_{pz} \dot{m}_A T_{pz}} \left[ A - \frac{C}{q_{sz}} \exp(0.0014 T_{sz}) \right] \left[ \text{Aromatic Content} + B \right] \quad (60)$$

The above equation shows that combustion pressure and primary-zone fuel/air ratio are the main factors governing the output of smoke. However, fuel type also has a strong influence, as evidenced by the relationships between soot concentration and aromatics content, shown plotted in Figs. 64 to 67. Although total aromatics content was selected as the best indicator of a fuels' propensity for soot formation, the form in which it is included in Eq. (60) is unsatisfactory, since different combustors require different values of B. More work is needed to clarify the role of fuel composition and combustion chemistry on soot formation and smoke. Carefully controlled experiments, conducted at high pressures on selected fuels, incorporating accurate measurements of spray characteristics, should provide a more definite indication of the relative importance of hydrogen content and aromatics type than can be deduced from the existing data.

#### 8. Pattern Factor

This is described with good accuracy by the following equation

$$\frac{T_{\max} - T_4}{T_4 - T_3} = 1 - \exp - Q' \left[ \frac{\Delta P_L}{q_{\text{ref}}} \left( \frac{L_L}{D_L} - \frac{0.33 \dot{m}_A D_o^2}{\rho_g A_L D_L \lambda_{\text{eff}}} \right) \right]^{-1} \quad (68)$$

where appropriate values of  $Q'$  are 0.70 and 0.50 for turbo-annular and annular combustors respectively. The above equation shows that the two main parameters controlling pattern factor are the pressure drop across the liner and the liner  $L/D$  ratio. It also accounts for the influence of evaporation time in reducing the time available for mixing within the liner. At the high pressure conditions where pattern factor is of most concern, the evaporation time is always quite short in comparison to the total residence time of the combustor, and so the dependence of pattern factor on fuel type is fairly small, as illustrated in Fig. 74.

With reduction in engine power the evaporation time increases due to increase in  $D_0$  and reduction in  $\lambda_{eff}$ . This produces a deterioration in pattern factor as indicated by Eq. (68) and also by Figs. 70 to 73, which demonstrate for all engines that pattern factor at idle is distinctly worse than at take-off. These considerations highlight the importance of measuring pattern factor only at the correct combustor inlet conditions of  $\dot{m}_A$ ,  $P_3$ ,  $T_3$  and  $q_{ov}$ , corresponding to engine operation at max power. Tests carried out at simulated conditions at lower pressure levels give misleading results, as shown in Fig. 73. First, they yield values that are overly pessimistic and, second, they show a dependence of pattern factor on fuel type which greatly exaggerates the dependence actually observed at high pressure.

## SECTION XII

### CONCLUSIONS

1. The most important factors governing liner durability and combustion performance are liner size, liner pressure drop and combustor operating conditions, with fuel effects playing a secondary role. However, since in modern high pressure ratio engines the combustor is called upon to perform satisfactorily for long periods at extreme conditions on current fuels, it follows that any factor, however secondary, that creates a more adverse combustor environment, will have a large and disproportionate effect on combustion performance and liner durability.
2. Analysis of the experimental data, which cover a range of fuel types from JP4 to DF2, shows that fuel chemistry, as indicated by hydrogen content and/or aromatics content, has a significant effect on flame radiation, liner wall temperature and smoke emissions.
3. The influence of fuel chemistry on ignition performance, weak extinction limits, combustion efficiency, and CO and NO<sub>x</sub> emissions, is quite small, and stems from the effects of slight variations in lower calorific value on combustion temperature.
4. The physical properties that govern atomization quality and evaporation rates affect lightup characteristics, weak extinction limits, combustion efficiency, and CO emissions. Other important performance parameters, such as NO<sub>x</sub> emissions, smoke emissions and liner wall temperature, are sensibly independent of physical properties over the range of fuels studied.

5. Fuel chemistry has no direct influence on pattern factor. However, physical properties have an effect that is appreciable at low power conditions but which diminishes in importance with increase in engine power, becoming very small at the highest power setting, where the effect of pattern factor on vane life is most significant.

SECTION XIII  
RECOMMENDATIONS

1. Additional work is recommended to extend the scope of the present report to include correlations for the prediction of unburned hydrocarbons (UHC). During this program the data on unburned hydrocarbons contained in references 1 to 6 were examined to the extent that it was found feasible to obtain correlations, although not to the same degree of accuracy as for CO and NO<sub>x</sub>. However, lack of time precluded the establishment of a satisfactory correlation for UHC.
2. The correlations presented in this report should be re-examined with a view to further improvement and refinement. For example, the present soot correlation is based on the total aromatic content of the fuel. However, it is quite possible that not all of the various types of aromatics (1-ring, 2-ring, etc.) are equally effective in producing soot; and thus a better correlation of smoke emissions might be achieved by neglecting certain aromatic constituents of the fuel. Also worthy of further investigation is the use of hydrogen content, instead of percentage aromatics, as an indicator of propensity to soot formation.
3. It is strongly recommended that efforts be made to measure the mean drop sizes (SMD's) produced by the fuel nozzles actually used in the fuels research programs described in references 1 to 6. Accurate knowledge of drop sizes over the entire engine operating range would not only allow the fairly complete correlations achieved for the J79-17A, J79-17C, F101, and TF41 to be applied to the TF39, J85, TF33

and F100, but would also enable these correlations to be rewritten in a more basic and general form that would facilitate their application to all other gas turbine combustors.

## REFERENCES

1. Gleason, C. C., T. L. Oller,  
M. W. Shayeson and D. W. Bahr,  
Evaluation of Fuel Character Effects  
on J79 Engine Combustion System,  
AFAPL-TR-79-2015, June 1979.
2. Gleason, C. C., T. L. Oller,  
M. W. Shayeson and D. W. Bahr,  
Evaluation of Fuel Character Effects  
on F101 Engine Combustion System,  
AFAPL-TR-79-2018, June 1979.
3. Vogel, R. E., D. L. Troth  
and A. J. Verdouw,  
Fuel Character Effects on Current,  
High Pressure Ratio, Can-Type Turbine  
Combustion Systems, AFAPL-TR-79-2072,  
April 1980.
4. Gleason, C. C., T. L. Oller,  
M. W. Shayeson and M. J.  
Kenworthy,  
Evaluation of Fuel Character Effects  
on J79 Smokeless Combustor, AFWAL-  
TR-80-2092, November 1980.
5. Oller, T. L., C. C. Gleason,  
M. J. Kenworthy, J. D. Cohen,  
and D. W. Bahr,  
Fuel Mainburner/Turbine Effects,  
AFWAL-TR-81-2100, May 1982.
6. Russel, P. L.,  
Fuel Mainburner/Turbine Effects,  
AFWAL-TR-81-2081, Sept. 1982.
7. Longwell, J. P.,  
Jet Aircraft Hydrocarbon Fuels  
Technology, NASA Conference  
Publication 2033, June 7-9, 1977.
8. Lefebvre, A. H.,  
Airblast Atomization, Prog. Energy  
Combust. Sci., Vol. 6, pp. 231-261,  
1980.
9. Lefebvre, A. H.,  
Gas Turbine Combustion, McGraw Hill,  
1983.
10. Lefebvre, A. H.,  
Theoretical Aspects of Gas Turbine  
Combustion Performance, College of  
Aeronautics Note, Aero. No. 163,  
Cranfield, Bedford, England, 1960.
11. Chin, J. S. and  
A. H. Lefebvre,  
Effective Values of Evaporation  
Constant for Hydrocarbon Fuel Drops,  
Proceedings of the Twentieth Automotive  
Technology Development Contractors  
Coordination Meeting, pp. 325-331, 1983.
12. Moses, C. A.,  
Studies of Fuel Volatility Effects on  
Turbine Combustor Performance, Joint  
Spring Meeting of Western and Central  
States Sections of the Combustion Institute,  
San Antonio, Texas, 1975.

13. Ballal, D. R. and A. H. Lefebvre, Weak Extinction Limits of Turbulent Flowing Mixtures, Trans. ASME, J. Eng. Power, Vol. 101, No. 3, pp. 343-348, 1979.
14. Ballal, D. R. and A. H. Lefebvre, Weak Extinction Limits of Turbulent Heterogeneous Fuel/Air Mixtures, Trans. ASME, J. Eng. Power, Vol. 102, No. 2, pp. 416-421, 1980.
15. Lefebvre, A. H., An Evaporation Model for Quenching Distance and Minimum Ignition Energy in Liquid Fuel Sprays, Paper presented at Fall Meeting of Combustion Institute (Eastern Section), 1977.
16. Foster, H. H. and D. M. Straight, Effect of Fuel Volatility Characteristics on Ignition Energy Requirements in a Turbojet Combustor, NACA RM E52J21, January 1953.
17. Wigg, L. D., The Ignition of Flowing Cases, Selected Combustion Problems II, Butterworth Scientific Publications, London, pp. 73-82, 1956.
18. Rao, K. V. L. and A. H. Lefebvre, Minimum Ignition Energies in Flowing Kerosene/Air Mixtures, Combustion and Flame, Vol. 27, No. 1, pp. 1-20, 1976.
19. Ballal, D. R. and A. H. Lefebvre, General Model of Spark Ignition for Gaseous and Liquid Fuel/Air Mixtures, Eighteenth Symposium (International) on Combustion, pp. 1737-1746, 1981.
20. Lefebvre, A. H. and M. V. Herbert, Heat-Transfer Processes in Gas-Turbine Combustion Chambers, Proc. Inst. Mech. Engrs., Vol. 174, No. 12, pp. 463-473, 1960.
21. Kretschmer, D. and Odgers, J., A Simple Method for the Prediction of Wall Temperatures in a Gas Turbine Combustor, ASME Paper No. 78-GT-90, 1978.
22. Blazowski, W. S., Combustion Considerations for Future Jet Fuels, Sixteenth Symposium (International) on Combustion, The Combustion Institute, pp. 1631-1638, 1977.
23. Jackson, T. A., Fuel Character Effects on the J79 and F101 Engine Combustion Systems, Symposium on Aircraft Research and Technology for Future Fuels, NASA Lewis Research Center, 1980.

24. McAdams, W. H., Heat Transmission, 3rd ed., McGraw-Hill Book Co., New York, 1954, Chapter 4 by H. C. Hottel.
25. Environmental Protection Agency. Control of Air Pollution from Aircraft and Aircraft Engines, Fed. Regist., 38, No. 136, 19103, 1973.
26. Environmental Protection Agency. Control of Air Pollution from Aircraft and Aircraft Engines, Fed. Regist., 43, No. 58, 1978.
27. Lipfert, F. W., Correlation of Gas Turbine Emissions Data, ASME Paper No. 72-GT-60, 1972.
28. Roffe, G. and K. S. Venkataramani, Emissions Measurements for a Lean Premixed Propane/Air System at Pressures up to 30 Atmospheres, NASA CR-159421, 1978.
29. Anderson, D. N., Effects of Equivalence Ratio and Dwell Time on Exhaust Emissions from an Experimental Premixing Prevaporizing Burner, ASME Paper 75-GT-69, 1975.
30. Fenimore, C. P., Formation of Nitric Oxide in Premixed Hydrocarbon Flames, Thirteenth Symposium (International) on Combustion, The Combustion Institute, Pittsburgh, pp. 373-380, 1971.
31. Merryman, E. L. and A. Levy, Nitrogen Oxide Formation in Flames: The Role of NO<sub>2</sub> and Fuel Nitrogen, Fifteenth Symposium (International) on Combustion, The Combustion Institute, Pittsburgh, pp. 1073-1083, 1975.
32. Laurendeau, N. M., Fast Nitrogen Dioxide Reactions: Significance of Decomposition During NO and NO<sub>2</sub> Formation, Combustion Science and Technology, Vol. 11, No. 3/4, pp. 86-96, 1975.
33. Graham, S. C., J. B. Homer, and J. L. J. Rosenfeld, The Formation and Coagulation of Soot Aerosols Generated by the Pyrolysis of Aromatic Hydrocarbons, Proc. Roy. Soc. London A, Vol. 344, pp. 259-285, 1978.
34. Graham, S. C., J. B. Homer, and J. L. J. Rosenfeld, The Formation and Coagulation of Soot Aerosols, Int. Shock Tube Symposium, 10th Proceedings, pp. 621-631, July 1975.

35. Blazowski, W. S.,  
Dependence of Soot Production on  
Fuel Blend Characteristics and  
Combustion Conditions, J. Eng. Power,  
Vol. 102, pp. 403-408, April 1980.
36. Naegeli, D. W. and  
C. A. Moses,  
Effect of Fuel Molecular Structure on  
Soot Formation in Gas Turbine Engines,  
ASME Gas Turbine Conference, New  
Orleans, Paper 80-GT-62.
37. Schalla, R. L. and  
R. R. Hibbard,  
Smoke and Coke Formation in the  
Combustion of Hydrocarbon-Air Mixtures,  
Chapter IX, Adaptation of Combustion  
Principles to Aircraft Propulsion  
Vol. 1: Basic Considerations in the  
Combustion of Hydrocarbon Fuels with  
Air, NACA RM ES4107, 1955.
38. Lefebvre, A. H. and  
T. Durrant,  
Design Characteristics Affecting Gas  
Turbine Combustion Performance, SAE  
Preprint 240C; also Esso Air World,  
Vol. 13, No. 3, pp. 64-69, 1960.
39. Clarke, A. E., T. G.  
Hunter, and F. H. Garner,  
The Tendency to Smoke of Organic  
Substances on Burning, Part I,  
Journal of the Institute of Petroleum,  
Vol. 32, No. 274, pp. 627-642, October  
1946.
40. Hunt, R. A.,  
The Relation of Smoke Point to  
Molecular Structure, Industrial and  
Engineering Chemistry, Vol. 45,  
No. 3, pp. 602-606, March 1953.
41. Odgers, J.,  
Air Pollution by Gas Turbines -- Is  
Control Possible? Canadian Aeronautical  
and Space Journal, Vol. 16, No. 8,  
pp. 339-344, October 1970.
42. Holderness, F. H. and  
J. J. Macfarlane,  
Soot Formation in Rich Kerosine  
Flames at High Pressure, Paper No. 18,  
Atmospheric Pollution by Aircraft  
Engines, AGARD CP-125, Advisory  
Group for Aerospace Research and  
Development, 1973.
43. Norster, E. R. and  
A. H. Lefebvre,  
Effects of Fuel Injection Method on  
Gas Turbine Combustion, Emissions  
from Continuous Combustion Systems,  
ed. by W. Cornelius and W. G. Agnew,  
Plenum Press, New York, pp. 255-278,  
1972.

44. Toone, B.,  
A Review of Aero Engine Smoke Emission, Combustion in Advanced Gas Turbine Systems, ed. by I. E. Smith, Cranfield International Symposium Series, Vol. X, Pergamon Press Ltd., London, pp. 271-296, 1968.
45. Lefebvre, A. H.,  
Factors Controlling Gas Turbine Combustion Performance at High Pressure, Combustion in Advanced Gas Turbine Systems, ed. by I. E. Smith, Cranfield International Symposium Series, Vol. X, Pergamon Press Ltd., London, pp. 211-226, 1968.
46. Jones, R. E. and J. Grobman,  
Design and Evaluation of Combustors for Reducing Aircraft Engine Pollution, Paper No. 31, Atmospheric Pollution by Aircraft Engines, AGARD CP-125, Advisory Group for Aerospace Research and Development, 1973.
47. Grobman, J.,  
Effect of Operating Variables on Pollutant Emissions from Aircraft Turbine Engine Combustors, Emissions from Continuous Combustion Systems, ed. by W. Cornelius and W. G. Agnew, Plenum Press Ltd., New York, pp. 279-303, 1972.
48. Bahr, D. W.,  
Control and Reduction of Aircraft Turbine Engine Exhaust Emissions, Emissions from Continuous Combustion Systems, ed. by W. Cornelius and W. G. Agnew, Plenum Press, New York, pp. 345-372, 1972.
49. Bahr, D. W.,  
Technology for the Reduction of Aircraft Turbine Engine Exhaust Emissions, Paper No. 29, Atmospheric Pollution by Aircraft Engines, AGARD CP-125, Advisory Group for Aerospace Research and Development, 1973.
50. Henderson, R. E. and W. S. Blazowski,  
Aircraft Gas Turbine Pollutant Limitations Oriented Toward Minimum Effect on Engine Performance, Paper No. 33, Atmospheric Pollution by Aircraft Engines, AGARD CP-125, Advisory Group for Aerospace Research and Development, 1973.

51. Jones, R. E., L. A. Diehl,  
D. A. Petrash, and J. Grobman,  
Results and Status of the NASA Aircraft Engine Emission Reduction Technology Program, NASA TM 79009, 1978.
52. Appleton, J. P.,  
Soot Oxidation Kinetics at Combustion Temperatures, Paper No. 20, Atmospheric Pollution by Aircraft Engines, AGARD CP-125, Advisory Group for Aerospace Research and Development, 1973.
53. Fenimore, C. P. and  
G. W. Jones,  
Coagulation of Soot to Smoke in Hydrocarbon Flames, Combust. Flame, Vol. 13, No. 3, pp. 303-310, 1969.
54. Caretto, L. S.,  
Mathematical Modelling of Pollutant Formation, Progress in Energy and Combustion Science, Vol. 1, No. 2/3, pp. 47-71, 1976.
55. Fletcher, R. S. and  
J. B. Heywood,  
A Model for Nitric Oxide Emissions from Aircraft Gas Turbine Engines, AIAA Paper No. 71-123.
56. Mosier, S. A. and  
R. Roberts,  
Development and Verification of an Analytical Model for Predicting Emissions from Gas Turbine Engine Combustors during Low Power Operation, AGARD CP-125, 1973.
57. Roberts, R., L. D. Aceto,  
R. Kollrack, D. P. Teixeira,  
and J. M. Bonnell,  
An Analytical Model for Nitric Oxide Formation in a Gas Turbine Combustor, AIAA Journal, Vol. 10, No. 6, pp. 820-826, 1972.
58. Mador, R. J. and  
R. Roberts,  
A Pollutant Emission Prediction Model for Gas Turbine Combustors, AIAA Paper No. 74-1113, 1974.
59. Edelman, R. and  
C. Economos,  
A Mathematical Model for the Jet Engine Combustion Pollutant Emissions, AIAA Paper No. 71-714, 1971.
60. Mongia, H. G. and  
K. Smith,  
An Empirical/Analytical Design Methodology for Gas Turbine Combustors, AIAA Paper No. 78-949, 1978.
61. Bruce, T. W., H. C. Mongia,  
and R. S. Reynolds,  
Combustor Design Criteria Evaluation, Vol. 1, UASRTL-TR-78-55A, 1979.
62. Swithenbank, J., A. Turan,  
and P. G. Felton,  
Three-Dimensional, Two Phase Mathematical Modelling of Gas Turbine Combustors, Gas Turbine Combustor Design Problems, Hemisphere, pp. 249-314, 1980.

63. Pratt, D. T., Coalescence/Dispersion Modelling of Gas Turbine Combustors, Gas Turbine Combustor Design Problems, Hemisphere, pp. 315-330, 1980.
64. Hung, W. S. Y., An Experimentally Verified NO<sub>x</sub> Emission Model for Gas Turbine Combustors, ASME Paper No. 75-GT-71, 1975.
65. Hung, W. S. Y., Accurate Method of Predicting the Effect of Humidity on Injected Water on NO<sub>x</sub> Emissions from Industrial Gas Turbines, ASME Paper No. 74-WA/GT-6, 1974.
66. Hung, W. S. Y., A Diffusion Limited Model that Accurately Predicts the NO<sub>x</sub> Emissions from Gas Turbine Combustors Including the Use of Nitrogen Containing Fuels, ASME Paper No. 75-Pwr-11, 1975.
67. Hung, W. S. Y., Modeling and Measurement of NO<sub>x</sub> Emissions from Burning Synthetic Coal Gas in Gas Turbine Combustors, ASME Paper No. 75-WA/GT-3, 1975.
68. Fletcher, R. S.  
R. D. Siegel, and  
E. K. Bastress, The Control of Oxides of Nitrogen Emissions from Aircraft Gas Turbine Engines, NREC 1162, FAA-RD-71-111, Vols. I, II, and III, Northern Research and Engineering Corp., Cambridge, MA, 1971.
69. Hammond, D. C. (Jr.)  
and A. M. Mellor, Analytical Calculations for the Performance and Pollutant Emissions of Gas Turbine Combustors, Combustion Science and Technology, Vol. 4, No. 3, pp. 101-112, 1971.
70. Hammond, D. C. (Jr.) and  
A. M. Mellor, Analytical Predictions of Emissions from and within an Allison J-33 Combustor, Combustion Science and Technology, Vol. 6, No. 5, pp. 279-286, 1973.
71. Mellor, A. M., Semi-Empirical Correlations for Gas Turbine Emissions, Ignition, and Flame Stabilization, Prog. Energy Combust. Sci., Vol. 6, pp. 347-358, 1981.

72. Rubins, P. M. and  
N. R. Marchionna,  
Evaluation of NO<sub>x</sub> Prediction-  
Correlation Equations for Small Gas  
Turbines, Journal of Aircraft,  
Vol. 15, No. 8, pp. 497-502, 1978.
73. Sullivan, D. A. and  
P. A. Mas,  
A Critical Review of NO<sub>x</sub> Correlations  
for Gas Turbine Combustors, ASME Paper  
75-WA/GT-7, 1975.
74. Odgers, J.,  
Current Theories of Combustion within  
Gas Turbine Chambers, Fifteenth  
Symposium (International) on Combustion,  
The Combustion Institute, pp. 1321-  
1338, 1975.
75. Shaffernocker, W. M.  
and Stanforth, C. M.,  
Smoke Measurement Techniques, SAE  
Paper C80346, 1968.